*UCRL-53809-96*
*Distribution Category UC-700*

***Institute of***

***Geophysics and***

***Planetary***

***Physics***

***Lawrence Livermore***

***National Laboratory***

# *1996*

# *Annual Report*

*October 1, 1995 through*
*September 30, 1996*

***Edited by***
***Frederick J. Ryerson***
*Institute of Geophysics and Planetary Physics*
*University of California*

UCRL-53809-96

Work performed under the auspices of the U.S. Department of Energy by Lawrence Livermore National Laboratory under Contract W-7405-Eng-48.

*UCRL-53809-96*
*Distribution Category UC-700*

***Institute of***

***Geophysics and***

***Planetary***

***Physics***

***Lawrence Livermore***

***National Laboratory***

# *1996*

# *Annual Report*

*October 1, 1995 through*
*September 30, 1996*

***Edited by***
***Frederick J. Ryerson***
*Institute of Geophysics and Planetary Physics*
*University of California*

## Acknowledgments

This report was edited and produced by Jan Tweed, who also prepared the manuscript and graphics. Kem Cook and Charles Alcock assisted in the technical reviews. Marsha McInnis provided assistance with graphic design and technical illustration. We would also like to thank Carolin Middleton, who edited IGPP's annual reports from 1991–1995, for her valuable contributions to this report.

# Section I. Overview

The Institute of Geophysics and Planetary Physics (IGPP) is a Multicampus Research Unit of the University of California (UC). IGPP was founded in 1946 at UC Los Angeles with a charter to further research in the earth and planetary sciences and in related fields. The Institute now has branches at UC campuses in Los Angeles, San Diego, and Riverside, and at Los Alamos and Lawrence Livermore national laboratories.

The University-wide IGPP has played an important role in establishing interdisciplinary research in the earth and planetary sciences. For example, IGPP was instrumental in founding the fields of physical oceanography and space physics, which at the time fell between the cracks of established university departments. Because of its multicampus orientation, IGPP has sponsored important interinstitutional consortia in the earth and planetary sciences. Each of the five branches has a somewhat different intellectual emphasis as a result of the interplay between strengths of campus departments and Laboratory programs.

The IGPP branch at Lawrence Livermore National Laboratory (LLNL) was approved by the Regents of the University of California in 1982. IGPP–LLNL emphasizes research in seismology, geochemistry, cosmochemistry, and astrophysics. It provides a venue for studying the fundamental aspects of these fields, thereby complementing LLNL programs that pursue applications of these disciplines in national security and energy research.

IGPP–LLNL is directed by Charles Alcock and was originally organized into three centers: Geosciences, stressing seismology; High-Pressure Physics, stressing experiments using the two-stage light-gas gun at LLNL; and Astrophysics, stressing theoretical and computational astrophysics. In 1994, the activities of the Center for High-Pressure Physics were merged with those of the Center for Geosciences.

The Center for Geosciences, headed by Frederick Ryerson, focuses on research in geophysics and geochemistry. The Astrophysics Research Center, headed by Charles Alcock, provides a home for theoretical and observational astrophysics and serves as an interface with the Physics and Space Technology Department's Laboratory for Experimental Astrophysics and with other astrophysics efforts at LLNL.

The IGPP branch at LLNL (as well as the branch at Los Alamos) also facilitates scientific collaborations between researchers at the UC campuses and those at the national laboratories in areas related to earth science, planetary science, and astrophysics. It does this by sponsoring the University Collaborative Research Program (UCRP), which provides funds to UC campus scientists for joint research projects with LLNL.

The goals of the UCRP are to enrich research opportunities for UC campus scientists by making available to them some of LLNL's unique facilities and expertise, and to broaden the scientific program at LLNL through collaborative or interdisciplinary work with UC campus researchers.

UCRP funds (provided jointly by the Regents of the University of California and by the Director of LLNL) are awarded annually on the basis of brief proposals, which are reviewed by a committee of scientists from UC campuses, LLNL programs, and external universities and research organizations. Typical annual funding for a collaborative research project ranges from $5,000 to $25,000. Funds are used for a variety of purposes, including salary support for visiting graduate students, postdoctoral fellows, and faculty; released-time salaries for LLNL scientists; and costs for experimental facilities.

Although the permanent LLNL staff assigned to IGPP is relatively small (presently about five full-time equivalents), IGPP's research centers have become vital research organizations. This growth has been possible because of IGPP support for a substantial group of resident postdoctoral fellows; because of the 20 or more UCRP projects funded each year; and because IGPP hosts a variety of visitors, guests, and faculty members (from both UC and other institutions) on sabbatical leave. To focus attention on areas of topical interest in the geosciences and astrophysics, IGPP–LLNL hosts conferences and workshops, and also organizes seminars in astrophysics and geosciences. Section IV lists the seminars given in FY 1996.

Figures 1 and 2 give a statistical overview of IGPP–LLNL's UCRP (colloquially known as the mini-grants). Figure 1 shows the distribution of UCRP awards among the UC campuses, by total amount awarded and by number of proposals funded. Figure 2 gives the distribution of awards by center.

Since FY 1987, IGPP–LLNL has maintained a bibliography of published research papers resulting from UCRP projects and from research by the IGPP's staff, postdoctoral fellows, and consultants. These lists are published each year in the annual report. Section V gives the bibliography for FY 1996. As a measure of research productivity, the results are gratifying. The abundance of publications from IGPP collaborative projects is a measure of the significance of the results obtained in these projects. This refereed-journal publication rate for IGPP-related projects corresponds to more than 1 paper/year for each faculty member, 2 papers/year for each IGPP postdoctoral fellow, and 2 papers/year for each IGPP staff member.

Figure 3 compares the total papers published in refereed journals or conferences for the last five years. (Note: Because of the extensive peer-review process for most scientific journals, several papers submitted by the principal investigators are still in progress. Therefore, we cannot give an accurate total of 1996 papers published until we receive formal notification from the journals and authors. Final 1996 totals will be available in our 1997 report.)

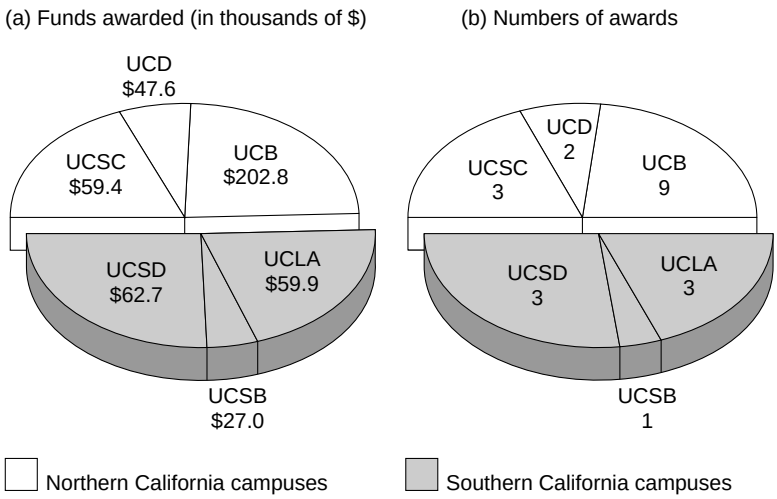


*Figure 1. Distribution of FY 1996 UCRP awards to UC campuses from IGPP–LLNL.*

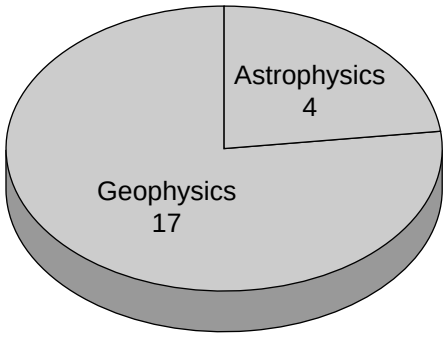


*Figure 2. Distribution of awards by IGPP–LLNL center.*

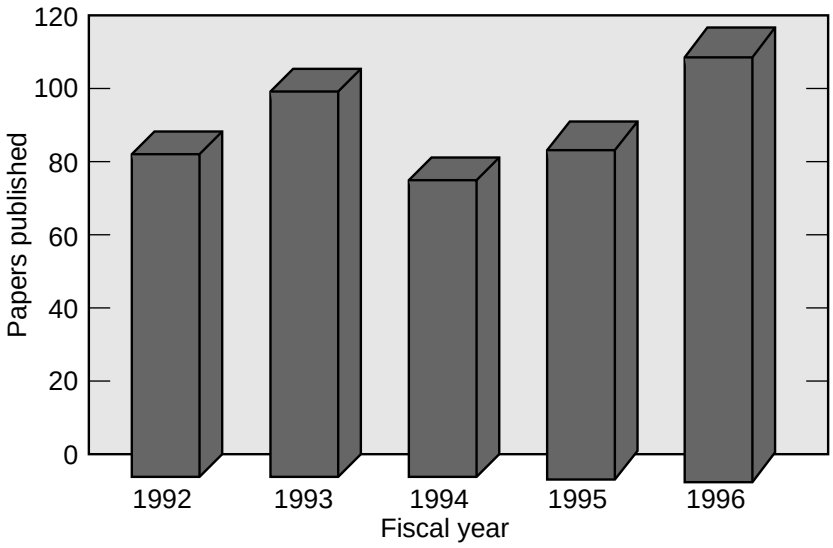


*Figure 3. Total number of papers published in refereed journals and conference proceedings from 1992 through 1996.*

# Section II. Highlights of Fiscal Year 1996

## *Astrophysics Research Center*

The Astrophysics Research Center serves the aims of IGPP–LLNL in astrophysics. These goals include managing the astrophysics part of the UCRP and facilitating contacts between UC scientists and their LLNL counterparts. The Astrophysics Research Center also serves as the focus of astrophysics activities at LLNL by organizing the weekly astrophysics colloquium, by hosting visitors and collaborators, by editing an annual Observatory Report that covers astrophysics activities at LLNL (and is published in the *Bulletin of the American Astronomical Society*), and by providing a variety of other service functions. The staff and postdoctoral researchers of the Astrophysics Research Center carry out a significant program of research.

The scientific staff of the center are Charles Alcock (Center Head), Kem Cook, Claire Max, and Willem van Breugel. Administrative support is provided by Christina Budwine (Operations Manager), and by secretaries Jan Tweed and Valerie Knighten. Debbie Santa Maria manages the network of computers in the center.

Postdoctoral fellows perform most of the research in the Astrophysics Research Center. Some fellows are supported entirely by IGPP funds, while some are supported partially by other groups at LLNL. In FY 1996, the postdoctoral fellows were David Bennett (Notre Dame), Michael Brotherton (U/Texas, Austin), Andrea Cimatti (Arectri Obs., Italy), Seran Gibbard (U/Arizona), Michael Gregg (Australian National University), Karsten Jedamzik (UC San Diego), Sally Laurent-Muehleisen (UC Davis), Matthew Lehnert (Leiden Obs., The Netherlands), Bruce Macintosh (UC Los Angeles), Stuart Marshall (UC San Diego), Dante Minniti (U/Arizona), Ed Moran (Columbia University), Sun Hong Rhie (Stanford University), Adam Stanford (U/Washington), and Hien Tran (UC Santa Cruz).

The center hosts several scientific visitors, not only from the UC campuses but also from around the world. These visitors stay for a day to a year. Some who are affiliated with local institutions spend large, ongoing portions of their time in the center.

The center and its offices are in Building 319, which is close to the offices of many LLNL astrophysicists and is subject to minimal access controls. These features make the center ideal for the many collaborations that have developed between UC researchers and LLNL scientists.

The Astrophysics Research Center has access to a variety of machines for computing. Most day-to-day work, which includes code development, image processing, and symbolic manipulation, is carried out on the center's

network of Sun workstations. This network has been used for large-scale processing by the exploitation of codes that utilize a large fraction of the network for parallel processing. This level of processing is especially effective at night, when most of the network is otherwise quiet and when the "invasive" code will not adversely affect the image-processing work. In addition, much greater computing power is available in other parts of LLNL.

## Research Highlights

The Astrophysics Research Center has developed a research program that exploits the traditional strengths in astrophysics at LLNL and opens new areas of study. This research ranges from smaller-scale theoretical and observational projects to large collaborative ventures. The following pages summarize some of this research.

### Laser Guide Stars

Claire Max, Scott Olivier, Jim Brase, Don Gavel, Bruce Macintosh, and Herbert Friedman, working with four LLNL collaborators and five collaborators from three UC campuses, are developing laser guide stars for astronomical adaptive optics. The goal of this project is to improve the angular resolution achieved at ground-based observatories. If the project is successful, the angular resolution at major observatories might be improved by 10 to 100%.

The angular resolution of ground-based telescopes with apertures larger than 10 to 20 cm is limited to about a second of arc because of turbulence in the atmosphere. In principle, if one deforms a flexible secondary mirror to make the wavefront nearly flat, then adaptive optics can be used to correct for the wavefront distortions, which are measured with a wavefront sensor.

This correction would allow ground-based telescopes to be operated at or near their diffraction-limited bounds. For example, at a wavelength of 0.5 mm, the diffraction-limited resolution would be 0.04 arcsec for a 3-m telescope and 0.01 arcsec for a 10-m telescope. These represent improvements in resolution of factors of 25 and 100, respectively, relative to the atmospheric resolution of about 1 arcsec.

To correct the visible range, one needs a bright reference object within a few arcseconds of the object being imaged. The statistics of bright stars are such that a few percent of the sky is accessible for diffraction-limited viewing, using nearby bright stars as the wavefront reference.

To make up for the lack of bright reference stars, this consortium is developing the ability to produce artificial stars using a powerful laser. The idea is to use a laser tuned to the sodium D lines to resonantly excite the atmosphere sodium layer at 90-km altitude, which makes an artificial star to serve as a reference beacon.

A wavefront sensor detects the tilts of the reference wavefront, and a wavefront computer uses the reference wavefront to calculate the adaptive-

optics corrections. Finally, the correction is applied to a deformable mirror. The images recorded using the deformable mirror, with the telescope's primary mirror, will have most of the atmospheric distortions removed.

A 20-W dye laser and an adaptive optics system (both developed at LLNL) have been installed on the Lick Observatory 3-m Shane telescope. The laser is based on technology developed for the LLNL Atomic Vapor Laser Isotope Separation (AVLIS) program and produces an eighth magnitude artificial guide star, sufficient for adaptive optics correction of the 3-m telescope at wavelengths of 1 to 2 μm.

In September 1996, the system produced near-diffraction-limited images using the laser guide star as a wavefront reference. This is the first ever demonstration of a sodium laser guide star high-order adaptive optics system. The results will appear in *Science* in September 1997. Based on experience gained during this run, the system is being redesigned, not only to increase reliability, but to deal with calibration issues (which remain the dominant error term in laser guide star adaptive optics).

The system also demonstrates excellent performance using bright natural guide stars as references. Natural-guide-star science programs studying young stellar objects, binary stars, and the outer planets will be carried out in collaboration with Prof. Andrea Ghez (UC Los Angeles), Prof. Ben Zuckerman (UC Los Angeles), and Prof. James Graham (UC Berkeley.) Science programs using the laser guide star to study fainter targets will also be carried out. The LLNL group is also working on the adaptive optics and laser guide star system for the 10-m W.M. Keck telescope.

## The Massive Compact Halo Objects Project

The Massive Compact Halo Objects (MACHO) Project is an experimental search for the dark matter, which makes up at least 90% of the mass of our galaxy. It was initiated at LLNL and involves Charles Alcock, Kem Cook, Stuart Marshall, and Dante Minniti (LLNL); Robyn Allsman, Tim Axelrod, and Alex Rodgers (Mt. Stromlo Obs., Australia); David Bennett (Notre Dame); Mark Pratt (U/Washington); Christopher Stubbs (CfPA at U/Washington); Kim Griest (CfPA at UC San Diego); Doug Welch (McMaster University); Will Sutherland (Oxford University); and Kenneth Freeman, Bruce Peterson, and Peter Quinn (European Southern Obs., Chile).

The Milky Way's dark matter is thought to be distributed in a large, spherical halo. Its constitution is unknown, because it emits no detectable radiation. Most hypotheses for its constitution before the Project involved speculations from particle physics. Our experiment searches for planets, brown dwarfs, and black holes or any other massive objects (MACHOs) having a mass range of $10^{-7}$ M=FE << M << 1 M=FE.

If the dark matter consists of MACHOs, it will occasionally magnify light from extragalactic stars by the gravitational lens effect. An event can

be recognized by fitting a theoretical light curve to the observations (four-parameter fit) and by its lack of color variation (it is achromatic). Unambiguous recognition of microlensing requires adequate data points on the light curve (10) and measurements in at least two filter bands. To detect events, one must monitor millions of stars for several years. The experiment has been operating for four years, and we have an agreement to operate through 2000.

The MACHO Project uses the 130-cm reflecting telescope of the Mt. Stromlo Observatory, near Canberra, Australia. Operating at prime focus with an innovative optical system gives a field of view 1 deg in diameter. We use a dichroic filter for simultaneous imaging in two spectral bands, doubling the effective exposure rate.

The beams leaving the beam-splitter are imaged onto mosaics of four 2048- $\times$ 2048-pixel charge-coupled devices (CCDs). The typical exposure is 300 s, followed by about 60 s to read the CCD chips. The experiment generates more than 4 Gbytes of data per night. A dedicated computer system and software process the data.

This system measures, twice per night, the brightness of stars in the Magellanic Clouds. Measuring in the regions at the central bar in the Large Magellanic Cloud (LMC), the system can record more than 500,000 stars in one image. In the more crowded regions near the center of the Milky Way, the system can record more than 600,000 stars in one image.

The system was extraordinarily successful in FY 1996. We have implemented an alert system, which identifies microlensing events well before their peak, and this system has allowed spectroscopic confirmation of the microlensing hypothesis. We have detected much more microlensing toward the center of the Milky Way than had been predicted. This is strong evidence for the Milky Way being a strongly barred spiral galaxy—a new point of view.

We have also analyzed two years of data on the central bar of the LMC and found eight microlensing events. A complete analysis of these events suggests that MACHOs constitute about half of the halo dark matter with masses of about 0.5 $M_{\odot}$.

### Searching for Asteroids

Kem Cook (LLNL); Christopher Stubbs and A. Diercks (U/Washington); and Ted Bowell and B. Koehn (Lowell Obs., Arizona) have completed an innovative 4096- $\times$ 4096-pixel scanning CCD camera, which will operate at prime focus on a 24-in. Schmidt telescope on Anderson Mesa in Arizona.

This thermoelectrically cooled camera will scan the sky along great circles of declination at up to 12 times the sidereal rate. This system is the heart of the Lowell Observatory Near-Earth Object Survey (LONEOS), and allows about 1000 square degrees per night to be triple-scanned to detect near-Earth objects through their rapid apparent motion.

The 24-in. Schmidt refurbishment is near completion, and first light is expected in early 1997.

## Galaxy Clusters at High Redshift

In collaboration with P. Eisenhardt (JPL) and M. Dickinson (JHU), Adam Stanford of LLNL has been carrying out a ground-based optical-to-near–IR imaging survey of 40 high redshift galaxy clusters from $z = 0$ to 0.9. For a subset of this sample (19 clusters), HST/WFPC2 images were obtained from the STScI Archive and examined to produce Hubble types for all cluster galaxies.

The optical-to-near–IR colors of the resulting samples of E/S0 galaxies were then compared with both galaxy evolution models and the colors of present epoch early-type galaxies to search for evolutionary trends with redshift.

Stanford found a clear and nearly monotonic change toward bluer colors in the cluster E/S0s with increasing redshift. This result is in agreement with the passive evolution expected for ellipticals formed at very high redshift.

Furthermore, he found that the intrinsic scatter in the colors was small and nearly constant with redshift, indicating that the early-type galaxies form an old, coeval population, which must have formed at a redshift $z > 3$.

Finally, the relationship between the color and the luminosity of the galaxies appears to be constant with redshift, indicating that this relationship depends on the metallicity of the stellar populations. A paper reporting these results was recently accepted for publication in *The Astrophysical Journal*.

At even higher redshifts, there are very few known galaxy clusters. An emerging method of finding such clusters is through deep wide-field near-IR imaging. In collaboration with R. Elston (U/Florida) and P. Eisenhardt (JPL), Stanford has been working on an imaging survey that covers 100 square arcminutes and reaches a K band limiting magnitude of 21.5.

While analyzing this dataset, Stanford discovered a spatially concentrated group of very red objects. The redshifts of a number of these galaxies were obtained using the Keck Telescope in collaboration with H. Spinrad (UC Berkeley). The galaxies appear to have the properties of a massive galaxy cluster at $z = 1.27$, which makes this one of the most distant clusters discovered thus far. A program to obtain HST/WFPC2 images of the candidate cluster is scheduled to examine their morphologies.

## Jet-Induced Star Formation in a Very High Redshift Radio Galaxy

W. van Breugel (LLNL), together with previous IGPP postdoc A. Dey (now at the Johns Hopkins University), W. Vacca (Institute for Astronomy, Hawaii), and Prof. R. Antonucci (UC Santa Barbara), has discovered jet-induced star formation in the very high redshift ($z = 4$) radio galaxy

4C41.17. The observations were the most sensitive of this kind, using a total integration time of 9-1/2 hours on the Keck II 10-m telescope.

The observations were made using a spectropolarimeter and were aimed to determine whether the rest-frame UV light in 4C41.17 is due to scattered light from a hidden quasar or young stars.

Previous observations using this instrument had shown that the UV continua in radio galaxies at moderate redshifts ($z$ = 1) are strongly polarized, suggesting that this light is due to dust or electron scattering of ionizing radiation from hidden quasars at their galaxy centers. The observations of 4C41.17 showed that its continuum is unpolarized and instead contains strong stellar absorption lines.

From deep images with the Hubble Space Telescope, we know that the continuum light in 4C41.17 is aligned with a powerful radio jet. Together, our Keck and HST observations then show that the jet is triggering a large burst of star formation (of several hundred solar masses per year) due to shocks propagating through the gaseous medium of this forming galaxy.

*A Keck near-infrared image of the first massive elliptical galaxy discovered at very high redshift.*

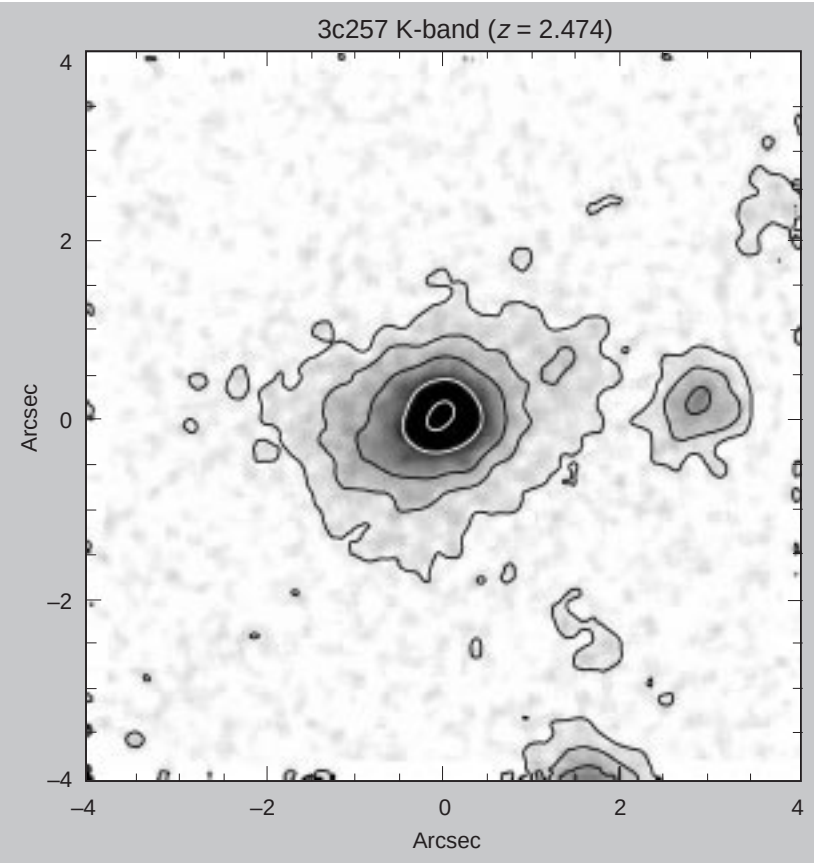

## Morphological Evolution of High Redshift Radio Galaxies and the Formation of Massive Elliptical Galaxies

Deep near-infrared observations of high redshift radio galaxies with the Keck I 10-m telescope by W. van Breugel and A. Stanford (LLNL) and Profs. H. Spinrad and J. Graham and graduate student D. Stern (UC Berkeley) have shown strong evolution of the galaxy morphologies at rest-frame visual wavelengths. At the highest redshifts, $z = 3$, the galaxies display large-scale low-surface brightness emission with occasionally bright elongated features aligned with the radio structure.

These morphologies change dramatically at $2 < z < 3$, where the HzRGs have smooth, compact structures without bright, radio-aligned features. Several of these lower redshift objects have elliptical shapes and surface brightness profiles similar to those of dynamically relaxed elliptical galaxies in the present epoch.

These results provide strong observational support for hierarchical galaxy formation models in which massive ellipticals are thought to form through the merging of sub-galactic stellar systems within a few years after the Big Bang.

# Center for Geosciences

The primary purpose of the IGPP–LLNL Center for Geosciences is to promote collaborative research in the geosciences between LLNL and the various UC campuses. LLNL's mission-oriented programs in national security and energy research employ many subdisciplines within the geosciences. IGPP draws upon these capabilities and expertise and acts as a focal point for research in the fundamental aspects of these areas. We hope to consolidate many unique talents and capabilities at LLNL and to provide an easily identifiable avenue for LLNL–UC collaborations.

The Center for Geosciences is the focus of these interactions, with visitors from academic (UC and other universities), industrial, and governmental research institutions. The center's research emphasis is on the physics and geochemistry of the solid Earth, including seismology, geochemistry, experimental petrology, mineral physics, environmental geochemistry, hydrology, and active tectonics.

The center is housed in the Geophysics & Global Security and Geosciences & Environmental Technologies divisions of LLNL's Earth and Environmental Sciences (EES) Directorate. It is involved with several programs within EES and also with the Isotope Sciences Division of LLNL's Chemistry and Materials Science Directorate, which is a major contributor in the area of geochemical expertise and analytical facilities.

Rick Ryerson and George Zandt have shared the responsibilities for operation of the center in past years. Zandt, a seismologist with interests in upper mantle and crustal structure and tectonics, left LLNL in 1996 for a position in the Department of Geosciences at the University of Arizona. Ryerson is a petrologist with interests in diffusion in rock-forming minerals, and high temperature and pressure phase equilibria. He oversees projects in experimental geochemistry and mineral physics. Postdoctoral fellows James Brenan, Daniel Farber, and William Minarik, along with staff members Henry Shaw, Ian Hutcheon, and Douglas Phinney, played active roles in this area of research.

In the past few years, the center has also developed a program in the tectonics of Asia associated with the Indo-Asian collision. Zandt and Ryerson, with Mark Caffee and Bob Finkel (LLNL), have participated in this effort. Zandt has been working with Tom Owens (U/South Carolina) and Dan McNamara (a postdoc at LLNL) on interpreting seismic data from a previous Lhasa-Golmud seismic deployment.

Rick Ryerson conducted fieldwork in Nepal this year with Mark Harrison and An Yin (UC Los Angeles), investigating the thermal and structural history of the Main Central Thrust.

We also began a program in active tectonics working with colleagues from the Jet Propulsion Lab, the Institut de Physique du Globe de Paris, the University of Washington, and the Chinese Institute of Remote Sensing,

attempting to measure the slip-rates on active faults using offset measurements and cosmic-ray exposure dating.

The dating is performed at LLNL's Center for Accelerator Mass Spectrometry (CAMS), a facility that plays a large role in the center's internal and UCRP research programs. Anne-Sophie Meriaux, a graduate student of Paul Tapponnier at Institut de Physique du Globe de Paris, is currently working with the CAMS group on this problem, as a guest at LLNL.

## Research Highlights

The research program at the Center for Geosciences concentrates on problems in experimental petrology and tectonics. The following pages summarize some of this research.

### Dating Inverted Metamorphism within the Central Himalaya

Rick Ryerson, working with Mark Harrison, An Yin, and Oscar Lovera (UC Los Angeles) and Patrick Le Fort (CNRS, Grenoble), provided new age constraints on the timing of deformation associated with the uplift of the Himalayas, by dating the metamorphism along the Main Central Thrust (MCT).

The spatial association of intracontinental thrusting and inverted metamorphism, recognized in the Himalaya more than a century ago, has inspired continuing efforts to identify its causal relationship. Perhaps the best known sequence of inverted metamorphism is that found immediately beneath the Himalayan Main Central Thrust (MCT), generally thought to have been active during the Early Miocene. It has been widely assumed that the pattern of inverted metamorphism also developed at that time.

Using a new approach, *in situ* Th-Pb dating of monazite included in garnet, the researchers have discovered that the peak metamorphic recrystallization recorded in the footwall of the MCT fault occurred at ca. 5 Ma. The apparent inverted metamorphism resulted from activation of a broad shear zone beneath the MCT zone, which juxtaposed two right-way-up metamorphic sequences.

Recognition of this remarkably youthful phase of metamorphism resolves outstanding problems in Himalayan tectonics. If Late Miocene activation of the MCT zone and the subsequent development of inverted metamorphism were a widespread occurrence across the Himalaya, two long-standing geodynamic and geomorphological puzzles would be easily resolved. Although the surface expression of the presently active Main Frontal Thrust and recently active Main Boundary Thrust are exposed at elevations of <1 km, it is the MCT zone that marks the most dramatic topographic break in slope within the Himalaya.

If the MCT zone had been inactive for the past ~20 m.y., why would this feature persist? Although a shallow (~15°) ramp on the decollement at ~20 km depth may be a contributory factor in elevating the MCT zone, it

would not produce a sharp break in slope over such a short distance unless the overlying rocks were unusually flexurally weak. More likely, this feature simply reflects the fact that significant displacement along the MCT zone was occurring as recently as 4 Ma.

The one common element among the numerous attempts to account for the thermal energy required by Tibetan Slab anatexis is the requirement for some extraordinary process to have aided melting. A variety of special mechanisms have been proposed, including high (100 MPa) shear stress along the MCT, mantle delamination, very long (>25 m.y.) or short (≤1 m.y.) thermal incubation periods, high concentrations (many 100's of ppm) of B, F, and Li, or rapid (>5 mm/yr) decompression.

Although the juxtaposition of rocks undergoing partial melting with the relatively cold rocks of the adjacent MCT zone undergoing endothermic reactions appears enigmatic, our hypothesis provides a simple explanation. The (presumably higher grade) footwall rocks that were juxtaposed against the thrust flat of the MCT during anatexis have since been displaced northward and replaced by a tectonically telescoped section of lower grade rocks.

As a consequence, any attempt to explain the present juxtaposition of Tibetan Slab and Midlands Formations without recognizing the diachroneity of deformation is ordained to require extraordinary circumstances.

## Fluids in Subduction Zones

A major problem that faces Earth scientists that study convergent margins is the origin of volcanism above a zone into which cold oceanic crust is penetrating. The current paradigm that apparently resolves this dilemma is that melting within the mantle wedge is driven by the fluxing action of aqueous fluids driven from the subducted oceanic crust in response to a series of pressure-dependent dehydration reactions. Boron is an element that is thought to be a particularly sensitive tracer of the slab-to-mantle transfer of water, owing to its:

- enrichment in both oceanic crust that has been altered hydrothermally and in pelagic sediments;
- apparent mobility during metamorphic devolatilization; and
- low intrinsic abundance in upper mantle reservoirs.

The chemistry of island arc lavas also appears to reflect the transfer of a boron-rich component from the oceanic crust to their mantle source. For example, high boron concentrations in island arc lavas have been correlated with elevated levels of other indicators of slab involvement (e.g., $^{10}$Be, boron isotopes), and most notably, arc lavas are typified by their high ratios of boron to beryllium and niobium (elements that behave similarly to boron during the melting process but are considered to be comparatively immobile during dehydration). Thus, a robust test of the perceived link between subduction and volcanism at convergent margins is to needed determine the

mobility of boron in high pressure aqueous fluids, both in an absolute sense and relative to elements that are interpreted to be immobile.

To provide this test, James Brenan, Henry Shaw, and Rick Ryerson conducted piston-cylinder experiments at 2.0 GPa and 900$^{o}$C to determine the boron, beryllium, and niobium content of aqueous fluid coexisting with phases that may be residual during high-pressure slab dehydration (i.e., garnet, clinopyroxene, amphibole, and rutile).

The results of these high-pressure experiments reveal that dense aqueous fluids are capable of efficient mobilization of boron relative to elements like beryllium and niobium during the devolatilization process that is thought to accompany subduction of oceanic crust at convergent margins. Such results are in qualitative agreement with the observed reduction in boron concentration and B/Be ratio in metamorphic rocks having similar protoliths, but subject to increasing metamorphic grade and having lower water contents.

In addition, selective loss of boron, relative to beryllium or niobium, is anticipated to produce fluids with initially high B/Be and B/Nb at the onset of dehydration, with a progressive reduction in these values as fluid escapes and produces a boron-depleted residue. Owing to the strong depth dependency of dehydration reactions in the subducted crust, the fluid input from the slab to the mantle wedge beneath island arcs should reflect this diminution of B/Be and B/Nb.

This anticipated variation in fluid composition to the mantle wedge is indeed the interpretation for the observed reduction in B/Be and B/Nb in lavas erupted at progressively greater height above the subducted slab in the Kurile and Izu island arcs.

Moreover, our results also have implications for the composition of the dehydrated oceanic crust that is returned to the convecting portion of the mantle. Due to the preferential loss of boron from the oceanic crust, material with low B/Be and B/Nb will be returned to the mantle during subduction. Such a process is thus capable of preventing the excess boron acquired during near-surface alteration of oceanic crust from being cycled into the mantle, thus maintaining the distinction in B/Be and B/Nb for mantle and crustal reservoirs.

Additionally, incorporation of this boron-depleted residue into the source region of ocean island basalts is a viable mechanism to reduce their observed B/Be and B/Nb ratios relative to mid-ocean ridge basalts, and to produce many of the other distinct geochemical features of this magma type.

## Imaging the Tibetan Crust and Upper Mantle

It is widely accepted that the high, uniform elevation of the Tibetan Plateau is, to a large extent, the result of crustal thickening in response to the collision of the Asian and Indian plates beginning 45–55 Myr ago. Although it has been known for at least a decade that the crustal thickness and crustal

seismic properties are not uniform throughout the plateau, until recently our ability to resolve the details of these lateral variations was limited, so little effort has been made to seek a systematic explanation for these differences.

Since 1991, a series of Sino-American and Sino-French seismological expeditions have gathered the first extensive data sets within the plateau itself, thus providing an opportunity to map crustal properties in greater detail.

George Zandt and Tom Owens (U/South Carolina) have made new observations of shear-coupled teleseismic P waves sampling the interior of the Tibetan Plateau. They find that the crust thins by up to 20 km from south to north, with a concomitant increase in Poisson's ratio from normal values in the south to unusually high values in the north, suggesting that the crust in the north may be partially molten.

Changes in crustal properties appear to be associated with changes in upper-mantle structure and properties. The upper mantle beneath northern Tibet is anomalous in many properties, indicative of high temperatures. Hence, while elevated topography in southern Tibet is supported by thick, low-density crust, elevation in northern Tibet may be supported by a relatively thin, partially molten crust underlain by hot mantle.

# Section III. Research Summaries of Collaborative Projects

## *Astrophysics*

## Unified Models and the Alignment Effect in Radio Galaxies and Quasars (AP96-35)

Principal Investigator: Robert Antonucci (UC Santa Barbara)
LLNL Collaborators: Wil van Breugel and Andrea Cimatti
Student: Todd Hurt (UC Santa Barbara)

### Abstract

*We have been carrying out extensive Lick, Keck, and Hubble Space Telescope (HST) observations relating to the Alignment Effect in high-z radio galaxies, the Unified Model for active galactic nuclei and quasars, and the search for active objects at ever higher redshifts. These include Lick and Keck observations revealing hidden quasars in radio galaxies and infrared sources at low and high redshifts, a surprising non-confirmation of polarization in the prototypical aligned high-redshift radio galaxy 3C368, and discovery of a z = 3.54 radio galaxy at Lick, which turned out to be the first radio-loud broad-absorption line object. Follow-up spectropolarimetry at Keck suggests that the latter is actually an immense unobscured starburst, with the absorption troughs formed in the winds of individual hot stars.*

### Objectives

Our goal was to use Lick, Keck, and HST polarization observations to determine the meaning of the "Alignment Effect" and the implications for the active galaxy Unified Model. We have also been searching for and detecting new active objects at very high redshifts, including an ultraluminous starburst with broad absorption lines.

### Progress

Our collaboration has been going very well, resulting in

- A Lick polarization survey of nearby infrared-loud radio galaxies, which produced, among other results, strong evidence for a hidden quasar in the radio galaxy Coma A.
- Three successful Keck runs dedicated to spectropolarimetry of high redshift "aligned" radio galaxies, with a fourth scheduled. The data argue strongly for hidden quasars in many objects.[1–3]
- The surprising non-confirmation of high polarization in the prototypical aligned radio galaxy 3C368 using HST polarization imag-

ing. This observation shows that intrinsic emission must also play a role in the alignment phenomenon.

- We have also been investigating several samples of radio sources in the hopes of finding high-redshift quasars and radio galaxies. Chambers, Miley, and van Breugel (ApJ, **327**, L47, 1988) have shown a correlation between radio spectral index ($\alpha$) and redshift ($z$) for Jansky-level radio sources. Since this $\alpha$–$z$ correlation provides a method for selecting high-$z$ objects, we have been observing several samples of faint ($S_{20}$ cm ~10–100 mJy), ultra-steep-spectrum ($\alpha < -1$, $S_\nu \propto \nu^\alpha$) radio sources.

In collaboration with W. van Breugel and H. Röttgering, we cross-correlated the 7C survey at 151 MHz (Visser *et al., A&A Supp.*, **110**, 419, 1995) with the first data from the VLA FIRST survey at 1400 MHz (Becker, White, and Helfand, *ApJ*, **450**, 559, 1995) to produce an extremely sensitive sample of faint, ultra-steep spectrum (USS) radio sources. After defining the sample, optical imaging is used to search for possible source identifications. Follow-up spectroscopy can then provide the redshift. The spectroscopy is aided by the fact that some high-$z$ radio galaxies exhibit strong emission lines; others contain Ly$\alpha$ lines with observed equivalent widths $\geq$ 1000Å (Lilly, *ApJ*, **333**, 161, 1988).

In April 1995, we took deep optical images of about 15 of the radio fields with the Lick 3-m telescope. In August 1995, with our observations of a brighter sample of USS sources, we discovered a radio galaxy, 1909+72, at $z$ = 3.54 (Röttgering *et al.*, in preparation). Subsequent observations at Keck by our group plus H. Spinrad have shown that it is a radio galaxy with a broad absorption line (BAL) system (Fig. 1). This is the first radio-loud BAL known.

The BALs in 1909+72 could be due to absorbing gas near the AGN (as in BAL quasars; Weymann, Caswell, and Smith, *ARAA*, **19**, 41, 1981) or possibly to outflows from massive stars. The latter possibility is supported by the low polarization measured by us at Keck, and the strong spectral similarity to certain nearby starburst knots such as that in *NGC1741* (Ebbels *et al.*, *MNRAS*, **281**, 175, 1996). In addition, our Lick image shows evidence for rest-frame UV emission extended along the radio axis. Some of the mJy radio sources are quite red.

Figure 2 shows our RIJK data of 0642+44 plotted with model stellar populations as $z$ = 1.5. The model spectra were obtained from a Web site maintained by G.Worthey. The models in Figure 2 employ a single burst of star formation with a Salpeter initial-mass function and solar metallicity. Clearly, our data are well fit by a highly evolved (8 Gyr) stellar population. Models of ~4 Gyr underpredict the K-band flux but otherwise have the correct shape. However, a Q = 1 universe has an age of only 1.6 $(h_{100})^{-1}$ Gyr at $z$ = 1.5. This inconsistency might suggest either reddening or cosmological absorption and thus *ultrahigh z* for 0642+44. Sources similarly red in I–J exist in the literature, but without the ultrasteep mJy radio pedigree. A

follow-up IRTF IR Grism spectroscopy run was snowed out, but has been rescheduled for January 1997.

## References


1. Dey, A., A. Cimatti, W. van Breugel, R. Antonucci, and H. Spinrad, "On the Origin of the UV Continuum Emission From the High Redshift Radio Galaxy 3C256," *ApJ* **465**, 157 (1996).
2. Cimatti, A., A. Dey, W. van Breugel, R. Antonucci, and H. Spinrad, "Spatially Resolved Spectropolarimetry of the Distant Radio Galaxy 3C324," *ApJ* **465**, 145 (1996).
3. Cimatti, A., A. Dey, W. van Breugel, T. Hurt, and R. Antonucci, "Keck Spectropolarimetry of Two High-*z* Radio Galaxies: Discerning the Components of the Alignment Effect," *ApJ*, in press (1996).


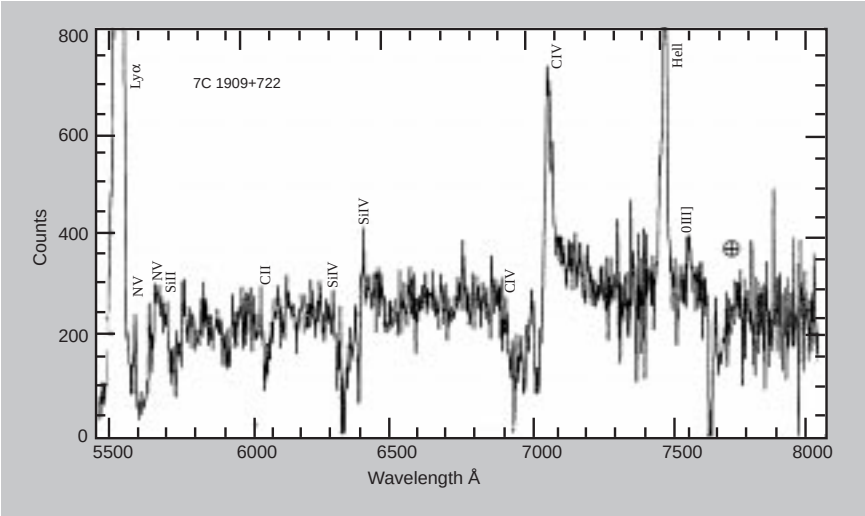


*Figure 1*

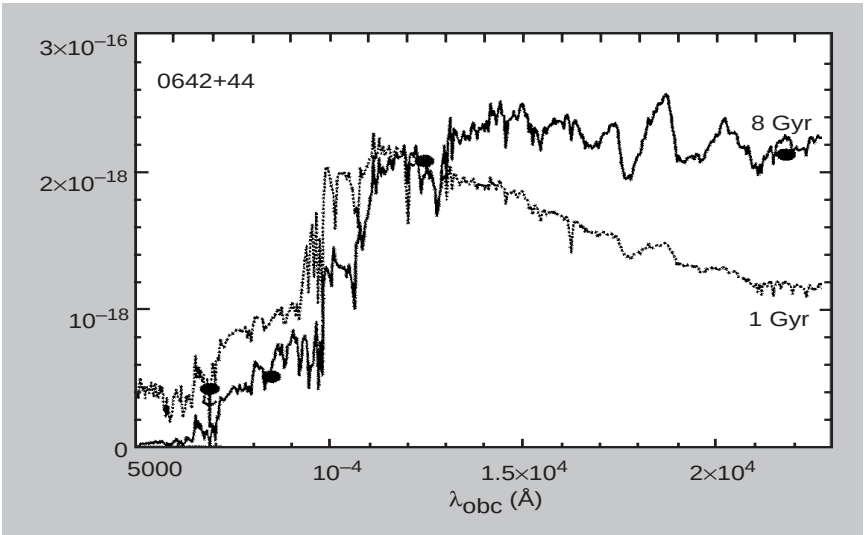


*Figure 2*

# A VLA Survey of the Sky at 1400 MHz (AP96-38)

Principal Investigator: Robert Becker (UC Davis)
LLNL Collaborator: Wil van Breugel
Davis Collaborator: Sally Laurent-Muehleisen

## Abstract

*The FIRST (Faint Images of the Radio Sky at Twenty centimeters) survey completed the analysis of the third season of observing, which has resulted in an expanded catalog of 230,000 discrete radio sources for ~3000 square degrees of sky. Using the expanded catalog, research has continued on the FIRST bright QSO survey,[1] on a search for distant clusters of galaxies, and on a search for extremely high-redshift radio galaxies.*

## Objectives

The primary objective is the creation of an accurate, high-dynamic-range image of the radio sky at 1400 MHz. The survey will allow astronomers to identify rare objects to brightness levels several orders of magnitude fainter then previously possible. This, in turn, will allow us to explore the evolution of quasars, radio galaxies, and clusters of galaxies out to very high redshifts.

## Progress

A number of studies are presently underway. Our bright QSO survey is gaining significant recognition in the community and is successfully competing for optical telescope time to determine redshifts for our candidate QSO. We are currently getting time at Kitt Peak National Observatory, Apache Point Observatory, Lick Observatory, and the Multi-Mirror Telescope.

The QSO survey is discovering a number of unusual objects, including the first examples of radio-loud broad absorption line QSOs. We have gotten time at Keck Observatory to get high-resolution spectra of these previously unheard of objects.

We have also used Keck Observatory to study several new high-redshift clusters of galaxies discovered in the FIRST survey by imaging the area around bent double radio galaxies.

Lastly, a comparison between the FIRST Survey and the low frequency WENNS radio survey is finding numerous steep spectrum radio sources, which are often associated with high-redshift radio galaxies. Optical spectroscopy of these sources is indeed turning up new examples of these high redshift galaxies.

## References

1. Gregg, M. D., R. H. Becker, R. L. White, D. J. Helfand, R. G. McMahon, and I. M. Hook, “The FIRST Bright QSO Survey,” *AJ* **112**, 407 (1996).

# Numerical Studies of Fragmentation in Star-Forming Regions (AP96-40)

Principal Investigator: Christopher F. McKee (UC Berkeley)
LLNL Collaborator: Richard I. Klein
Student: J. Kelly Truelove (UC Berkeley)

## Abstract

*With support from IGPP–LLNL, we have developed and applied a new code for simulation of self-gravitational hydrodynamics. This 3-D code employs adaptive mesh refinement (AMR), a technique whereby the computational volume is evolved on a hierarchy of recursively finer grids. Multiple grids at multiple levels of resolution are dynamically inserted, positioned, and removed as dictated by the changing requirements of the simulated flow. The efficiency obtained with this technology relative to single-grid codes is essential for the study of problems involving gravitational collapse across many orders of magnitude in density at unpredictable locations in the computational volume.*

*With this code, we have determined that, under certain conditions, perturbations arising from numerical errors can grow through a physical mechanism into artificial fragments. We have confirmed this process is not unique to our code, and we have investigated what measures must be taken to suppress it. We have also evaluated the impact of this effect on prominent calculations in the literature. This work has built the foundation for simulations we shall perform of the collapse and fragmentation of molecular clouds, which will be the most realistic to date.*

## Objectives

A key step in the star formation process is fragmentation, whereby molecular clouds or clumps within more massive clouds gravitationally collapse and break up into substantially less massive components that can, in turn, condense into stars. Answers to basic questions concerning this process remain elusive. What is the qualitative nature of the fragmentation process: hierarchical, single-step, or some hybrid? What determines the fraction of an unstable cloud that will fragment into protostellar objects? What influences the distribution of fragment masses, and therefore the initial stellar mass function? What determines the pattern of stellar clustering into binaries and multiple systems?

Our work seeks to address these questions through direct numerical simulation. These simulations are enabled by new numerical technology that we have developed for 3-D adaptive mesh refinement simulation of self-gravitational hydrodynamics. This technology, coupled with realistic initial conditions and a novel equation of state, allows for the most accurate simulations of fragmentation in star-forming regions heretofore possible.

## Progress

In the past year, we debugged and verified our code on a standard test suite of problems for self-gravitational hydrodynamics codes, setting new benchmarks for accuracy on each. This suite includes the pressureless collapse problem described by Hunter;[1] the standard binary fragmentation problem introduced by Boss and Bodenheimer;[2] and the angular momentum conservation test problem of Norman, Wilson, and Barton.[3]

As a bridge to the application stage of our project, we also ran two published calculations that display fragmentation beyond a simple binary. In these simulations, we used the resolutions of the best published results. One, a problem treated by Boss[4] with a low-resolution spherical code, was recently repeated by Burkert and Bodenheimer[5] using a higher-resolution rectangular code.

This problem involves the simulation of a solar mass, centrally condensed molecular cloud core through collapse and multiple fragmentation. Fragmentation is stimulated by an initial 10% amplitude, m = 2 sinusoidal perturbation in azimuthal angle. We reproduced the results of Burkert and Bodenheimer using their resolution.

The second complex calculation we ran was the problem introduced by Burkert and Bodenheimer.[6] Again, using their resolution, we confirmed their general evolutionary scenario. This problem differs from the previous one only in that the simulated cloud core is initially of uniform density.

In the pressureless collapse and angular momentum conservation test problems, both of which have axisymmetric initial conditions and thus axisymmetric analytic solutions, we discovered a key new effect: the formation of artificial fragments from numerical perturbations. Out of concern that this process could equally well occur in nonaxisymmetric problems and be difficult to discern from real fragmentation, we have invested considerable effort in studying it.

We have determined that the artificial fragmentation is a resolution-dependent effect, and we have identified the ratio of the cell size to the Jeans length as the key parameter to adjust to control it. We are investigating the importance of artificial fragmentation in the context of the cloud core calculations described above, which show complex evolutions.

A solid appreciation of artificial fragmentation is prerequisite to approaching the general collapse and fragmentation problems that are the ultimate goal of the project. In preliminary tests, we have utilized conservative spatial resolution and completed the first simulations of collapse from realistic, asymmetric, power-law perturbation initial conditions. These serve as prelude to future calculations of larger clouds.

A discussion of some of the above work is contained in the UC Berkeley Ph.D. thesis of John Holliman. Our progress was described by LLNL collaborator Klein in a talk at the 1996 Star Formation Workshop, July 22–25, 1996, in Wellesley, MA, and in a poster by graduate student Truelove at the

same meeting. Additional computational resources were requested and secured from the Pittsburgh Supercomputing Center to continue the project.

## References


1. Hunter, C., *ApJ* **136**, 594 (1962).
2. Boss, A. P., and P. Bodenheimer, *ApJ* **234**, 289 (1979).
3. Norman, M. L., J. R. Wilson, and R. T. Barton, *ApJ* **239**, 968 (1980).
4. Boss, A. P., *Nature* **351**, 298 (1991).
5. Burkert, A., and P. Bodenheimer, *MNRAS* **280**, 1190 (1996).
6. Burkert, A., and P. Bodenheimer, *MNRAS* **264**, 798 (1993).

# A New Technology for X-Ray Astrophysics and Particle Cosmology (AP96-41)

Principal Investigator: Bernard Sadoulet (UC Berkeley)
LLNL Collaborators: Carl A. Mears, Simon Labov, and Matthias Frank
Student: Sunil Golwala (UC Berkeley)

## Abstract

*In the past year of IGPP funding, we have made great progress in developing the hot electron tunneling (HET) sensor for use in a variety of X-ray and particle detection applications. We have also instrumented cryogenic test setups at Lawrence Livermore National Laboratory (LLNL) and at the Center for Particle Astrophysics at University of California, Berkeley (UCB). Concurrently, our collaboration with San Francisco State University (SFSU) has paved the way for large-scale implementation of the HET sensor via photolithographic fabrication techniques.*

## Progress

**SQUID Installation**: A necessary part of our work has been cryostat instrumentation at LLNL and UCB for testing the HET devices. We have chosen SQUID current amplifiers to measure pulses from our devices, because of their low source impedance (typically a fraction of an ohm). To match the speed of the HET sensor, the readout system must have a bandwidth of approximately 1 megahertz. Commercially available SQUID systems typically are limited to tens of kilohertz. A few companies have begun to develop higher bandwidth SQUID systems for applications such as ours, and we immediately began testing SQUIDs from Quantum Magnetics and Hypres.

While the Quantum Magnetics SQUID displayed extremely good noise performance, we found that it was nevertheless too slow for the HET signals. The Hypres SQUID features a novel array design that obviates the usual superconducting transformer and lock-in technique used in conventional SQUIDs. Because of this, the Hypres SQUID is more convenient to use; more importantly, it also has a wider bandwidth than the Quantum Magnetics SQUID.

The results of our tests were presented at last year's Low Temperature Detectors conference (LTD-6).[1] Based on these tests, we have settled on the Hypres SQUID for our device testing. Unfortunately we have had problems with the reliability of the Hypres SQUIDs; this delayed use of the UCB cryostat for pulse measurements until well into the year. We have overcome this hurdle and can now quickly test devices at UCB.

A major use of the grant has been in the purchase of SQUID chips and the necessary electronics. In addition, a nontrivial amount of effort has also gone into understanding and improving the SQUID electronics, primarily the feedback circuit. While the Hypres SQUID itself is capable of stewing

at the needed speed to measure the HET signals, the presently available feedback electronics do not match this performance. Without the feedback circuit, the SQUIDs are somewhat inconvenient to use because the open loop gain must be measured as data is taken. We believe we can increase the speed of the feedback, and we expect to implement this improvement soon.

An important point is that the collaborative effort funded by this grant has enabled both groups to learn from Dr. Frank's experience in SQUID use. We have applied this knowledge to testing devices fabricated at LLNL, and also to evaluating HET sensors made by our SFSU collaborators and other sensor technologies under development by both groups.

**Sensor Design Issues**: We have significantly increased the sophistication of our understanding of the HET sensor this past year. This advance has been strongly influenced by the frequent exchange of ideas between LLNL and UCB personnel, which is facilitated by this grant.

First, recall the principle of operation of the HET sensor: the tunneling current from the normal (N) electrode to the superconducting (S) electrode is primarily due to tunneling of hot electrons from the tail of the Fermi-Dirac distribution in the N electrode. The number of electrons in this tail is extremely dependent on the temperature of the electrons in the N electrode; in brief, this is why the HET sensor promises to provide a sensitive measurement of energy deposition in the N electrode. When calculated in more detail, this model makes a number of clear predictions:

1. The maximum pulse height should continue to increase as temperature decreases;
2. The bias voltage yielding this maximal pulse height should increase (become closer to the superconductor's gap voltage) as temperature decreases, with the value being independent of the normal state resistance (Rn) of the junction; and
3. The DC tunneling current near the gap should continue to visibly decrease as temperature decreases.

IV curves for a number of devices indicate that the sub-gap current in fact seems to remain unchanged below about 200 to 300 mK. Our measurements of maximal pulse height indicate a saturation at low temperature. Finally, we find that, though the bias voltage of maximal pulse height does increase as temperature is decreased, the actual value is strongly dependent on Rn.

These observations prompted us to investigate one of the main assumptions of the naive model, which is that the electrons, having tunneled to the S electrode, somehow leave the junction area. The main effect of relaxing this assumption is that the quasiparticle population in the S electrode is heated by the tunneled electrons. Because the electron-hole symmetries in the N and the S are different due to the bias voltage, it can be shown that warming up the S quasiparticle population, even in a manner that maintains thermal equilibrium in the S, can lead to tunneling events that heat the N

electrode. In addition, the excess quasiparticle density in the S electrode leads to a higher production rate of recombination phonons; these may interact with the N metal electrons, also heating them. A more macroscopic point of view is that the IV power provided by the voltage bias must be dissipated somewhere; the naive model assumes that this power is removed from the junction in an unspecified way.

We have numerically modeled these microscopic effects and have seen that the N and S electrode temperatures can be significantly elevated by this local power dissipation. This realization has led us to consider designs in which a normal metal layer is placed in contact with the S electrode. Because the gap in this N metal will be zero or at least greatly suppressed relative to that in the S, the hot quasiparticles can be trapped in this region, away from the junction area.

By heat-sinking this N "cooling trap" well, we hope to remove the injected quasiparticles from the junction before they can give rise to any kind of backtunneling. Our power dissipation model makes clear qualitative predictions for behavior of pulse height and decay time that will allow us to see if the cooling traps are effective.

Another important consideration we have begun to investigate is the application of electrothermal feedback to the HET sensor. Electrothermal feedback is a general phenomenon in which electrical and thermal circuits are linked via the power that the electrical current can dissipate in or remove from a device.

We have determined that electrothermal feedback can occur for a voltage-biased HET sensor in which the cooling trap works efficiently. More specifically, we expect that the cooling trap will make the tunneling current effective in removing energy from the N electrode electrons; this reduces the N electrode temperature below that of the substrate.

The interesting practical consequence is that the HET sensor would operate at a colder temperature than the refrigerator; effectively, the HET sensor would act as a second-stage refrigerator for itself. This would reduce the N electrode heat capacity and increase the sensor responsivity, resulting in an increase in pulse height. This could yield "dilution refrigerator-equivalent" performance with the substrate actually cooled using a cheaper and simpler technology such as adiabatic demagnetization or helium-3 refrigeration. In addition, there are two other effects we may be able to exploit:

1. Negative electrothermal feedback acts to suppress tunneling shot noise. Tunneling events cool the N electrode because the hot tunneling electron is replaced by one at the N metal Fermi level. This cooling reduces the junction current on the timescale of the device's decay time constant. Hence, for timescales slower than the thermal time constant, shot noise events are counteracted. The degree of cancellation depends on the relative importance of the electrical cooling

path and the standard thermal cooling path (typically electron-phonon coupling); the more important the electrical cooling, the more effective the shot noise suppression.

2. The tunneling current measures the power leaving the HET sensor via the electrical cooling path; by integrating this power, we can find the amount of energy that leaves by this path. If the electrical cooling path dominates, then all the energy leaves via the electrical path, and the tunneling current measurement provides an independent measurement of the energy deposited in the sensor. This will be very useful in analyzing the effectiveness of various schemes in which the HET sensor is coupled to some large absorber, because it gives an independent measurement of the efficiency of the HET sensor in collecting energy from the large absorber.

Another realization we have made regarding sensor design is the need for a vertical, instead of lateral, structure. Because signal size decreases as the N electrode heat capacity increases, it is advantageous to have as little unneeded normal electrode as possible. By fabricating the junction vertically, the full cross-sectional area of the junction is exposed to the absorber and to the tunnel barrier; that is, the N electrode is 100% active. In addition, the distance between the trapping region and the tunneling barrier is only the film thickness (order of 1 μm), reducing the importance of loss mechanisms such as phonon emission.

With these different issues in mind, we have started designing the mask for a large-area phonon absorber to be deposited on a dielectric crystal. Our initial estimates indicate that such a detector, using many HET sensors in parallel and coupled to large Al phonon absorbers, promises a resolution that is competitive with estimates for other technologies.[2] We recently extended this work to include our more sophisticated model for HET sensor operation.

**Device Fabrication and Test Results**: We fabricated devices using thermal evaporation and sputtering through shadow masks. Since no etching steps are involved, device production is extremely quick and flexible, both in terms of geometric design and materials choice.

Traditionally, shadow mask tunnel junctions have been produced with a "lateral" design philosophy: one electrode is deposited, a tunnel barrier is formed, a counterelectrode is deposited over the edge of the base electrode, and an absorber is deposited at another edge of the counterelectrode. Our first attempts (the SANIS mask) at HET sensor fabrication used designs of this kind. While we were able to achieve 100 eV full-width half-maximum resolution with these devices, we also concluded that the lateral structure was problematic because the N electrode is very large and the junction is formed over the edge of the S electrode.

To ameliorate the situation, we fabricated vertical structures. A base electrode (and possibly an Al seed layer) is deposited and oxidized. A coun-

terelectrode is deposited on top of the barrier. To avoid the edges of the lower film, the counterelectrode has a smaller area than the base electrode. A silicon oxide layer is deposited and patterned via a liftoff process, and a wiring layer is deposited on top of this insulating layer. In order to simulate the fully vertical structure we would like to make, a large Al base layer is deposited first to simulate a quasiparticle diffusing film or superconducting crystal. The tunnel junction is fabricated on this film with the N electrode at the bottom. At present, we use Ag for the N electrode.

Both LLNL and UCB personnel fabricate devices in the facilities available at LLNL, primarily the deposition systems maintained by the Labov group. We successfully produced high-quality junctions (low temperature leakage resistances are typically 1,000 to 10,000 times the normal resistance) using this process. We test these devices by absorption of 5.89 keV X-rays in the N electrode.

Using the variation in rise time, we are able to distinguish events that occur under the active junction area from those on the periphery of the Ag film. This rise time difference is a measure of the diffusion time in the Ag electrode. We also observe a pulse height deficit, indicating an energy loss process (most probably by phonon emission) that acts on the timescale of diffusion time; the value of the deficit gives a measure of the electron-phonon coupling in the Ag film. Measurement of these parameters is extremely useful because they define the optimal sensor architecture. These results were presented at the Applied Superconductivity Conference (ASC).[3]

A problem we discovered with the above structure is that the yield is only about 50%. We studied this problem by fabricating devices in which the Ag electrode is as large as the underlying Al film. We found that the yield for such devices is 100%. Our explanation is that the Al seed layer does not adhere well to the Ag, i.e., the Al atoms are very mobile on the Ag.

When the Ag electrode is small, it is easy for the Al to diffuse off the Ag and stick to the Al underlayer. With the large Ag electrode, there is no Al nearby, so the Al seed layer has enough time to adhere to the Ag. This is corroborated by our observation that the photoresist used in the liftoff process also does not stick well when Ag is used as the counterelectrode. While the large Ag layer solves the yield problem, its extra heat capacity is unacceptable. We are beginning to investigate the use of a different N metal, a switch that is easy to make with our shadow mask fabrication technique.

While the device presented at ASC was useful for measuring materials parameters of Ag, the position dependence is undesirable for a practical detector. Therefore, we fabricated a device (NPT2) in which the large Al base layer is used as the S electrode and is immediately oxidized. A small Ag layer is deposited on top of this; electrical contact is made by an Al film through a hole in the SiO insulation layer.

Because the full area of the Ag is active junction, we expected no position dependence, such as was seen in the ASC device. The observed spectra, in fact, display a number of different peaks and bands, suggesting that the Al wiring layer is introducing a position dependence because it is not in contact with the whole Ag film.

The sloping edges of the Ag may also have an effect. We do not yet have a complete model for this device; however, there are indications that back-tunneling may be suppressed in this device because of the thick (400 nm), large S electrode: it provides a large volume for tunneled quasiparticles to diffuse into, away from the junction area. The primary evidence is a dip and then increase in decay time with bias voltage. This agrees with our microscopic model when electrical cooling is effective. Furthermore, this observation is clearly different from similar measurements in previous junctions that obviously suffered from self-heating due to power dissipation; in such devices, the decay time decreased as the bias was increased.

Another aspect of the work with the vertical structure junctions has been the study of proximitization of the N electrode by Al films. In all the above devices, the Ag displayed superconductivity due to proximitization by the Al. By applying a small magnetic field to exceed the critical field of the proximitized Ag, we could drive the silver normal and study the devices as HET sensors. We varied the film thicknesses to determine how this proximitization depends on the Ag and Al film thicknesses.

We find that the degree of proximitization is strongly dependent on the Al film thickness; for example, the NPT2 device, with a 200 nm Ag electrode and a 500 nm Al wiring layer, displayed a gap of 110 μeV, a critical field of 50 gauss, and a critical temperature of 1 K. We would like to make the Al films as thick as possible to maximize quasiparticle diffusion lengths; this will necessitate thick N electrodes. We plan to investigate different normal metals in the hope that we can find one that is less susceptible to proximitization by Al.

**SFSU Collaboration**: The cryostat at UCB has been extensively used to test HET devices fabricated by Professor Barbara Neuhauser's group at SFSU. Devices are produced there using photolithographic methods. While more difficult to develop, photolithography promises better uniformity and much better dimensional control than shadow mask fabrication; these advantages will be important for fabricating practical, large-scale detectors.

We clearly confirmed self-heating due to power dissipation in the SFSU devices and presented these results at the Low Temperature XXI conference.[4,5] We investigated the dependence of self-heating on the size of the Al S electrode and found none; however, we have only tested very thin (120 nm) Al films and expect improvement with thicker films.

We also studied the variation of the leakage resistance on barrier thickness and geometry; we find that junction quality scales with area rather than perimeter, and that if there is any dependence on barrier thickness, it is that

junction quality improves as barrier thickness is decreased. To reduce self-heating effects in the SFSU devices, we are fabricating devices with both thicker Al S electrodes and extreme aspect ratios. We expect these variations to improve diffusion of tunneled quasiparticles away from the junction area and thereby promote cooling as observed with NPT2.

**Summary**: We have made significant progress on HET sensor development in our understanding of sensor design issues and by fabricating test devices. In particular, this work has greatly benefited from the collaborative efforts of the two groups. Dr. Frank's experience with SQUID instrumentation has benefited members of both groups. Without this experience, it would certainly have taken much longer for the UCB graduate student funded by this grant to bring the UCB test facility to full operation.

Exchanges on theoretical issues between Dr. Mears, Dr. Josef Jochum of UCB, and Mr. Golwala have greatly clarified and extended our model of the HET sensor. The combined efforts of Harrie Netel of LLNL, Dr. Jochum, and Dr. Mears have yielded the interesting devices whose results are discussed above. Finally, our experience with the devices produced at LLNL has strongly influenced the development path of SFSU fabrication.

## References


1. Frank, M. *et al.*, "High-Resolution X-Ray Detectors with High-Speed SQUID Readout of Superconducting Tunnel Junctions," *Nucl. Instr. and Meth.* **A370**, 41 (1996).
2. Sadoulet, S., "Comparison Between Phonon Detection Schemes," *Nucl. Instr. and Meth.* **A370** (1996).
3. Netel, H., *et al.*, "Proximity Effect and Hot Electron Diffusion in $Ag/Al_2O_3/Cu$ Tunnel Junctions," Proceedings of the Applied Superconductivity Conference, Pittsburgh, PA, August 1996.
4. Castle, J. P., *et al.*, "Preparation and Characterization of $Al/Al_2O_3/Cu$ SIN Tunnel Junctions Microfabricated with a Full Wafer Process," Proceedings of the Low Temperature XXI Conference, Prague, Czech Republic, August 1996.
5. Cunningham, M. F., *et al.*, "Investigation of Quasiparticle Diffusion away from the Tunneling Regions of SIN X-Ray Sensors," Proceedings of the Low Temperature XXI Conference, Prague, Czech Republic, August 1996.

# Three-Dimensional Modeling of Regional Broadband Waveforms (GS96-04)

Principal Investigators: Barbara Romanowicz and Douglas Dreger (UC Berkeley)

LLNL Collaborator: Shawn Larsen

Student: Mike Antolik (UC Berkeley)

## Abstract

*During FY 1995–1996, we investigated the effects of lateral heterogeneity on broadband waveforms along several source-receiver paths using a two-dimensional (2D) fourth-order finite difference code. Results of modeling across the San Joaquin Valley indicate that broadband waveforms can be well explained by a simple model with a Moho dip of approximately 5° toward the east. Waveforms recorded at station CMB in the central Sierra Nevada foothills from sources in the central Coast Ranges are also controlled by a velocity increase in the mid-crust, probably representing termination of the Franciscan basement against the Sierran basement somewhere beneath the Great Valley. Major body-wave reflections as well as the surface wave dispersion can be well matched to frequencies of 1 Hz using this model. Farther north, however, wave propagation is much more affected by three-dimensional (3D) structure, as paths from the northern Coast Ranges to the Sierra Nevada show abnormally long surface wave durations, possibly due to refraction from the edge of the Sacramento Valley or from the volcanic intrusion of the Sierra Buttes.*

## Objectives

The goal of this project is to develop a regional three-dimensional crustal and upper mantle velocity model for central and northern California, which can describe propagation effects on waveforms recorded by the 10-station broadband Berkeley Digital Seismographic Network (BDSN) to frequencies up to 1 Hz. Currently, simple laterally homogeneous models are routinely used at UC Berkeley to determine locations and source parameters of earthquakes throughout the region. However, several recent studies have shown a large contribution of basin structures and lateral heterogeneity to broadband waveforms.[1,2]

Many of the recent tomographic studies being conducted in the region yield information on the P-wave velocity structure and only for relatively high frequency waves. This study utilizes the entire broadband wavefield and yields important constraints on the shear velocity structure. The final three-dimensional model will be used to refine the accuracy of source parameter estimation and to identify areas of potential ground motion amplification in large earthquakes.

## Progress

During this fiscal year, we collected broadband data from the BDSN from several recent M4 or larger events occurring in central and northern California. The seismograms from these events were modeled using a 2D finite difference (FD) scheme, because the 3D elastic code developed at LLNL was not ready for use at the time this project was initiated.

During the development of this work, however, we found that 2D modeling made sense in that it allowed the number of variable parameters to be kept low (thus reducing the computational demand), and it helped to gain insight into which features of the data can be explained by 2D structure and which other features require further 3D modeling. This point is important because the goal of the project is not simply to create a 3D model and perform the calculations, but also to find a 3D model that also fits the recorded data.

We investigated structure along several profiles where 1D velocity models do not explain the observed features of the waveforms. One such example (Fig. 1, top) shows transverse component displacement records from BDSN station CMB for the January 16, 1993, earthquake near Gilroy, California (M5.3). The path to CMB crosses the central Coast Ranges and the San Joaquin Valley at an approximate right angle.

We constructed a hybrid 2D model for this path by combining two regional 1D models used at UC Berkeley for routine moment tensor estimation.[3] The cross section for this path requires a generally increasing crustal thickness from west to east as well as increasing shear wave velocities in the mid-crust.

The absence of a head wave on the initial shear wave arrival (SmS reflection) requires an eastward dipping Moho throughout the model or a gradient increase in velocity from lower crust to upper mantle (Fig. 1, bottom). We include the sharp Moho boundary in this model because independent generalized ray modeling indicates the presence of such a sharp boundary under both the Coast Ranges and the Sierra Nevada. The increase in S-wave velocity from west to east in the mid-crustal layer is required to explain the absence of large amplitude crustal reflections in the data. However, the exact nature of this boundary cannot be determined from data recorded solely at CMB.

The addition of lower velocity layers within the Great Valley is necessary in order to match the observed surface wave dispersion. The final model obtains a very good match to both the body wave phases and surface wave train. Good fits are also obtained for the radial and transverse components (not shown).

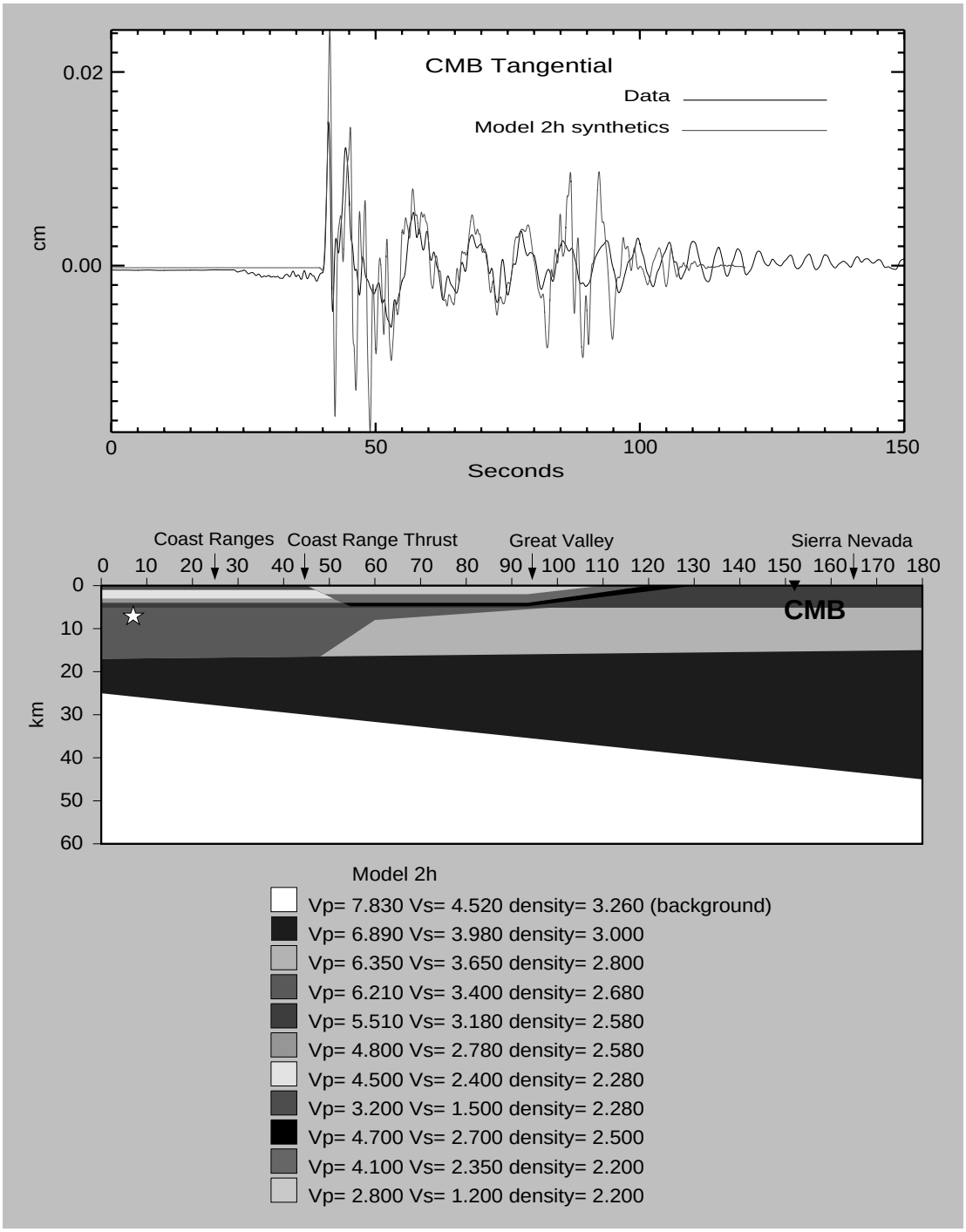


*Figure 1. (Top panel) Tangential component data at station CMB from an earthquake near Gilroy, CA, is compared to FD synthetics constructed from the 2D model shown in the bottom panel. (Bottom Panel) Best fitting 2D model for the path from Gilroy, CA, to station CMB. Hypocenter location is indicated by the star. See text for details.*

Additional modeling has been completed for paths across the Sacramento Valley and down the Coast Ranges for an earthquake near Healdsburg, California. These results show that a similar 2D model does not adequately explain features of wave propagation at station ORV (northern Sierra foothills). Only at long periods (20 sec) is an adequate fit obtained. This indicates that regional attenuation is much higher in the northern Coast Ranges, possibly due to recent magmatic intrusions associated with passage of the Mendocino Triple Junction and the presence of the Geysers geothermal field. Anomalously long surface wave durations are also observed along this path. In addition, a crustal low velocity anomaly, previously identified from teleseismic travel time delays, has been identified from regional waveform modeling near the Geysers region.

Concurrent with the waveform modeling, we have also assembled all available information on subsurface geology in the region. Results from modeling of magnetic and gravity data,[4] as well as recent reflection profiles from the BASIX seismic imaging experiment,[5] have been collected. Along with information obtained from the 2D profiles, these data are being used to construct the initial model of 3D structure in central California.

## References


1. Somerville, P., and J. Yoshimura, "The Influence of Critical Moho Reflections on Strong Ground Motions Recorded in San Francisco and Oakland during the 1989 Loma Prieta Earthquake," *Geophys. Res. Lett.* **17**, 1203 (1990).

2. Amirbekian, R., *Effects of Seismic Wave Scattering in Strong Motion Seismology*, Ph.D. thesis, University of California, Berkeley, 180 pp. (1995).

3. Dreger, D. S., and B. Romanowicz, "Source Characteristics of Events in the San Francisco Bay Region," USGS Open-File Report 94-176, 301 (1994).

4. Jachens, R. C., A. Griscom, and C. W. Roberts, "Regional Extent of Great Valley Basement West of the Great Valley, California: Implications for Extensive Tectonic Wedging in the California Coast Ranges," *J. Geophys. Res.* **100**, 12,769 (1995).

5. Holbrook, W. S., T. M. Brocher, U. S. ten Brink, and J. A. Hole, "Crustal Structure beneath the San Francisco Bay Block and the Central California Continental Margin," submitted to *J. Geophys. Res*. (1995).

# Empirical Determination of a Soil Production Law using Topographic Data, Measurements of Soil Depth, and Cosmogenic Nuclides (GS96-05)

Principal Investigators: William E. Dietrich and Kunihiko Nishiizumi (UC Berkeley)

LLNL Collaborator: Robert C. Finkel

Student: Arjun M. Heimsath (UC Berkeley)

## Abstract

*We measured concentrations of* in situ*-produced cosmogenic $^{26}Al$ and $^{10}Be$ nuclides in bedrock samples taken from under different soil depths on divergent ridges. During FY 1995–1996, we completed sampling and sample processing from two of our field sites with similar hillslope morphology, but markedly different hillslope processes—the Oregon Coast Range near Coos Bay and the coastal hills near San Francisco (Tennessee Valley).*

*Measurements were made to determine the long-term soil production rate of each sample. Under steady-state conditions, this defines the rate at which bedrock disintegrates into erodible material as a function of soil depth. We also intensely measured the divergence of slope and soil depth at our California site to test the theoretical result that soil thickness varies with hillslope curvature.*

*Results from both methods from this site offer the first empirical evidence for the hypothesized inverse exponential soil production law. We found that soil production rates from both field sites decrease exponentially with increasing soil depths, while soil production rates for exposed bedrock at the Oregon site suggest different processes are dominant under shallow soil depths. These data offer the first quantitative understanding of a fundamental geomorphic assumption.*

## Objectives

Our goal was to develop two independent field-based methods to test, for the first time, the validity of the hypothesized depth dependency in the soil production rate. For over 100 years it has been assumed that the rate of disintegration of bedrock into erodible soil depends on the thickness of the overlying soil mantle. This assumption underlies the belief that there are weathering-limited and transport-limited landscapes, which is not supported by any field data. It also identifies a key linkage between climate, topography, geology, and erosion.

Recent analysis suggests that on divergent hillslopes (ridges), where soil production is in balance with soil removal by diffusive processes, the product of the diffusion coefficient and hillslope curvature equals the soil production rate.[1] We hypothesize that, if soil production rate depends on soil thickness, then soil thickness should vary with topographic curvature. If this

is found to be the case, we can then fully quantify the soil production law if the diffusion coefficient is known for the study site.

We also sought to independently determine the soil production law by measuring *in situ*-produced cosmogenic $^{10}$Be and $^{26}$Al in quartz extracted from bedrock under different soil depths. This approach is analogous to erosion rate estimates previously done on exposed bedrock using cosmogenic nuclides, but we sampled target rock beneath the surface, at the distinct soil-bedrock interface, as well as bedrock exposed at the surface of the landscape.

## Progress

**Geomorphology**. We surveyed four divergent ridges in Tennessee Valley, California, at 1–3 m resolution and measured soil depth at 400 locations. We calculated hillslope curvature for each location and found 80 stable locations where curvature does not vary with grid size. Figure 1 shows the observed relationship between soil production and local soil depth.[2] Soil production is calculated by multiplying the regional diffusivity and bulk of the density ratio. We find a clear inverse relationship between inferred soil production rate and soil depth, although the scatter is considerable. This scatter is to be expected even for steady-state soil thickness because of

- fine-scale heterogeneity (fracture density, bedding, etc.) in the resistance of the underlying bedrock to soil production;
- fine-scale curvature variation due to the same mechanism; and
- short-term variation in biologic activity (which will affect local soil depth more than curvature) such as gopher burrowing.

Using various topographic grid sizes to determine hillslope curvature, we found that curvature was normally distributed across all grid sizes and that the larger grid sizes decreased variance in curvature. Despite the variance, these data seem to support a simple exponential production function rather than one with a maximum at some non-zero depth for the northern California field site.

We also surveyed and measured soil depth from the divergent areas from our Coos Bay, Oregon, study site and found the hillslope processes and steep slopes complicate the relationship between soil depth and hillslope curvature. Both sites are underlain by greywacke and were used to fully develop our methodology.

**Geochemistry**. We completed collecting and processing bedrock samples from two of our project areas and successfully measured $^{10}$Be and $^{26}$Al concentrations to calculate long-term soil production rates assuming steady-state conditions. We processed 22 samples from our Marin County, California, site and 30 samples from our Oregon Coast Range site. Results from some samples were eliminated because of divergence from the expected steady-state value for the ratio $^{26}$Al/$^{10}$Be; others were rejected because of

sampling error. The remaining data for Tennessee Valley are plotted (Fig. 1) with soil production rates calculated from curvature measurements to show the strong correlation with the geomorphologically derived soil production function. The Oregon results are shown in Figure 2.

The California samples show a clear inverse exponential relationship between soil production and soil depth. The Oregon samples show a clear relationship between soil production and soil depth, although the deeper samples could have been influenced by shallow landsliding.

If shallow landslides tend to remove the upper layer of the underlying, weathered bedrock, then our soil production function from Oregon may still apply. The Oregon results seem to support a soil production function with a maximum at a depth of about 20–30 cm. Results from both sites fit well with previously estimated long-term erosion rates.[1,3]

We have used our cosmogenic nuclide-based method, which depends on the high analytical sensitivity of the LLNL Center for Accelerator Mass Spectrometry (CAMS), to provide both an evaluation of the procedure and some insights about the assumption of steady-state soil production. Our measurements of $^{10}$Be and $^{26}$Al concentrations, with their different half-lives, allowed us to directly assess the assumption of steady-state soil thickness, because the ratio of the nuclide concentrations will differ from the steady-state case if the soil mantle thickness is not steady through time.

The $^{26}$Al/$^{10}$Be ratios from both sites suggest that the local soil depths have been in steady state. To independently determine local diffusivity, we intend to combine measurement of soil production rate through cosmogenic nuclide analysis on ridge crests, where bedrock typically is exposed, with our measurements of hillslope curvature.

## References

1. Dietrich, W. E., R. Reiss, and D. R. Montgomery, "A Process-Based Model for Colluvial Soil Depth and Shallow Landsliding using Digital Elevation Data," *J. Hydrologic Processes* **9**, 383–400 (1995).

2. Heimsath, A. M., W. E. Dietrich, K. Nishiizumi, and R. C. Finkel, "Soil Production and Landscape Equilibrium: Hillslope Analysis using Cosmogenic Nuclides in Northern California and Coastal Oregon," *EOS Trans. Am. Geophys. Union. Fall Supplement* **F112** (1996).

3. Reneau, S. L., and W. E. Dietrich, "Erosion Rates in the Southern Oregon Coast Range: Evidence for an Equilibrium between Hillslope Erosion and Sediment Yield," *Earth Surface Processes and Landforms* **16**, 307–322 (1991).

*Figure 1. Tennessee Valley, Marin County, California: The soil production function from both field methods, showing an inverse exponential relationship. Dots and triangles with error bars show the nuclide samples, including two different basin average erosion rates from stream sediment measurements from two second order creeks.*

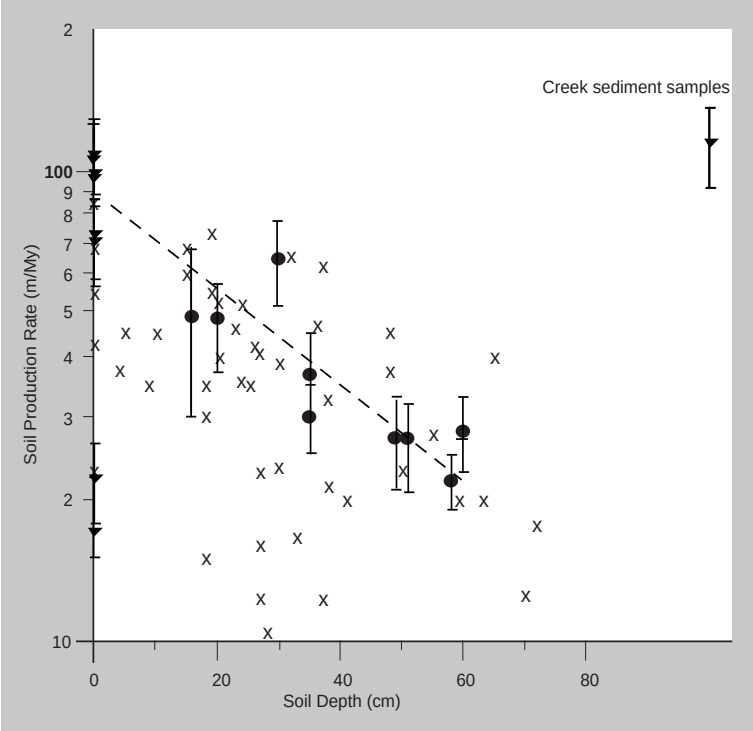


*Figure 2. Coos Bay, Oregon: The soil production function from* in situ*-produced, cosmogenic $^{26}Al$ and $^{10}Be$ measurements made from bedrock sampled under different soil depths.*

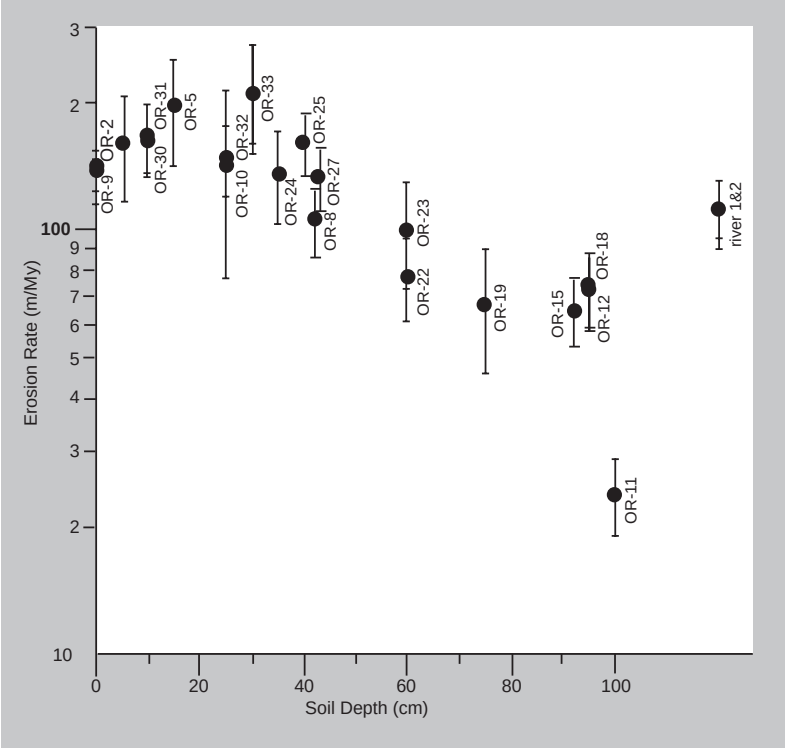

# Crustal Thickening in Southern Tibet: The Renbu-Zedong Thrust (GS96-07)

Principal Investigators: T. Mark Harrison and An Yin (UC Los Angeles)
LLNL Collaborator: F. J. Ryerson

## Abstract

*Near Lang Xian, southeastern Tibet, the Renbu-Zedong Thrust (RZT) places epidote-amphibolite facies Tethyan metasediments atop the Gangdese batholith. U-Pb zircon results indicate that this portion of the batholith was emplaced between 100–70 Ma, with most intrusions formed at ~85 Ma. K-feldspar and biotite $^{40}Ar/^{39}Ar$ results from a NW-SE transect through footwall granitoids reveal disturbances to their isotopic systems immediately beneath the RZT. This effect systematically decreases with increasing distance from the RZT.*

*Inverse modeling of the K-feldspar $^{40}Ar/^{39}Ar$ results yields thermal history data that indicate that the RZT was active in the interval 19–11 Ma. In conjunction with a numerical thermal model, the results constrain the minimum average slip rate and displacement along the ramp between 19–15 Ma to 2 mm/yr and 12 km, respectively, but likely higher.*

*A cooling episode recorded by all the K-feldspar age spectra beginning at ~10 Ma may reflect either denudation following regional uplift caused by displacement along a ramp on the Main Himalayan Thrust or topographic collapse following cessation of RZT thrusting. RZT activity between 19–11 Ma places this backthrust out of the generally southward progression of thrusting, but occupies a period that appears to otherwise be unrepresented by contractional motion in the Himalaya.*

## Objectives

The Indo-Asian collision is our best natural laboratory in which to understand the interplay between the various factors (e.g., lithospheric thickening, injection of the ductile lower crust, temperature increases or density decreases in the lithosphere and underlying mantle) that control surface elevation. Although central to understanding the geologic evolution of the collision zone, the history of crustal scale thrusting in southern Tibet and the Himalaya is incompletely known. Geologic investigations conducted in southern Tibet by UCLA and LLNL personnel led to the recognition of two previously undocumented thrust systems: the north-dipping Gangdese Thrust (GT) and the younger south-dipping Renbu-Zedong Thrust (RZT).

The Gangdese Thrust is known to have been active near Zedong in southeastern Tibet between 27 and 23 Ma. The younger RZT is, in most places, thrust over the trace of the GT, obscuring its exposure, and the development of both systems has obscured the suture between India and Asia. Although we now have reasonably good control on the timing of motion on the GT, constraints on RZT motion are poor. To improve our understanding

of this important structure, we undertook an investigation to determine the thermochronologic and thermobarometric evolution of the upper and lower plates of the RZT in order to constrain the timing and magnitude of slip on this feature.

## Progress

Cretaceous granitoids of the Gangdese batholith, southeastern Tibet, were overthrust by upper greenschist to epidote-amphibolite facies Tethyan rocks derived from the Indian shelf along the north-directed (~30° dip) Renbu-Zedong Thrust. Thermochronological results obtained from a NE-SW transect near Lian Xian show evidence of thermal effects related to thrusting.[1] Granitoids immediately beneath the RZT exhibit considerable recrystallization to greenschist facies assemblages. Biotite and K-feldspar $^{40}Ar/^{39}Ar$ ages measured along the traverse into the footwall increase systematically away from the RZT.

The timing of initial upward displacement of the RZT hanging wall is constrained to have occurred at ~18 Ma from the hornblende ages and the two K-feldspar samples closest to the fault. K-feldspars up to 15 km from the thrust yield 9–12 Ma ages for the initial ~20% of $^{39}Ar$ release. Distal samples yield $^{40}Ar/^{39}Ar$ ages nearly as old as the 70–110 Ma ion microprobe $^{206}Pb^{*}/^{238}U$ ages determined for coexisting zircons.

We have integrated our thermal history results with numerical heat-flow models and found that while reheating to 320–280°C at shallow (~7 km) levels due to rapid (>15 mm/yr) slip along the RZT at ~10 Ma is capable of explaining the initial portion of the K-feldspar age spectra, a prior common thermal history experienced by all samples cannot satisfactorily account for all the $^{40}Ar/^{39}Ar$ results. Instead, we find our thermal history constraints to be more completely explained by a numerical model in which

1. rocks currently at the surface originated from different depths;
2. footwall samples in close proximity to the RZT experienced fault drag from 19–15 Ma; and
3. post-thrusting denudation of the region involving localized tilting occurred at ~10 Ma.

The minimum average slip rate and displacement along the ramp during this period are 2 mm/yr and 12 km, respectively, but are likely to have been greater. The cooling episode recorded in all the K-feldspar age spectra beginning at ~10 Ma may reflect either denudation following regional uplift due to displacement along the ramp of the Main Himalayan Thrust[2] or topographic collapse following cessation of RZT thrusting.[3]

Our inference that the RZT was active in the interval 1811 Ma places this feature out-of-sequence in an otherwise general pattern of propagation of south-directed thrusts toward the foreland. However, it appears to fill a gap in time that is not represented by current estimates of the timing of the other recognized thrust faults.

## References

1. Quidelleur, X., M. Grove, O. M. Lovera, T. M. Harrison, A. Yin, and F. J. Ryerson, "The Thermal Evolution and Slip History of the Renbu-Zedong Thrust, Southeastern Tibet," *J. Geophys. Res.* (in press).

2. Hauck, M. L., K. D. Nelson, *et al.*, "Ramping of the Main Himalayan Thrust and Development of the South Tibetan Detachment and Kangmar Basement Dome: INDEPTH Reflection Profiles in Southern Tibet," *Geol. Soc. Am. Abs. w. Progs.* **27**, A336 (1995).

3. Yin, A., T. M. Harrison, F. J. Ryerson, W. Chen, W. S. F. Kidd, and P. Copeland, "Tertiary Structural Evolution of the Gangdese Thrust: Southeastern Tibet," *J. Geophys. Res.* **99,** 18,175 (1994).

# Structural and Cosmogenic Investigation of Quaternary Slip Rates along the Left-Slip Altyn Tagh Fault, Central Asia (GS96-08)

Principal Investigators: An Yin and T. Mark Harrison (UC Los Angeles)

LLNL Collaborators: Frederick J. Ryerson, Marc W. Caffee, and Robert C. Finkel

## Abstract

*We conducted an integrated field investigation and cosmogenic dating of active thrusts in the southern Nan Shan region of northwestern China. Thrusts in the Nan Shan are kinematically linked with the left-slip Altyn Tagh Fault; thus, their ages are indicative of the slip history of the Altyn Tagh Fault. The initiation age of the thrust system in the study area is constrained by magnetostratigraphic analysis and sedimentological studies, which suggest that a dramatic increase in sedimentation rates and input of conglomerates occurred at about 28.5 Ma.*

*Because the dated strata show growth-faulting relationship (i.e., their dip angles decrease upsection), we interpret the 28.5 Ma age as the minimum initiation age for the thrust system and related Altyn Tagh Fault. Estimates of slip rates along the active frontal thrust were investigated by modeling four topographic profiles using diffusion models. This analysis indicates that the active frontal thrust moves at rates no more than 5 mm/yr.*

*Because the studied thrust system is one of four or five active thrusts in the Nan Shan, which are all linked with the Altyn Tagh Fault, our result implies that the total shortening rate across the Nan Shan is likely to be 20–25 mm/year. This rate would be the slip rate along the Altyn Tagh Fault as it terminates at the Nan Shan thrust belt.*

## Objectives

The inability of plate tectonics to describe the kinematics of continental deformation has motivated the development in recent years of a variety of mechanical models, which range from treating the continents as a continuous, ductile medium to a collage of rigid blocks bounded by a few large faults. These drastically different views on how continents deform are best illustrated by the two well known end-member views for the Indo-Asian collision: the distributed shortening and lateral extrusion hypotheses. The first emphasizes the role of thrusting in absorbing the N-S shortening, whereas the second stresses the role of eastward translation of continental blocks in accommodating the N-S convergence.

Debate on the nature of the Indo-Asian collision and its potential in relating the simple oceanic-plate kinematics to the complex dynamics of continental deformation have led us to focus on arguably the largest active intracontinental strike-slip fault system on Earth—the Altyn Tagh Fault, northern Tibet/western China. This fault is a key feature in either the lateral

extrusion or crustal shortening hypotheses. In addition, it has played a critical role in the two first-order issues of continental dynamics: the evolution of the Tibetan Plateau and continental subduction in the western Kunlun. Because of its central role in resolving these fundamental problems, we have conducted an integrated investigation to constrain its slip rate and magnitude of slip.

The Nan Shan thrust belt lies along the northern edge of the Tibetan Plateau where the Altyn Tagh Fault terminates. Its age and magnitude of shortening are key to understanding when and how the Altyn Tagh Fault, as well as the Tibetan Plateau, have been developed in response to the Indo-Asian collision in the Late Cenozoic. To address the questions of when the Altyn Tagh Fault initiated and at what rate it has moved, we conducted detailed stratigraphic, structural, and geomorphological investigations in the Subei area, Gansu Province of northwestern China.

## Progress

Geologic mapping was conducted at a scale of 1:100,000. Samples were collected for both cosmogenic dating and sedimentological studies. The first-order structure in the area is the Altyn Tagh Fault, which makes a sharp turn from an ENE strike to an E-W strike. The change in strike correlates with a change in fault kinematics from left-slip faulting to N-directed thrusting. The N-directed thrust system consists of two faults. One separates the Upper Precambrian-Lower Paleozoic magmatic-arc sequence (metavolcanics) in its hangingwall from Tertiary sedimentary strata in its footwall.

The second thrust is also N-directed and lies north of the first at a lower structural level. This fault juxtaposes the Tertiary sequence over a Quaternary alluvial sequence. A stratigraphic section was measured within the Tertiary sequence. The stratigraphic data constrain

- facies evolution;
- chronostratigraphy via magnetostratigraphic analysis; and
- the sandstone provenance of the Late Cenozoic sequences.

The facies in the section varied from lacustrine mudstones and interbedded siltstones at the base, grading upward into channelized meandering to braided fluvial systems, which in turn graded upward into channelized and sheet-flow alluvial fan deposits. This stratigraphic succession is interpreted to represent a progradational sequence located in the foreland basin of the propagating thrust belt.

We interpret the change from dominantly lacustrine mudstone deposition to dominantly channelized fluvial deposition as the minimum age of inception of thrusting in the area and initiation of slip on the northern-most strand of the Altyn Tagh Fault.

Other than an unconfirmed Oligo-Miocene age for this section, there is generally a dearth of biostratigraphic information about this area. Furthermore, the lack of any volcanic ash deposits makes it even more difficult to

constrain the geochronology. In order to better constrain the chronostratigraphy, over 400 siltstone and mudstone samples were taken for magnetostratigraphic analyses. These analyses, in conjunction with sedimentological studies, suggest that the southern Nan Shan thrust belt initiated at or prior to 28.5 Ma. This is a minimum age, because the thrusts in the field area may have propagated forward, which means the earlier foreland basins, if they existed, may have been eroded away in the hangingwall of the younger thrust.

As the thrust system in the Subei area links with the Altyn Tagh Fault, it implies that the Altyn Tagh Fault also began at or prior to 28.5 Ma. This age estimate implies that the average slip rate along the Altyn Tagh Fault, assuming its total slip is ~500 km (as indicated by the offset of a late Paleozoic magmatic belt), is no more than 17.5 mm/yr.

Sandstone samples were collected throughout the section in order to determine the temporal variation in composition. These data plot in the magmatic arc field on the Dickinson ternary diagrams. The most striking lithic type is metavolcanic. Based on our mapping, these sediments were most likely derived from Paleozoic basement rocks within the Nan Shan. These data are consistent with the interpretation that the Nan Shan/Qilian Shan was a Paleozoic suture.

The strikingly consistent composition of the sandstones suggests not only that pre-Oligocene(?) thrusting had uplifted and exposed the Paleozoic magmatic arc rocks by the inception deposition, but also that the amount of Cenozoic shortening in the area was not enough to uplift and expose structurally deeper rocks. Late Neogene-Quaternary slip rates along the active thrust were determined in three ways:

1. Our topographic profiles were measured across the active frontal thrust, which cut the prograding alluvial fans. Using existing diffusion models and reasonable assumptions about initial fan and fault geometry, we estimated (with the help of Prof. Ramon Arrowsmith at Arizona State University) that the active frontal thrust in the Subei area moved at a rate of ~5 mm/year.
2. A vertical traverse for apatite fission track samples was conducted within the thrust belt. The mineral separation has been finished, and the samples will be processed in the near future. The analysis of cooling ages based on these samples will provide constraints on the initiation of thrusting in the region. These data, combined with field-based estimates of total crustal shortening in the thrust belt, will be used to calculate total slip rates.
3. We used the $^{14}C$ method to date the ages of offset terraces by the active frontal thrust in the Subei area. The samples were analyzed at LLNL. Unfortunately, the organic materials collected yield essentially zero ages considering the analytical errors involved. We are still looking for the answer to this problem. Meanwhile, mineral

separation for cosmogenic dating is on the way. We expect to analyze these samples in the coming summer.

## References

1. Rumelhart, P. E., A. Yin, F. J. Ryerson, Z. X. Qiang, Z. Qing, and W. X. Feng, "Stratigraphic, Structural, and Geomorphological Constraints on the Evolution of the Nan Shan Thrust Belt, Northern Tibetan Plateau," 11th Himalaya-Karakorum-Tibet Workshop, Flagstaff, Abstract Volume, p. 125 (1996).

# Recurrence, Interaction, and Source Processes of Small Characteristic Earthquakes (GS96-10)

Principal Investigator: Thomas V. McEvilly (UC Berkeley)
LLNL Collaborators: Lawrence Hutchings and William Foxall
Berkeley Collaborator: Robert M. Nadeau

## Abstract

*We have improved constraints on characteristic earthquake models used to estimate conditional probabilities of occurrence in seismic hazard analysis. We have also enhanced understanding of the fundamental earthquake source processes underlying these models by greatly improving the resolution of space, time, and size characteristics of the microearthquake population at Parkfield and by automating statistical and waveform analysis techniques, which make the task of processing the vast number of continuing earthquakes tractable.*

*This work has provided many new and unexpected results, which have proven to be vital in furthering LLNL's capabilities in accurate probabilistic seismic analysis and site-specific ground motion prediction for critical facilities.*

## Objectives

The purpose of our research has been to improve the constraints on characteristic earthquake models that form the basis of current methods of time-dependent seismic hazard analysis, and to improve our understanding of the fundamental earthquake source processes underlying these models.

This was to be done by first developing and applying high resolution waveform analysis techniques to provide relative space, time, and size measurements of unprecedented resolution. This phase was to be followed by characterization of the highly resolved behavior using various techniques, including formulation of new statistical approaches capable of incorporating the detailed systematics manifest in the seismicity as a result of the increased resolution.

This effort has laid the groundwork for the mechanical modeling of a large system of well-defined small characteristic earthquakes recorded on the San Andreas Fault (SAF) at Parkfield.

## Progress

We have successfully developed and tested the automatic procedures for identifying similar repeating earthquakes, for locating these events with a high-precision relative location method, and for doing the descriptive statistics we plan to use to characterize the spatio-temporal behavior of the events. Progress at processing the data using these procedures was temporarily hampered by the unanticipated relocation of our computing facilities

at Lawrence Berkeley Laboratory in February and March, but despite this, we have managed to process a large portion of the data set. Processing is continuing at the accelerated pace made possible by the automation.

Subsequent to submitting the original proposal, we recognized the advantages of developing a more highly resolved size discriminant. Therefore, concurrent with development of the automated procedures discussed above, we also developed a relative moment methodology, which we have also applied to a significant fraction of the seismicity.

The improvement in resolution of our automated methods over routine catalogue determinations is illustrated in a paper submitted to *EOS*.[1] Our automated procedures provide detection and rapid analyses of large numbers of events. The resolution is adequate for discerning space-time-size systematics and for estimating various source parameters previously masked by uncertainties in the routine methods.

For example, estimates of source radius among rupture patches in multiple event-type clusters can be determined, assuming circular rupture, using the average separation distances of events of one type from those of another. In conjunction with seismic moment and recurrence time information, these radii can be used to infer slip per event and stress drop independent of spectra and can be checked against spectral-based analyses or other non-spectral-based results derivable from tectonic moment and slip rates on faults.

Our early analyses have already yielded significant and unexpected results. For example, the variability in fault-specific seismic moment for sequences of characteristic microearthquakes (as measured using the coefficient of variation [COV]—standard deviation divided by the average) was found to be nearly identical to that reported by geologists studying characteristic slip of large events.[2] Since seismic moment, Mo, and average slip, u, can be related[3] by

$$Mo = GuA,$$

the similarity in distributions provides supporting evidence for the existence of characteristic earthquake rupture. Furthermore, in the case of our microearthquake measurements, the COV can be directly related to moment magnitude, Mw.[4] The seismic moment results then indicate that the event size variability for microearthquakes generally corresponds to less than +/-0.1 Mw, typical of characteristic earthquake rupture.

Another unexpected finding has been the relatively elevated stress drops (i.e., over 500 bars) of microearthquakes (inferred using the non-spectral means discussed) when compared to those expected for a constant stress drop model (~3–300 bars). Further support for this finding is found in the recurrence scaling observed in Figure l, where lines of constant stress drop deviate significantly from the best-fit line taken from microearthquakes (lower left) through to large damaging SAF earthquakes (upper right), and from the longer-than-expected recurrence intervals observed for the charac-

teristic microearthquake sequences in general. The resolution obtained from our analyses of the data has helped to strengthen the validity of the recurrence scaling concept illustrated in Figure 1 by providing observations of similar scaling behavior within the microearthquake regime where asperities on a single fault plane and within ~l km of each other exist under relatively homogeneous fault mechanical conditions and tectonic slip rates (Fig. 2).

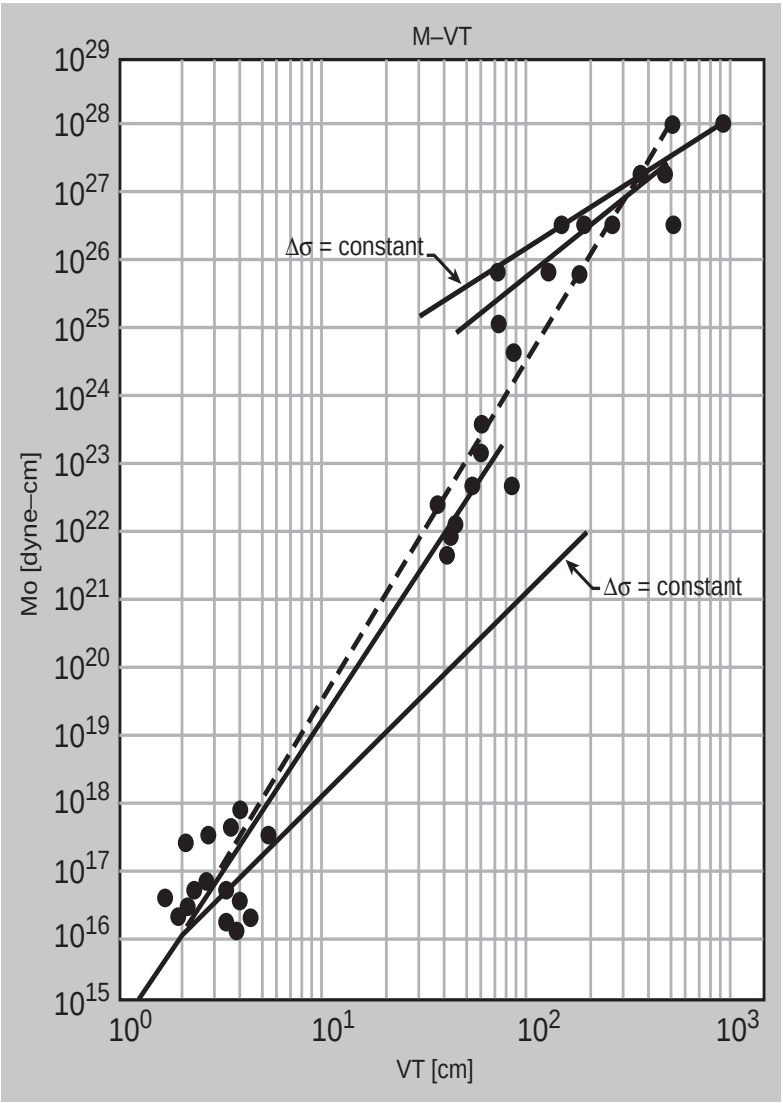


*Figure 1. Sequence average seismic moment verses (average recurrence time) × (inferred sliprate) for characteristic earthquake sequences ranging in size from ~$10^{16}$ dyne-cm to $10^{28}$ dyne-cm.*

*Dashed line shows least square fit to all the data; dark solid lines show separate fits to events of Mo below and above $10^{24}$ dyne-cm. Lines of constant stress drop (light solid lines) are based on a circular crack model for small events and a rectangular crack L-model for large events and show significantly different moveouts than the empirical fits to the data.*

*Parkfield microearthquakes plot to the lower left. Events between $10^{21}$ and $10^{24}$ are taken from Ellsworth,[5] and events above $10^{24}$ are taken from the Working Group on California Earthquake Probabilities.[6]*

*The empirical straight-line fit to the data suggests a moment-recurrence scaling model of $Mo=K(VT)^q$ where q ~5 for small events and ~3 for large events.*

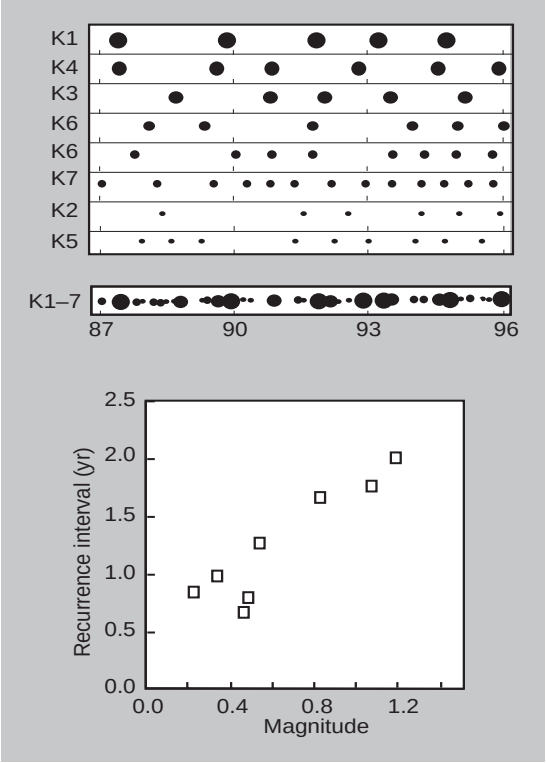


*Figure 2. (Top) Occurrence plot for eight closely spaced characteristic sequences (there are two in K6). Timeline K1-7 is a superimposition of the individual characteristic sequence timelines and shows the apparently chaotic recurrence pattern of the Kester group before the application of high resolution techniques, which resolve the events into their component sequences.*

*Symbol size is proportional to magnitude (in the range 0.2 to 1.4). There likely were undetected events in the sequences; therefore, the regularity could be greater than shown.*

*(Bottom) Sequence median recurrence interval vs. magnitude for the eight characteristic sequences. Repeat times for events in this magnitude range could be as short as a few months.*

## References


1. Nadeau, R. M., and T. V. McEvilly, "An Analysis of the Feasibility of Microearthquake Hypocenters as Drilling Targets," *EOS Trans. Am. Geophys. Union*, submitted (1996).
2. Hecker, S., and D. P. Schwartz, "The Characteristic Earthquake Revisited: Assessing the Geologic Record of Event-Size Variability on Faults," *EOS Trans. Am. Geophys. Union Suppl.* **76** (46), F361 (1995).
3. Aki, K., and P. G. Richards, *Quantitative Seismology Theory and Methods*, Vol. 1, W.H. Freeman and Company, New York, 557 pp., (1980).
4. Hanks, T. C., and H. Kanamori, "A Moment Magnitude Scale," *J. Geophys. Res.* **84**, 2,348 (1979).
5. Ellsworth, W. L., "Characteristic Earthquakes and Long-Term Earthquake Forecasts: Implications of Central California Seismicity," in *Urban Disaster Mitigation: The Role of Science and Technology*, F. Y. Cheng and M. S. Sheu, eds., Elsevier Science Ltd., in press (1995).
6. Working Group on California Earthquake Probabilities, *Probabilities of Large Earthquakes in the San Francisco Bay Region*, California, U.S. Geological Survey, Circular 1053 (1990).

# Trace Metal Concentrations in Otoliths: Salmon Differentiation in San Francisco Bay and Delta (GS96-11)

Principal Investigator: B. Lynn Ingram (UC Berkeley)
LLNL Collaborator: Ian Hutcheon

## Abstract

*In California, the Sacramento winter-run salmon population is critically low and listed as endangered due to upstream storage, water diversion, introduction of new fish species (such as the striped bass), and entrainment in delta pumps, which causes mortality of juvenile salmon.*

*Chinook salmon (or king salmon) mature in the Pacific Ocean and migrate through the San Francisco Bay estuary to spawn in the streambed gravels of the Sacramento-San Joaquin river system. There are four races (or runs) designated by the season in which the salmon enter fresh water to spawn:*

1. *a fall run that enters fresh water during July through November;*
2. *a late fall run that moves upstream during October through February;*
3. *a winter run that moves upstream during January through June; and*
4. *a spring run in the Sacramento River that moves upstream during March through July.*

*After hatching, young salmon (or smolt) move downstream and through the Delta and estuary to the ocean.*

## Objectives

To understand the geographic distribution of salmon in the river systems and to offset the declines of salmon populations, it is critical to distinguish between the various races of salmon that populate the different rivers. For example, in order to decrease the impact of delta pump mortality on endangered salmon, pumps are turned off after a certain number of individuals of the endangered salmon are taken into the pumps.

Presently, in the San Francisco Bay Delta, the various races of salmon are primarily distinguished on size or timing, both of which may be inaccurate due to overlaps in size and timing of out-migration of the different races of salmon.

We report results of a pilot study testing a new technique for evaluating the origin of juvenile salmon stocks by examining the Sr isotopic compositions and trace elemental concentrations of river waters, and variations along sequential growth layers of salmon otoliths (aragonitic ear bones). The approach used in this study relies on the natural geographic variation in trace elements and isotopic concentrations to determine the origin of salmon stock that migrate through the San Francisco Bay.

To use strontium isotopes and trace elements in tracing fish origin and migration, several conditions must be met:

1. freshwater sources in different drainages and tributaries have distinct $^{87}Sr/^{86}Sr$ ratios and trace elements;
2. the $^{87}Sr/^{86}Sr$ ratios and trace elements incorporated into the fish otoliths reflect the freshwater source; and
3. the $^{87}Sr/^{86}Sr$ ratios and trace elements remain fixed in the otolith.

Otoliths are composed of the three bodies present in the auditory systems of bony fish. The largest of these, the sagittae, are composed of aragonite (calcium carbonate). Morphologically they are elliptical, laterally compressed, and range in size from millimeters to centimeters. The center of a sagitta consists of the nucleus, which represents the earliest phase of growth, and concentric rings deposited around the nucleus in daily or seasonal increments. Strontium substitutes for calcium due to similar charge and ionic radius in the aragonitic otoliths. Strontium isotopic compositions and trace elemental concentrations in the otoliths should reflect those in the ambient water in which the fish grew.

## Progress

River waters were sampled from the Sacramento, Feather, San Joaquin, Tuolumne, Merced, and Stanislaus rivers (Fig. 1). Otoliths of adult fish from both hatcheries and the natural population from these tributaries were also sampled by the California Department of Fish and Game.

Trace element abundances of salmon otoliths and scales were measured with the ion microprobe in the Isotope Sciences Division at Lawrence Livermore National Laboratory (LLNL), which has the capability for automated traverses across otolith sections. The ion probe is also equipped with a resistive anode encoder detector system, which can be used for quantitative elemental mapping at part-per-million concentration levels.

Microprobe analyses of the abundances of up to 45 major, minor, and trace elements can be performed on C-coated, polished, otolith sections using standard energy-filtering techniques.

Strontium isotopic analyses will be made at the Center of Isotope Geochemistry at UC Berkeley. For Sr isotopic analyses, the sample is dissolved, evaporated under a heat lamp, and redissolved in 1.5 N HC1. One aliquot of the carbonate sample is used to determine Sr and Rb concentrations by isotope dilution using a spike solution of $^{84}Sr$ and $^{85}Rb$. Another aliquot is passed through an ion-exchange column to separate purified Sr for isotopic analysis.

Sr isotope measurements were made at the UC Berkeley Center for Isotope Geochemistry. An essential part of this study is the high-precision isotopic ratio measurements of Sr, which are accomplished using a multicollector mass spectrometer with peak-switching by magnetic scanning. The $\Delta^{87}Sr$ notation is used: $\Delta^{87}Sr = \{(^{87}Sr/^{86}Sr_{sample})\ ^{87}Sr/^{86}Sr_{standard})\} \times 100{,}000$. The EN-1 seawater standard (a modern *Tridacna* shell from the Eniwetok Lagoon), prepared by the U.S. Geological Survey, has an $^{87}Sr/^{86}Sr$ ratio of 0.709198. Samples requiring high precision are normally measured twice, with reproducibility of $^{87}Sr/^{86}Sr$ ratio, or $\Delta^{87}Sr$ value,

as determined from measurements of standards. The statistically determined uncertainties vary between $\Delta^{87}$Sr.

Preliminary measurements of river water chemistry (using ICP-MS) suggest that trace elemental concentrations (such as Rb, Sr, Ba, Mg, Zn, Pb, Al, Fe, Cu, and Mn) vary naturally in California rivers because of variations in bedrock lithology.

Sr isotopic measurements of tributaries from the San Joaquin and Sacramento drainage basins have demonstrated large differences in the $^{87}Sr/^{86}Sr$ ratio between the two drainages, as well as between individual tributaries within these basins. Sr isotopic ratios in the Sacramento River drainage vary between 0.705 and 0.706, while those in the San Joaquin tributaries vary between 0.707 and 0.708.

Strontium isotopic measurements and trace elemental contents of adult salmon otoliths (sampled from the center, middle, and outer edge of the otolith) were made from the Yuba and Feather rivers, and from the Feather and Merced river hatcheries. In addition, adult otoliths were sectioned and polished to allow a detailed scan across the otolith using the ion microprobe at LLNL.

Preliminary ion microprobe scans across adult otoliths indicate large differences between the center and rim of the otolith, indicating that the chemical signal incorporated in the otolith is retained even after the salmon migrate to the ocean.

The preliminary Sr isotope results indicate that the $^{87}Sr/^{86}Sr$ ratio varies from center to rim, with the rim close to the oceanic $^{87}Sr/^{86}Sr$ ratio. The center appears to lie in between the oceanic value and the riverine value, indicating either that we did not sample the very center of the otolith with the drill or that the $^{87}Sr/^{86}Sr$ ratio of the center re-equilibrates with seawater during growth in the ocean.

These preliminary results have allowed us to prepare a proposal to the California Department of Water Resources and Department of Fish and Game to obtain further funding.

*Figure 1*

# Quaternary Downcutting Rate of the New River, Virginia, Measured from Differential Decay of Cosmogenic $^{26}$Al and $^{10}$Be in Cave-Deposited Alluvium (GS96-12a)

Principal Investigator: James W. Kirchner (UC Berkeley)
LLNL Collaborator: Robert C. Finkel
Student: Darryl E. Granger (UC Berkeley)

## Abstract

*The concentrations of the cosmogenic radionuclides $^{26}$Al and $^{10}$Be in quartz can be used to date sediment burial. This technique is applicable to a range of problems in surface process studies and neotectonics. We have used $^{26}$Al and $^{10}$Be in cave-deposited river sediment to date the time of sediment emplacement. Sediment burial dates from a vertical sequence of caves along the New River constrain the Quaternary downcutting rate to 27.3 ± 4.5 m/m.y., and may provide evidence of regional tectonic tilt.*

## Objectives

River downcutting rates are important for understanding rates of erosion, landform evolution, and tectonic uplift. Measurements of river downcutting rates provide first-order estimates of landscape lowering rates. Moreover, because large rivers tend to preserve characteristic longitudinal profiles, the spatial pattern of uplift along a river's course can be inferred from variations in downcutting rates along the river's profile. However, reliably measuring rates of river incision is difficult, since datable river terrace surfaces are often poorly preserved.

River downcutting rates can, however, be measured by dating buried alluvium (preserved beneath terraces or within caves) using the cosmogenic radionuclides $^{26}$Al and $^{10}$Be. Quartz grains are exposed to cosmic rays and acquire $^{26}$Al and $^{10}$Be during exhumation from hillslopes and transport through river networks. After these quartz grains are subsequently buried and shielded from cosmic radiation, their $^{26}$Al will decay faster than their $^{10}$Be. The $^{26}$Al/$^{10}$Be ratio will therefore decrease through time, recording the time since burial.

Quartz river sediment deposited in caves is ideal for burial dating with $^{26}$Al and $^{10}$Be. Alluvium deposited deep within caves is well shielded from cosmic rays, so only radioactive decay—not neutron spallation or muon capture—will alter the concentrations of $^{26}$Al and $^{10}$Be after burial. Because cave-deposited river sediments remain fixed relative to bedrock while the river incises, the emplacement times of ancient river sediments in caves, now high above the modern river, can be used to infer river downcutting rates. Our objective was to test the practicality of cosmogenic nuclide burial dating, by measuring the Quaternary downcutting rate of the New River.

## Progress

The New River drains the crystalline Blue Ridge Mountains and cuts across the Valley and Ridge province of Virginia. As the river flows across cave-forming dolomites in the Valley and Ridge province, its bedload spills into caves that open onto the river bed (underwater caves opening onto the modern river bed have been observed by SCUBA divers). River incision leaves these caves abandoned high in riverside cliffs.

Granger explored every known cave along the New River in the Valley and Ridge (more than 50 caves in all), and found 5 caves with emplaced river sediment, as much as 35 m above the modern river. The cave deposits can be distinguished by well-rounded gravels and cobbles in a well-sorted, clast-supported fabric, and extend ~10 m to >100 m into the cave entrances.

We measured $^{26}$Al and $^{10}$Be concentrations in distinctive clasts of vein quartz gravels derived from the New River's headwaters in the metamorphic Blue Ridge, more than 75 km upstream. Thus, we know that these clasts were derived from New River alluvium, rather than from the local host rock.

Results from $^{26}$Al and $^{10}$Be analyses of the five cave samples are shown in Table 1. Sediment emplacement times inferred from these samples range from 0.29 ± 0.18 Ma for a cave 12 ± 2 m above the modern river, to 1.47 ± 0.22 Ma for a cave 29 ± 2 m above the river. Regressing the elevation of caves above the modern river by the age of sediment emplacement shows that the New River's downcutting rate is 27.3 ± 4.5 m/m.y. (Fig. 1).

**Table 1: Burial ages and erosion rates from $^{26}$Al and $^{10}$Be in cave and river sediment**

| Sample | Height above river (m) | $^{26}$Al ($10^6$ at/g) | $^{10}$Be ($10^5$ at/g) | Burial age (m.y.) | Erosion rate (m/m.y.) |
|---|---|---|---|---|---|
| *Pearisburg caves* | | | | | |
| Virginian Cliff #1 | 12 ± 2 | 1.86 ± 0.07 | 3.68 ± 0.11 | 0.29 ± 0.18(0.08) | 12.0–2.8(0.6) |
| Quartz Cobble | 27 ± 2 | 1.63 ± 0.07 | 4.84 ± 0.10 | 1.02 ± 0.19(0.09) | 6.0 ± 1.4(0.3) |
| Virginian Cliff #3 | 31 ± 2 | 0.019 ± 0.002 | 0.059 ± 0.013 | 1.25 ± 0.50(0.46) | 451 ± 153(112) |
| Klotz Quary | 35 ± 2 | 2.29–0.09 | 7.27 ± 0.15 | 1.09 ± 0.19(0.08) | 3.7 ± 0.9(0.2) |
| *Eggleston cave* | | | | | |
| Benton Williams #1 | 29 ± 2 | 1.43 ± 0.09 | 5.48 ± 0.11 | 1.47 ± 0.22(0.12) | 4.0 ± 1.0(0.3) |

*Burial ages and exposure times assume $^{26}$Al and $^{10}$Be production rates of 53.2 ± 10.6 and 8.8 ± 1.8 atoms $g^{-1}$ $a^{-1}$ estimated from Nishiizumi et al. (1989) and corrected for latitude (37°) and elevation (550 m) as in Lal (1991), and production rate ratio $P_{26}/P_{10}$ of 6.04 ± 0.54. Uncertainties are stated as ±1 standard error, and are shown as both random uncertainty (in parentheses, based on analytical uncertainties), and total uncertainty (including uncertainty in production rates, production rate ratio, penetration depth, and radioactive meanlife).*

Figure 1 shows that a single river downcutting rate regressed through the data deviates from 3 of the 5 data points by >1.5 standard errors, implying that either (1) we have underestimated our uncertainties, or (2) a single regression line does not fully explain the data. To examine the second possibility, we divided the sampled caves into two groups and analyzed each group separately. Four of the sampled caves are clustered together near the town of Pearisburg, while one cave is located ~10 km to the southeast, near the town of Eggleston.

Inferred river downcutting rates are slightly different at the two locations: the river is incising at 30.2 ± 5.5 m/m.y. at Pearisburg, and more slowly (19.7 ± 3.2 m/m.y.) at Eggleston.

Although only a single sample exists to constrain the Eggleston downcutting rate, the difference between the two rates (10.5 ± 3.5 m/m.y.) suggests regional tectonic tilt, in a direction consistent with inferred motion of an active seismic zone beneath the study area. (Uncertainty in the inferred tilt rate is calculated only from analytical uncertainties, because systematic uncertainties have little effect on the difference between the two incision rates.) The inferred tilt rate (1.05 ± 0.35 nanoradians/yr) would be difficult to detect by other methods.

Erosion rates inferred from the cave samples range from 3.7 ± 0.9 m/m.y. to 12.0 ± 2.8 m/m.y., with a single outlier at 451 ± 153 m/m.y. (Table 1). Despite large differences in inferred erosion rates, the four Pearisburg samples yield burial ages consistent with a constant river downcutting rate. This illustrates an important point: because the burial dating technique is based on the ratio of $^{26}$Al to $^{10}$Be, and not on absolute concentrations, it is not sensitive to the rate of erosion. Previous estimates of the New River's downcutting rate have ranged from 40 to nearly 300 m/m.y.; $^{26}$Al/$^{10}$Be burial dating provides better-constrained estimates of both New River incision and tectonic tilt rates.

Burial dating with $^{26}$Al and $^{10}$Be opens a new window into dating sediments and measuring geomorphic process rates, because its useful time scale (0.3–5 Ma) is beyond the limits of U-Th dating, and because the technique can be used to infer both burial dates and erosion rates. Furthermore, because $^{26}$Al/$^{10}$Be burial dating requires only quartz, this technique may be used where other datable materials are unavailable.

Burial dating with $^{26}$Al and $^{10}$Be can be applied to other sedimentary deposits (such as basin fills, alluvial fans, or river terraces) provided the sediment is buried tens of meters below the ground surface, beyond the influence of cosmic ray neutrons and muons. This study provides the first radiometric estimate of the New River's downcutting rate, thus demonstrating the utility of $^{26}$Al/$^{10}$Be burial dating for tectonic and geomorphic research.

## References


1. Granger, D. E., and J. W. Kirchner, "Downcutting Rate of the New River, Virginia, from $^{26}Al/^{10}Be$ in Buried River Gravels", *EOS Trans. Am. Geophys. Union* **76**, F689 (1995).

2. Granger, D. E., J. W. Kirchner, and R. C. Finkel, "Quaternary Downcutting Rate of the New River, Virginia, Measured from Differential Decay of Cosmogenic $^{26}Al$ and $^{10}Be$ in Cave-Deposited Alluvium," *Geology* (in review) (1996).


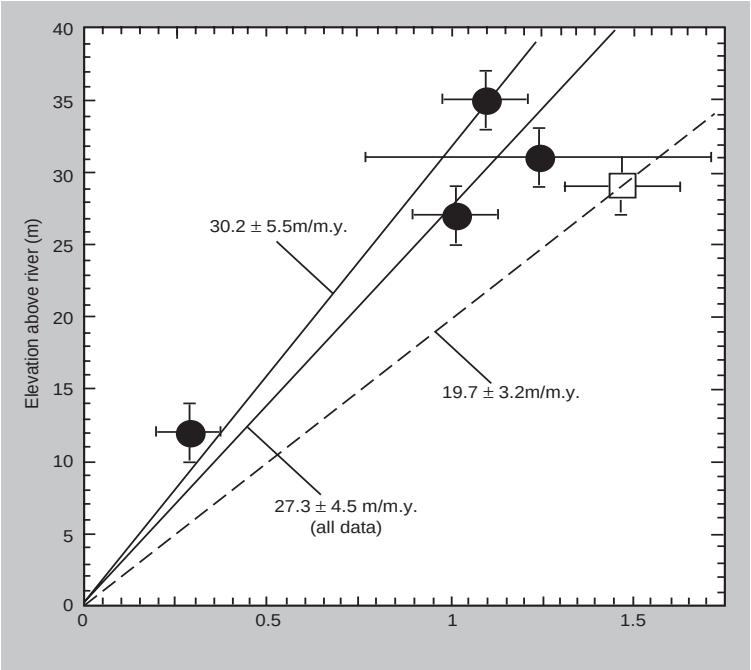


*Figure 1. Downcutting rates inferred from emplacement times of river gravels in caves high above New River. Regressing all data together indicates a downcutting rate of 27.3 ± 4.5 m/m.y. Separating data by cave location reveals that four caves near Pearisburg (circles) record a downcutting rate of 30.2 ± 5.5 m/m.y., while the single cave near Eggleston (open square) records a downcutting rate of 19.7 ± 3.2 m/m.y. The difference between downcutting rates suggests a regional tectonic tilt rate of 1.05 ± 0.35 m $km^{-1}$ $m.y.^{-1}$ near the Giles County seismic zone over late Quaternary. Downcutting rates are constrained to pass through origin. Error bars represent analytical uncertainty.*

# Climatic and Geomorphological Controls on Erosion Rates in Granitic Terrain, Determined using Cosmogenic Isotopes in Stream Sediment (GS96-12b)

Principal Investigator: James W. Kirchner (UC Berkeley)
LLNL Collaborator: Robert C. Finkel
Students: Darryl E. Granger and Clifford S. Riebe (UC Berkeley)

## Abstract

*We used cosmogenic isotopes in stream sediment to measure the erosion rates of a series of small subcatchments at Adams Peak and Fort Sage Mountain, California. These two sites have virtually indistinguishable bedrock, but sharply differing climates. At Fort Sage Mountain, which has a warm, dry, high-desert climate, erosion rates increase sharply with hillslope gradient. At Adams Peak, which has a cooler and wetter climate, erosion rates are roughly constant across a wide range of hillslope gradients. These results suggest that under different climatic regimes, different erosional processes are dominant. Thus, changes in climate can affect not only the rate but also the style of erosion and landform evolution.*

## Objectives

Understanding what controls long-term erosion rates is important for many reasons. For example, the tectonic consequences of erosional unloading have recently become a central concern for both tectonicists and geomorphologists. However, the mechanisms by which tectonic uplift accelerates erosion are poorly quantified, particularly in non-glacial terrain.

Similarly, the suggestion that orogenesis may accelerate weathering and erosion, consume atmospheric $CO_2$, and alter global climate highlights the need to understand how erosion responds to tectonic forcing. Likewise, we need to better understand how erosion rates respond to climate changes, in order to assess whether erosion and weathering (and the resulting consumption of atmospheric $CO_2$) can be an effective feedback mechanism regulating global climate on geologic timescales.

Cosmogenic nuclides record long-term erosion rates without requiring datable sedimentary deposits or erosion surfaces, and thus are applicable to many geomorphic problems. Cosmogenic nuclides in alluvial sediment permit us to directly measure the long-term, spatially averaged erosion rates of small catchments to within roughly ±20%.[1]

Using this method, we previously demonstrated that erosion rates vary systematically with hillslope gradient in granitic terrain under a desert climate.[1,2] But how do erosion rates vary with climate? In this study, we used cosmogenic nuclides to compare long-term erosion rates at two sites with similar lithology but contrasting climatic regimes.

## Progress

Our two study sites, Fort Sage Mountain and Adams Peak, are lithologically similar, having been formed from a single pluton that was broken by basin-and-range faulting. Fort Sage Mountain lies in the rain shadow of the Sierra Nevada and is therefore warm and dry (average annual temperature 8–10°C, annual precipitation 20–25 cm/yr). Adams Peak, by contrast, lies high in the eastern Sierra and is markedly cooler and wetter (average annual temperature 2–5°C, annual precipitation 40–50 cm/yr).

We sampled sediment from streams and gullies draining small subcatchments at Adams Peak. Samples were chemically purified at UC Berkeley and analyzed for $^{10}Be$ and $^{26}Al$ by accelerator mass spectrometry at Lawrence Livermore National Laboratory's Center for Accelerator Mass Spectrometry. The cosmogenic isotope measurements of erosion rates at Adams Peak were compared with previously measured erosion rates at Fort Sage Mountain (Fig. 1).

Figure 1 shows that erosion rates at the two contrasting sites have little in common. Erosion rates at Fort Sage Mountain (the warmer/drier site) increase dramatically with hillslope gradient, and we expected to see a similar pattern at Adams Peak. Instead, erosion rates at Adams Peak (the cooler/wetter site) are roughly constant over a wide range of hillslope gradients.

At Fort Sage Mountain, the relationship between erosion rate (ER, in cm/ka) and hillslope gradient (S) is described by the equation $ER = (0.53 \pm 0.27)e^{(5.1 \pm 01.4)S}$, whereas at Adams Peak, the best-fit line is instead $ER = (4.78 \pm 1.55)e^{(0.36 \pm 0.67)S}$. Although theoretical models of landscape evolution typically assume a simple "erosion law" linking erosion rates and hillslope gradients, our results suggest that no such universal relationship exists.

Figure 1 strongly suggests a shift in dominant erosion processes, and not simply erosion rates, between the two sites. We have several hypotheses that might account for the differences between the sites, but no definitive answers are possible at this point.

Steep slopes at Fort Sage Mountain show evidence of shallow landsliding, a strongly slope-dependent erosional process. By contrast, erosion rates at Adams Peak may be more strongly controlled by frost shattering, which may be independent of gradient (or which may be even more intense on shallow slopes because they retain water better).

The dominant vegetation differs between the two sites, reflecting their different climatic regimes; whereas Fort Sage Mountain is covered by desert forbs and shrubs, Adams Peak is covered by a sparse conifer forest. Treethrow may be an important erosional process at Adams Peak, and may not be strongly slope-dependent, because the density of tree cover is comparable on steep and shallow slopes. Furthermore, steep slopes at Adams Peak may actually be stabilized by the anchoring action of tree roots; steep slopes at Fort Sage Mountain have no such protection from erosion.

Finally, at Fort Sage Mountain, steep and shallow slopes alike are soil-mantled, whereas steep slopes at Adams Peak have prominent bedrock outcrops; these outcrops may weather slowly because they do not retain water. Further study will be needed to determine whether any of these hypotheses is adequate to explain the contrasting erosional behavior of these sites.

The profound difference in erosional behavior between these two sites highlights the need to better understand how variations in climate can affect erosion rates and processes.

We are now extending this study to eight sites throughout the Sierra Nevada, spanning a ten-fold range in annual precipitation and a 10°C range of mean annual temperature. In addition to measuring the relationship between erosion rates and hillslope gradients at each of these sites, we will also be evaluating the rate of chemical weathering and the degree of chemical alteration of erodible regolith. In this way we hope to develop a systematic understanding of how climatic and topographic factors control rates and processes of erosion in granitic terrain.

## References


1. Granger, D. E., J. W. Kirchner, and R. Finkel, "Spatially Averaged Long-Term Erosion Rates Measured from *In-Situ* Produced Cosmogenic Nuclides in Alluvial Sediment," *J. Geol.* **104**, 249 (1996).
2. Granger, D. E., and J. W. Kirchner, "Erosional Response to Tectonic Forcing Inferred from Cosmogenic Isotopes in Alluvial Sediment," *EOS Trans. Am. Geophys. Union* **75**, 289 (1994).


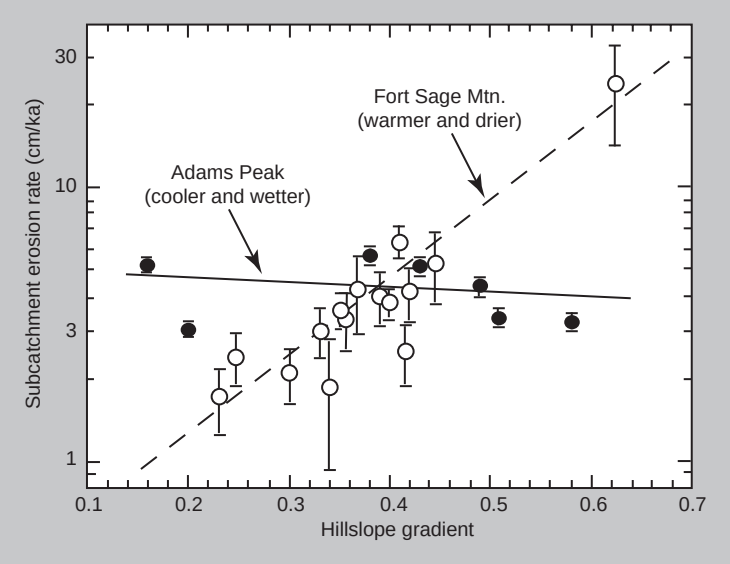


*Figure 1. Erosion rates measured using cosmogenic $^{26}Al$ and $^{10}Be$ for subcatchments at Fort Sage Mountain (open symbols) and Adams Peak (solid symbols), plotted as a function of average hillslope gradient in each subcatchment.*

# Shock Compression of Fayalite (GS96-18)

Principal Investigator: Raymond Jeanloz (UC Berkeley)
LLNL Collaborator: William J. Nellis
Student: Abby Kavner (UC Berkeley)

## Abstract

*Fayalite, the iron end-member of olivine, is an abundant planetary and meteoritic mineral that readily amorphizes under static compression at pressures over 39 GPa, yet resists any recoverable phase change, including amorphization, under shock processing at pressures up to 75 GPa. We have examined this apparent paradox by investigating the amorphization kinetics of fayalite through carefully controlled shock processing. The shock-recovered samples have been analyzed by X-ray diffraction and optical and electron microscopy, as well as by infrared spectroscopy.*

## Objectives

The purpose of this study is to investigate the transformation kinetics of single-crystal fayalite by comparing the effects of static compression and shock processing. The objectives are to understand how experiments performed on different experimental timescales may yield different results, and thus to predict the behavior over a range of timescales pertinent to planetary impact processes. In particular, our goal is to understand the shock "metamorphism" of iron-rich olivines, including the production of the high-pressure ringwoodite phase that is found within certain meteorites.

## Progress

Shock experiments on single-crystal fayalite were performed at the 7-m two-stage light gas gun facility at Lawrence Livermore National Laboratory. Three experiments were designed to complement previous shock experiments on fayalite powder. The first two shock experiments were performed in stainless steel capsules to peak pressures of 63.5 and 75 GPa; one was pre-cooled in liquid nitrogen, the other was maintained at room temperature. A third single-crystal fayalite was shocked to 75 GPa using a specially designed, impedance-matched titanium alloy target and capsule assembly. Each crystal was shocked along its c-axis. The recovered samples were analyzed using X-ray diffraction, optical and electron microscopy, and infrared spectroscopy.

Examination of the recovered samples showed samples fractured by shock processing, with tangles of strain-induced dislocations, but no evidence of amorphization or any other phase transformation. This result is at odds with the complete amorphization of fayalite in the diamond cell at quasi-static pressures exceeding 39 GPa. This result is also surprising because the recovered samples had been shocked well into fayalite's mixed-phase region on the hugoniot, where phase transformations are presumed to be occurring.

This is the first example of a pressure-induced phase transformation that clearly does not show a correspondence between the diamond cell and shock processing. The fact that no transformation is observed in the recovered product suggests one of two possibilities, each with interesting implications.

The first scenario is that during shock loading, the sample does not have the thermal energy required to overcome the kinetic barrier for transformation. This implies a reconstructive mechanism for the transformation to the higher pressure phase, clearly at odds with the observations of amorphization in the diamond cell, which is assumed to take place by a shear or displacive transformation.

The other possibility is that amorphization occurs during shock loading, and then back-transforms upon decompression, in accord with a quick displacive mechanism (martensitic-like) for the transformation. The fact that this experiment, designed to slow the kinetics of the back reaction by pre-cooling the sample prior to shocking, showed no evidence of a phase transformation also suggests that thermal activation is unimportant; that is, of a displacive-type mechanism.

It is highly unlikely that an equilibrium phase transformation occurs in fayalite during shock compression to the pressures and under the variety of shock conditions examined here. Instead, transformation to a partially amorphized phase may take place during shock loading, with reversion back to the original crystalline state upon the release.

For example, all of our results are consistent with a model of fayalite undergoing amorphization in only one dimension—along the c-axis—during compression, with reversion back to the crystalline state upon release of pressure. In contrast, there may not be enough thermal energy available during static compression for reversion back to single-crystal material upon decompression, thus allowing the amorphous state to be quenched.

# The Effect of Pressure on Oxygen and Silicon Diffusion in Olivine (GS96-19)

Principal Investigators: Daniel L. Farber and Kevin McKeegan (UC Los Angeles)

LLNL Collaborator: Frederick Ryerson (LLNL)

## Abstract

*Diffusion of atoms at high pressure is likely the rate-limiting step for viscous flow in the Earth's mantle. Thus, a detailed understanding of the effect of pressure on the slow diffusing species in olivine should yield insight into the viscosity structure of the upper mantle. We have developed new techniques to determine diffusion coefficients for slow diffusing species in olivine. The main technical difficulty associated with these measurements has been stabilizing a highly polished mineral surface and recovering it from high pressure. Although we have experimented with a number of techniques, to date we have found the most effective method to be deposition of thin films at 1 atm followed by a high pressure diffusion anneal.*

## Objectives

Recently there have been great advances in the understanding of the structure and dynamics of the Earth. However, there are still fundamental gaps in our knowledge of the inner workings of the planet. Indeed, an accurate model of plate tectonics depends on being able to model flow of material deep within the Earth's interior. Thus, a detailed understanding of the rheological properties of the minerals that comprise the Earth's mantle is critical for our understanding of the thermal and dynamical evolution of the planet.

Olivine is the most abundant mineral in the Earth's upper mantle. However, rheological studies of olivine have only been carried out at pressures appropriate to the base of the crust, and little rheologic data exists for materials at pressure and temperature conditions appropriate to the transition zone (400–670 km) and lower mantle (> 670 km). Moreover, rheologic studies at high pressure are extremely difficult and, to date, have produced controversial and inconsistent data sets.

This study is aimed at developing new high-pressure techniques to determine diffusion coefficients for slow diffusing species in olivine. As diffusion of these species should control viscous flow, these experiments will provide an independent check of the rheological measurements.

## Progress

We have conducted a number of experiments on silicon and oxygen diffusion in forsterite. To date, we have used both hydrothermal and solid state sources with limited success. We have primarily conducted experiments in the piston and cylinder apparatus at 10 kb and 900°C and have experimented with different methods of producing thin film sources on the polished sur-

face of olivine single crystals. We have also performed experiments using a fluid source for the $^{18}O$ at high pressure. In each case, the recovered surfaces had lost the high polish during the high pressure annea. We have, however, begun to have some success by depositing a layer of $Mg_2{}^{30}Si^{18}O_4$ directly on the surface at 1 atm. Using this technique, we have stabilized some highly polished olivine surfaces. These initial experiments hold promise for being able to recover undeformed polished surfaces from olivine at high pressure.

# Study of Seismic Attenuation in Northern California using BDSN Data (GS96-20)

Principal Investigator: Lane R. Johnson (UC Berkeley)
LLNL Collaborator: Kevin Mayeda
Student: Rouben Amirbekian (UC Berkeley)

## Abstract

*The study of seismic waves in the frequency band between 0.5 to 10 Hz is currently one of the most important and most difficult areas of basic seismological research. Such waves are of primary concern in the consideration of seismic hazards from local earthquakes, as most structures have their resonant modes in this frequency band. These waves are also essential to basic studies of earthquake sources, both in terms of precise locations of hypocenters and estimation of the physical processes taking place in the source region.*

*Related to this is the fact that this frequency band is critical to current research in support of a nuclear test ban treaty at thresholds below 1 kiloton. Finally, working in this higher frequency band has the potential of yielding increased resolution in any characterization of Earth structure.*

## Objectives

The objective of this research project was to perform a fundamental study of the attenuation of regional seismic waves in the frequency band between 0.5 and 10 Hz through an analysis of seismic coda waves. A newly developed method of separating intrinsic and scattering attenuation (the multiple lapse time window approach) was applied to broad-band waveform data recorded by the Berkeley Digital Seismic Network (BDSN). This method of analysis was implemented and some preliminary results were obtained with waveform data that sampled the northwestern Coast Ranges of California.

The first and primary task of this research project was to apply the multiple lapse time window analysis method to the extensive data set available at the BDSN. The objective of this analysis was to estimate the separate effects of intrinsic attenuation and scattering attenuation and their frequency dependence.

The use of data from the BDSN, which spans much of central and northern California, provides an excellent test of this method and at the same time has the potential to generate important new information about the properties of the crust on scales that range from regional down to the characteristic scale of the scatterers.

Another objective was to relate these estimates of intrinsic and scattering attenuation to geologic and tectonic features in central and northern California. The interpretation of the frequency dependence of the scattering can be related to the statistical properties of crustal heterogeneity, taking advan-

tage of recent theoretical and computational advances in the treatment of elastic scattering. A final objective was to investigate the possibility of using the coda measurements as a stable estimate of earthquake size.

## Progress

The first stage of the project was to develop the necessary computer programs for implementing the multiple lapse time window approach to coda analysis. This method takes advantage of differences between scattering and intrinsic attenuation in both the time and frequency domain.[1–5]

Using a multiple lapse time window analysis and a time domain representation of the multiple scattering solution,[6] this approach leads to a separation of intrinsic attenuation and scattering attenuation, which appears to be quite reliable. This part of the project was successfully completed, and test runs on data recorded by the BDSN produced results comparable to those obtained by other investigators.[3–5]

The next stage of the project was a systematic application of this method to broad-band seismic waveform data recorded by the BDSN. This network presently consists of 12 state-of-the-art broad-band seismographic stations spread out over a distance of about 700 km in central and northern California. The broad variety of geological conditions encompassed by this network provides an opportunity to investigate how the estimated parameters of intrinsic attenuation and scattering attenuation in the crust can vary between different geological provinces. The frequency dependence of these quantities can also lead to a better understanding of the physical mechanism, which is their cause.

This task began with a consideration of seismic events located in northwest California, because the high rate of seismicity in this region provides ample broad-band data. Waveforms from selected events from this region were analyzed for seismographic stations located in the California Coast Ranges and also farther east at stations near the Sierra Nevada. Results for stations located within the Coast Ranges were quite similar, suggesting that characteristic values of intrinsic attenuation and scattering attenuation for the crust of this region could be estimated.

Several practical problems were encountered in the application of the multiple lapse time window method. One of these problems is related to the occurrence of other seismic events during the time window used for coda analysis, which can be a few minutes in length. These other seismic events, which are often aftershocks but could also be other seismic events in the same general region, cause an interruption in the smooth decay of coda energy and thus interfere with the estimation of decay parameters. Various methods of mitigating the effects of these extra events were considered, but the most reliable approach was found to be carefully editing the data to select those events that were followed by a period of seismic quiescence.

Another practical problem involved the choice of the time window to be used for fitting the theoretical model to the coda decay function. This win-

dow has to be chosen differently for each frequency, as the coda levels for different frequencies fall below the background noise level at different times. The best guides for choosing the optimum window lengths were found to be the experience provided by numerical experimentation with a variety of window lengths, plus a careful inspection of noise levels.

The original plan for this project was to apply the multiple lapse time method to a wide variety of source and station pairs in central and northern California to look for regional patterns in differences in intrinsic attenuation and scattering attenuation in the crust. However, the grant period ended before this part of the project was completed.

From the research that was completed, it appears that the multiple lapse time method is a reliable approach to the problem of separating the effects of intrinsic attenuation and scattering attenuation and making separate frequency dependent estimates of these two parameters in the crust.

## References


1. Hoshiba, M., H. Sato, and M. Fehler, "Numerical Basis of the Separation of Scattering and Intrinsic Absorption from Full Seismogram Envelope: A Monte-Carlo Simulation of Multiple Isotropic Scattering," *Pap. Meteorol. Geophys.* **42**, 65 (1991).

2. Fehler, M., M. Hoshiba, H. Sato, and K. Obara, "Separation of Scattering and Intrinsic Attenuation for the Kanto-Tokai Region, Japan, using Measurements of S-Wave Energy vs. Hypocentral Distance," *Geophys. J. Int.* **108**, 787 (1992).

3. Mayeda, K., K. S. Koyanagi, and K. Aki, "A Comparative Study of Scattering, Intrinsic and Coda Q-1 for Hawaii, Long Valley, and Central California between 1.5 and 15 Hz," *J. Geophys. Res.* **97**, 6,643 (1992).

4. Hoshiba, M., "Separation of Scattering Attenuation and Intrinsic Absorption in Japan with the Multiple Lapse Time Window Analysis from Full Seismogram Envelope," *J. Geophys. Res.* **98**,15,809 (1993).

5. Jin, A., K. Mayeda, D. Adams, and K. Aki, "Separation of Intrinsic and Scattering Attenuation in Southern California using TERRAscope Data," *J. Geophys. Res.* **99**, 17,853 (1994).

6. Zeng, Y., F. Su, and K. Aki, "Scattering Wave Energy Propagation in a Medium with Randomly Distributed Isotropic Scatterers, 1. Theory," *J. Geophys. Res.* **96**, 607 (1991).

# Three-Dimensional Modeling of Upper Mantle Structure beneath the Western United States (GS96-22)

Principal Investigator: Yu-Shen Zhang (UC Santa Cruz)
LLNL Collaborator: Howard J. Patton

## Abstract

*We are developing a high-resolution shear-wave velocity model of the western United States. This project is a continuous study based upon Ammon and Patton's previous IGPP project. Due to differences of resolution scales, velocity structures in the uppermost mantle (less than 50 km) and below 200 km under the western United States are different in recent regional and global studies.*

*For example, there is a deep, slow velocity anomaly at depths between 100 and 300 km with horizontal radius of about 500 km in the southern Basin and Range, which has not been discussed before, but which may have important implications for the dynamics of the Basin and Range. These studies must be improved to allow geodynamic understanding of this tectonic active area.*

## Objectives

Using Love and Rayleigh waves dispersion measurements, which are associated with earthquakes (M >5) from 1980 to 1994, a three-dimensional (3-D) shear-wave velocity model for the upper 300 km of the mantle under the western United States will be developed. The surface waves at periods between 40 and 150 s are sensitive to the upper 300 km of the mantle. The final high-resolution shear-wave velocity model, with a resolution of about 200 to 400 km, will provide a framework for multidisciplinary studies and for understanding the possible geodynamic activities of the western United States.

## Progress

Our study has five phases: (1) data collection, (2) data analysis and dispersion measurement, (3) phase velocity variation, (4) shear-wave velocity structure, and (5) publication of the results. We have finished the first phase, and we are working on the second and third phases of the investigation.

The accumulated digital seismic data in the last decade have provided excellent path coverage. We have collected digital seismic waveforms from the Global Seismographic Network (GSN), the Lawrence Livermore National Laboratory (LLNL) network, and the United States Geological Survey (USGS) network.

The minor arc phases G1 and R1 associated with earthquakes (M >= 5.0) were selected. Each seismogram was visually inspected in the time and spectral domains and was compared with synthetics to ensure that the data

have energy at periods 40 and 150 s and to guarantee the reliability of the inversion results.

Three different experiments were performed in this study. The first experiment is the traditional approach. Using PREM as a starting model, we did phase velocity inversions in different periods. (Note that the present global investigations have successfully obtained the long-wavelength features, while these variations are hard to get in the regional study.)

In the second experiment, we used Zhang and Lay's[1] recent 3-D model as a starting model and did velocity inversion.

*A priori* information, such as the topography and crustal structure variations, was involved in the third experiment. Figures 1 and 2 are Love and Rayleigh waves phase velocity variations at a period of 100 s in the third experiment.

The other novel aspect of this study is that it departs fundamentally from the constant model parameterization approach, which has been used in most seismological tomographic studies. The large-scale features are investigated first, and then small-scale features beneath the western United States are studied.

## References

1. Zhang, Y-S, and T. Lay, "3-D S-wave velocity variations in the upper mantle," *EOS* **77**, 482 (1995).

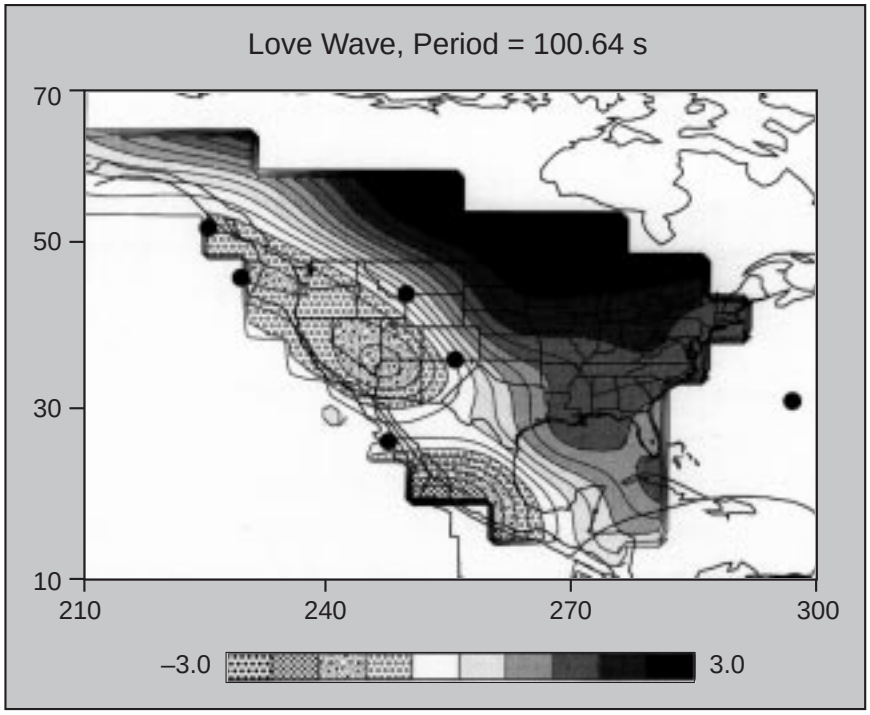


*Figure1. Love Wave at a period of 100 s. The unit is percent. The solid circles are hotspots in this area.*

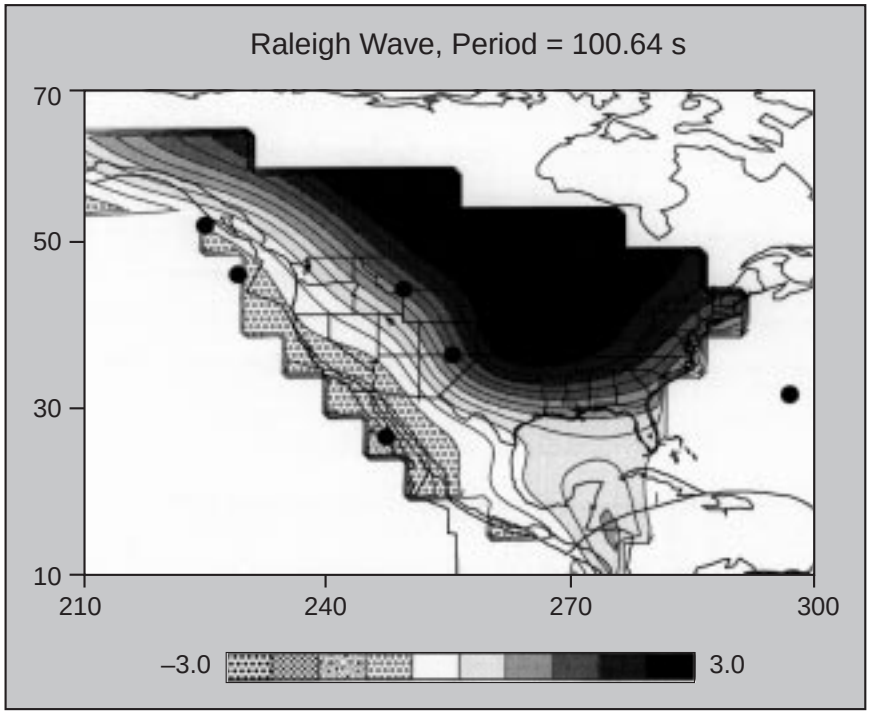


*Figure 2. Same as Figure 1, except for Rayleigh Wave.*

# Array Studies of Northern California Crust and Uppermost Mantle (GS96-23)

Principle Investigator: Justin Revenaugh (UC Santa Cruz)

LLNL Collaborator: William R. Walter

Students: Colin Reasoner, Jacob Lawrence, and Michael Hagerty (UC Santa Cruz)

## Abstract

*The regional seismograph arrays in California are a tremendous and under-utilized resource for seismologists. Originally intended to monitor seismicity in the state, the networks have been increasingly used in structural seismology. Travel time tomography is clearly the premiere application, producing maps of crust and upper mantle velocity heterogeneity over a broad-wave number range. Tomography, however, utilizes only a very small fraction of the information recorded by these networks.*

*We have begun a program consisting of several separate projects having in common extensive use of waveform information. The best developed of these projects is a scheme for back projecting, or migrating, locally scattered energy in teleseismic P wave coda. Working from a database of over 9,000 seismograms, we have constructed maps of P to Sg scattering potential (a dimensionless measure of local scattering strength) along a nearly 500-km long stretch of the San Andreas Fault system in northern and central California. The primary results to date are*

- *fault segment boundaries based on historic and paleoseismicity coincide with high along-fault gradients of scattering potential, suggesting that the basic building blocks of large San Andreas earthquakes can be defined independently of local seismicity; and*
- *removal of ~315 km of right-lateral offset optimally aligns cross-fault profiles of scattering potential, implying that present-day scattering potential depends (in part) on pre-fault crustal structure, which in this case is ≥20 Ma old.*

## Objectives

Our objective is to utilize regional array waveform information to map heterogeneity in the crust and uppermost mantle of northern and central California. Our primary focus is on the scattering properties of the crust. The sensitivity of seismic scattering extends to shorter scale length structures than can be imaged tomographically. Our hope is that by studying crustal scattering in and around major California fault zones, we may be able to improve the present understanding of the interactions of fault-zone structure and seismogenesis.

## Progress

Progress has been slow, primarily because it has been difficult to retrieve high-frequency records of teleseismic events. The data collection

and archiving strategies of the northern and southern components of the California State regional array system differ significantly. Our experience with the southern component led us to propose an overly ambitious research schedule for this project. Progress has been made, but most of it has come in the last few months, leaving little opportunity for active collaboration.

**The San Andreas in Central California.** Scattering correlates with seismic productivity (number of recorded earthquakes) along the San Jacinto fault zone[1] and component faults of the 1992 Landers mainshock.[2] A similar analysis is not possible in central California given the very long recurrence intervals of some segments of the San Andreas and the short instrumental seismicity catalog. However, we can compare fault segment boundaries[3] with scattering potential (Fig. 1).

Segment bounds delimit fault stretches that are ruptured singly or multiply in large earthquakes. Determined on the combined basis of historic and paleoseismicity and geologic constraints, the segment bounds are more representative of long-term fault behavior than the instrumental record alone.

We find that segment bounds coincide with high along-fault scattering gradient (profile slope). High scattering gradients are much more numerous than segment bounds, however, suggesting that the correspondence might be mere coincidence. This hypothesis can be tested by assuming that segment bounds are randomly placed with respect to scattering. If we define high along-fault gradient as any gradient with magnitude outside the standard deviation level (0.048 $km^{-1}$), then 33% of the imaged San Andreas Fault is "high gradient."

The likelihood that at least six out of nine randomly sited segments would fall upon high scattering gradient is 4.3%, leading us to accept the hypothesis that segment bounds are marked by high scattering gradient.

Fault stepovers and changes in strike frequently serve as the initiation and termination points of earthquake rupture, i.e., as segment bounds. The correlation of high scattering gradient and segmentation suggests that fault jumps and bends along the San Andreas occur in crust that is intrinsically associated with high scattering potential, or that the bends and jumps themselves produce scatterers.

Distinguishing these two hypotheses is a question of precedence that Figure 1, showing present-day scattering, cannot answer. Nonetheless, the correlation corroborates existing evidence that scattering and seismogenesis are related.[1,2]

To better understand the sources of crustal scattering and perhaps unravel the ontology of the correlation of scattering and seismogenesis, we are looking for evidence of offset markers in scattering potential. The idea is simple: we compute along-fault averages of scattering potential on both sides of the fault, then systematically offset them, searching for the offset that yields the greatest cross-fault correlation. If scattering is strongly tied

to crustal lithology and structure, one might expect the patterns of scattering to translate coherently with fault offset.

For the San Andreas in central California, that is exactly what we find. Removal of 315 km of right-lateral offset optimally realigns scattering potential. This offset removal agrees very well with the most accurate estimates of post-early Miocene offset, the most probable time of inception of slip on the present-day trace of the San Andreas.

Coupled with the correlations between segment bounds and scattering, this suggests that pre-fault structure has lasting control on present-day seismogenesis despite the accumulation of ~315 km of offset over ≥20 Ma.

## References


1. Revenaugh, J., "Relationship of the 1992 Landers, California, Earthquake Sequence to Seismic Scattering," *Science* **270**, 1344 (1995).
2. Revenaugh, J., "Relation of Southern California Seismicity to Seismic Scattering: Implications for Fault Rupture and Slip Repeatability," abstract, *EOS Trans. Am. Geophys. Union* **46**, 409 (1995).
3. Working Group on California Earthquake Probabilities, *Probabilities of Large Earthquakes Occurring in California on the San Andreas Fault*, U.S. Geological Survey Open-File Report **88-398**, 1 (1988).


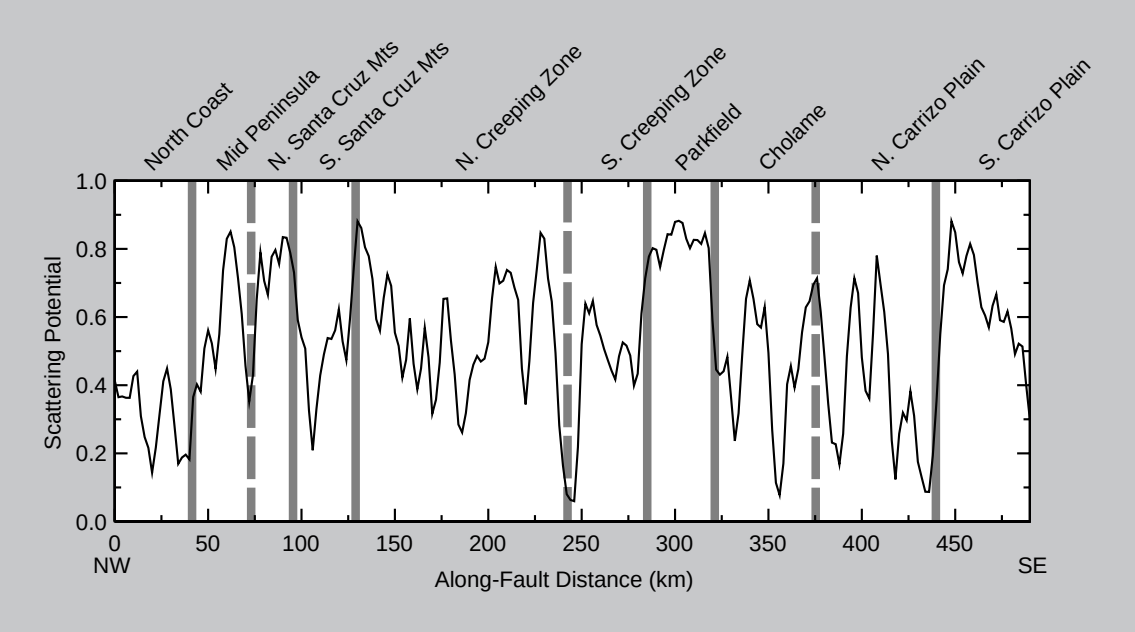


*Figure 1. Mean scattering potential along the San Andreas Fault plotted with segment boundaries (vertical bars) superposed. Six of nine boundaries (solid bars) coincide with regions of high along-fault scattering gradient (gradient magnitude outside the standard deviation level), an event <5% likely to occur by chance, implying structural expression of segment bounds. Along-fault distance increases to the southeast along the fault zone, which begins near San Francisco and extends to the juncture of the Garlock Fault.*

# Surface Diffusion/Conduction in Polycrystalline Olivine Rocks (GS96-27)

Principal Investigator: Steven Constable (Scripps Institution of Oceanography, UC San Diego)

LLNL Collaborator: Jeffery J. Roberts

## Abstract

*Measurements of conductivity and thermopower as a function of oxygen fugacity have been used to derive a model for conduction in olivine. Thermopower at 1000–1200°C is between 50 and 400 μVk and has a positive oxygen fugacity dependence; electrical conductivity exhibits approximately a 1/11 power dependence on oxygen fugacity.*

*However, small polarons (Fe+++ on a Fe++ site), considered to be the conducting defect in olivine at these temperatures, would produce a larger thermopower than observed, with a negative oxygen fugacity dependence, as well as a 1/6 power dependence of conductivity on oxygen fugacity.*

*At least one other conducting defect species must be invoked to explain the observed magnitude and oxygen fugacity dependence of thermopower. An electron/polaron model cannot be made to fit the conductivity and thermopower data well, but a polaron/magnesium vacancy model fits the data if a constant polaron or magnesium vacancy term is included.*

*Concentrations from our fits are consistent with predictions from theoretical models, and our analysis predicts a transition from polaron dominance in conduction to magnesium vacancy dominance at around 1300°C, as has been previously inferred from other data.*

## Objectives

An understanding of defect chemistry is important in the study of the electrical conductivity, rheology, and diffusion in Earth's mantle, and there have been several recent attempts to model the point defect structure in olivine. The objective of our project was to apply mathematical modeling to existing data sets of electrical conductivity for polycrystalline olivine collected at Lawrence Livermore National Laboratory.

Although the original proposal focused on modeling diffusion of re-equilibration with changes in oxygen fucacity, as the work proceeded we changed our attention to the thermoelectric effect, or thermopower. Typically, previous modeling efforts have been based on either the temperature dependence or the oxygen fugacity dependence of electrical conductivity.[1]

Thermopower, on the other hand, is determined by the sign and concentration of the dominant charge carrier, resulting from the migration of the conducting species from the hotter electrode of a sample in a temperature gradient. Because conductivity is a product of defect concentration and mobility, while thermopower is dependent only on concentration, a simulta-

neous model of conductivity and thermopower offers the possibility of estimating defect concentrations and mobilities independently.

## Progress

Our primary data for interpretation (Fig. 1) comprise thermopower and conductivity measurements published by Roberts and Duba.[2] The measurements were performed on a dunite from the San Quintin volcanic field, Baja California, Mexico. The sample was fine-grained (~300 μm grain size) and contains approximately 95% olivine ($Fo_{90.5}$), 3% clinopyroxene, and 2% spinel. Optical and scanning electron microscopy revealed no alteration.

The thermopower and conductivity data were collected at temperatures of 1000, 1100, and 1200°C, over a range of oxygen fugacities that span the olivine stability field, in the furnace design described by Duba *et al.*[3] Thermopower was determined using the method described by Schock *et al.*;[1] at a given temperature and oxygen fugacity, the sample was moved into an area of the furnace with a known temperature gradient.

The emf that results from charge-carrier migration from the hotter electrode is measured by a digital voltmeter with an accuracy of 10 μV. This was done for several temperature gradients at each temperature and oxygen fugacities (controlled by various gas mixtures).

The positive sign of the thermopower is consistent with the polaron model, and indeed was an important part of the basis for the polaron hypothesis.[1] Thermoelectric power is also inversely proportional to the concentration of charge carriers, and so the observed decrease with temperature (Fig. 1) is consistent with a thermally activated defect population.

However, thermopower increases with oxygen fugacity. This increase is not what would be predicted by an increased polaron population at high oxygen fugacity implied by the increased conductivity, because thermopower decreases with increased concentration.

Furthermore, if the magnitudes of observed thermoelectric data are interpreted in terms of polaron conduction only, unrealistically large Fe+++ to Fe++ ratios are implied. The largest Fe+++ to Fe++ ratios estimated by Hirsch and Shankland[4] predict a thermoelectric power of about 650 μV/K at 1200°C. In contrast, we observe thermopowers of about 100 μV/K at 1200°C; and even at 1000°C, thermopower does not exceed 500 μV/K.

Neither the slope of the conductivity-oxygen fugacity relationship nor the slope of the thermoelectric power-oxygen fugacity relationship support the simple polaron paradigm, and the data clearly suggest either a different conduction mechanism than polarons or mixed conduction.

We built a mathematical model of mixed conduction and used Marquardt inversion[5] to solve for mobilities and concentrations of polarons, magnesium vacancies, and electrons, using the conductivity and thermopower data at 1000, 1100, and 1200°C as constraints. The details of the modeling are described in Constable and Roberts.[6]

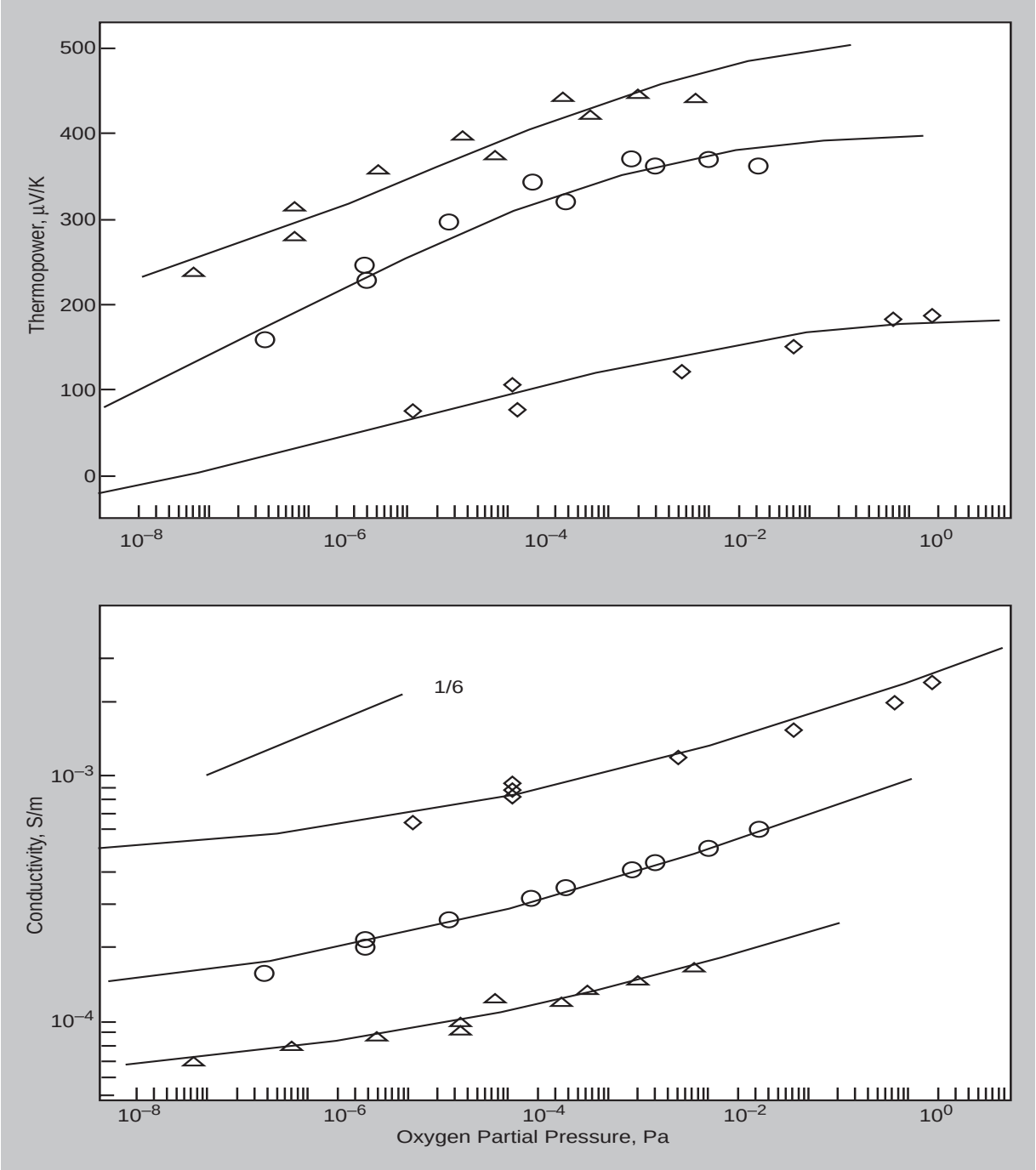


*Figure 1. Electrical conductivity data and thermopower data (symbols), along with model fits (solid lines) as described in the text. Data are collected at 1000°C (triangles), 1100°C (circles), and 1200°C (diamonds).*

On the order of 200 inversions were run from different starting models and with various constraints on model parameters. We rejected as inadequate any model that did not approach the estimated data error of about 5%, although inadequate models were usually evident immediately as a consequence of slopes of opposite sign or grossly incorrect conductivities and thermopowers.

We concluded that a second, negative charge carrier must exist alongside the polaron, both to drop the magnitude of the thermopower and to produce a positive thermopower-oxygen fugacity slope. This can be accomplished to first approximation using electrons, but the negative oxygen fugacity dependence of electron concentration produces models in which thermopower plunges steeply at low oxygen fugacity.

We cannot find any fits using a polaron-electron model that we consider adequate, and all acceptable models consist of polarons and magnesium vacancies. We were able to fit the data well using this model, with a root-mean-square misfit of 6%, which is about the accuracy of the data. Figure 1 shows the fits of our model to the data.

Our modeling demonstrates that mixed conduction can explain the behavior of both conductivity and thermopower. The defect concentrations we obtain are similar enough to those of Hirsch and Shankland[4] that we are confident the assumptions and approximations we have made are valid.

On the other hand, our results can be used to refine the theoretical model. For example, Hirsch and Shankland arbitrarily assigned a mobility to magnesium vacancies that was 10% of the polaron mobility. Our model indicates that it is closer to 20% of the polaron mobility. Electrons do not appear to play a significant role in conduction at these temperatures and oxygen fugacities.

This defect model will provide the basis for understanding the electrical properties and point defect diffusivity in olivine. For example, observations of an oxygen fugacity-dependent diffusivity (Constable, Duba, and Roberts, manuscript in preparation) can be readily understood to be caused by the changing relative contribution of the various defects as a function of oxygen fugacity.

Also, although there have been suggestions that a new conduction mechanism comes into play at higher temperatures, the change in activation energy of conductivity-temperature measurements at around 1300°C has proved somewhat difficult to model, because at these temperatures, iron loss to electrodes and sample metamorphism becomes a problem. Extrapolating the present model indicates near equal contributions to conduction from polarons and magnesium vacancies at 1300°C.

## References

1. Schock, R. N., A. Duba, and T. J. Shankland. “Electrical Conduction in Olivine,” *J. Geophys. Res.* **94**, 5,829 (1989).

2. Roberts, J. J., and A. G. Duba, "Transient Electrical Response of San Quintin Dunite as a Function of Oxygen Fugacity Changes: Information about Charge Carriers," *Geophys. Res. Lett.* **22**, 453 (1995).

3. Duba, A. G., R. N. Schock, E. Arnold, and T. J. Shankland, "An Apparatus for Measurement of Electrical Conductivity to 1500°C at Known Oxygen Fugacity," in *The Brittle-Ductile Transitions in Rocks*, A. G. Duba, W. B. Durham, J. W. Handin, and H. F. Wang, eds., *Geophys. Monogr. Ser.* **56** (*Am. Geophys. Union*, Washington, D.C.) pp.207–210 (1990).

4. Hirsch, L. M., and T. J. Shankland, "Quantitative Olivine-Defect Chemical Model: Insights on Electrical Conduction, Diffusion, and the Role of Fe Content," *Geophys. J. Int.* **114**, 21 (1993).

5. Marquardt, D. W., "An Algorithm for Least-Squares Estimation of Non-Linear Parameters," *J. Soc. Ind. Appl. Math* **11**, 431 (1963).

6. Constable, S., and J. J. Roberts, "Simultaneous Modeling of Thermopower and Electrical Conduction in Olivine," *Phys. Chem. Min*, in press (1997).

# Crustal and Uppermost-Mantle Structure from Observations of $SP_dP$ (GS96-29)

Principal Investigator: Peter Shearer (UC San Diego)
LLNL Collaborator: William Walter
Student: Paul Earle (UC San Diego)

## Abstract

*Recent studies using various methods support the presence of a seismic discontinuity (Hales discontinuity) at a depth near 80 km in some regions, which has been attributed to a phase change from spinet to garnet peridotite. However, the existence and possible origin of the Hales discontinuity are not universally accepted.*

*Observations of S-to-P-converted phases recorded on broad-band seismic stations in North America have previously been used to infer the existence of an increase in seismic velocity at a depth of 70 km.[1] Our study extends this previous work to a global survey and expands the synthetic seismogram modeling tests.*

*Reflectivity synthetic modeling has shown that care must be taken to isolate $SP_dP$ arrivals originating from top-side Moho reflections (Fig. 1) before a search for discontinuities in the uppermost mantle can proceed. Thus, we have developed and applied a method, using $SP_mP$ arrivals, to determine crustal thickness.*

*Examination of over 14,000 three-component seismograms has highlighted the complexity of $SP_dP$ phases. Stacking techniques have been applied to broad-band records to reveal similarities between these arrivals. Such stacks show energy arriving at a time and distance range consistent with reflections from a discontinuity in the uppermost mantle.*

## Objectives

Our objectives are to determine the global extent and properties (depth and impedance contrast) of discontinuities in the uppermost mantle from observations of *S*-to-*P*-converted phases and to place upper bounds on their magnitude in regions that produce no observable reflections. An improved knowledge of the seismological properties of these discontinuities would provide constraints on upper-mantle composition and dynamics.

## Progress

$SP_dP$ is a seismic phase that travels through the mantle as a shear wave (*S*) and is converted at the surface to a compressional wave (*P*), which undergoes a topside reflection from a seismic discontinuity at a depth *d* (Fig. 1). These phases arrive shortly after *S* and are sometimes of comparable amplitude, but with a distinctly different particle motion. For a range of source-receiver separations, governed by the depth and velocity contrast of

a possible seismic discontinuity, $SP_dP$ phases will undergo a post-critical reflection giving rise to enhanced $SP_dP$ amplitudes.

To determine if such energy can be clearly detected, we have computed synthetic seismograms, using the reflectivity method, to obtain the response expected for a suite of models with different crustal thickness, upper-mantle velocities *(Pn)*, and the possible inclusion of an 80-km discontinuity. The Moho reflected *SP* phase is a prominent feature, and knowing its behavior is crucial for avoiding possible misidentification of upper-mantle discontinuity phases.

Synthetics for varying crustal thickness show that increasing the crustal depth widens the separation between *S* and $SP_mP$ but does not significantly increase the distance to which $SP_mP$ *is* observed. Enhancing the *Pn* velocity of the models has the opposite effect, increasing the distance range of $SP_mP$ observations while only slightly changing the separation of the *S* and $SP_mP$ phase.

Difficulties arise when a thick crust is accompanied by an unusually large *Pn* velocity; under such conditions, synthetic seismograms predict energy arriving at distances and times consistent with a reflection from a shallow upper-mantle discontinuity *(*60–80 km). Thus, knowledge of the crustal depth is essential for accurate identification of discontinuity phases.

We developed a new method, utilizing the $SP_mP$ phase, for estimating crustal thickness. First, the radial and vertical components of the seismogram are rotated by an angle such that the *S* and the $SP_mP$ arrival appear distinctly on separate traces. Next, we take envelope functions of the traces to eliminate the effect of a phase shift of unknown magnitude occurring in the $SP_mP$ arrival. Finally, the first swing of the processed *S* and $SP_mP$ arrival are aligned by eye to obtain a differential travel time, which is converted to a crustal thickness estimate.

We have obtained high-quality observations of crustal thickness for 17 stations (Fig. 2). The only free parameter in our modeling is the average *P* velocity in the crust.

Our examination of approximately 14,000 three-component seismograms at the optimal source receiver separation highlighted the waveform complexities that arise from various effects, such as differing source time functions, crustal reverberations, and varying attenuation. In hopes of determining the global nature of possible uppermost-mantle discontinuities, we employ robust stacking techniques to reveal the underlying shared signal in the broadband waveforms.

The particle motion of the *S* and *SP* phases are roughly 90° out of phase, making it possible to sum the scaled radial and vertical components to suppress the *S* arrival and to magnify the *SP* arrival. Beyond 54°, the *iasp91* velocity model predicts a precritical reflection for $SP_mP$; thus, *SP* energy will begin sampling the upper-mantle. Our stack images *S*-to-*P*-converted energy to distances of 60° (Fig. 3). Energy of this magnitude is not seen in

synthetics calculated for ranges beyond 55° in Earth models with crustal and upper-mantle velocities similar to *iasp91*, which do not contain an uppermost-mantle discontinuity. Synthetic modeling has shown that our stacks can also be explained by an enhanced velocity gradient in the upper-mantle.

The stacking techniques and database developed during this research have proven useful in several additional studies on Earth structure, including the determination of the distribution of small-scale heterogeneities in the mantle, the imaging of the main teleseismic arrivals over a broad frequency range, estimation of the upper-mantle discontinuity sharpness, and tighter limits on core-mantle-boundary topography.

## References

1. Zandt, J., and G. E. Randall, *Geophys. Res. Lett.* **12**(9), 565 (1985).

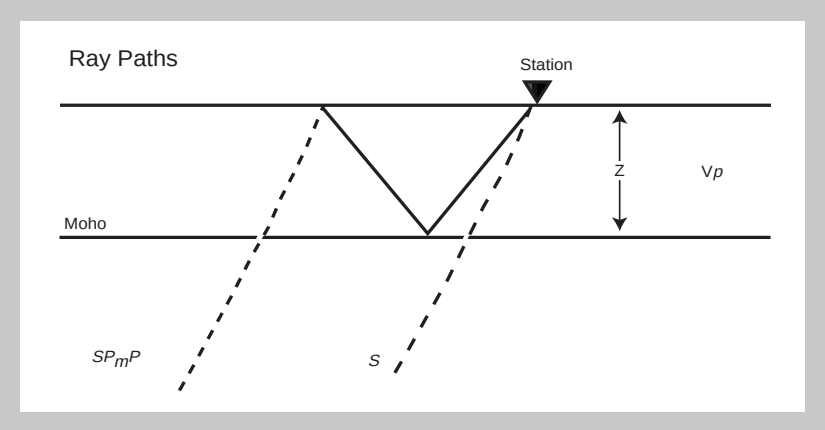


*Figure 1. Ray path for $SP_mP$ ($SP_dP$ phase resulting from the topside reflection from the Moho). The S-waves are shown as dashed lines; the P-waves are shown as solid lines.*

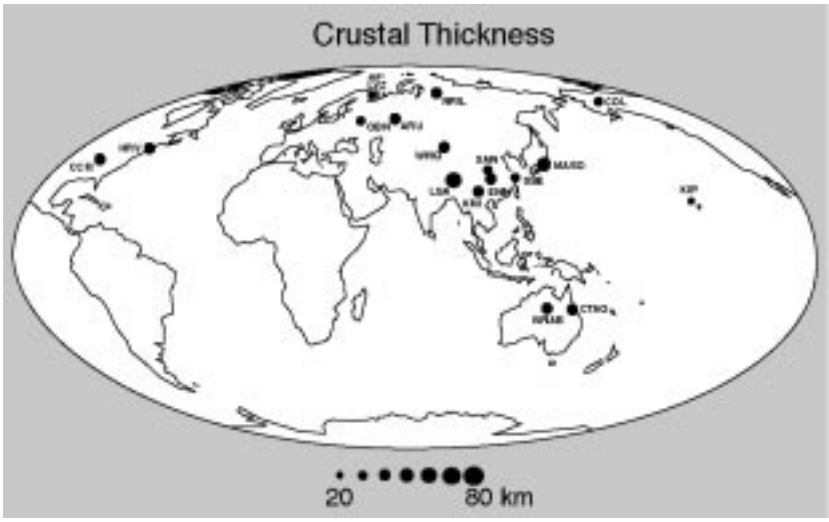


*Figure 2. Crustal thickness estimates.*

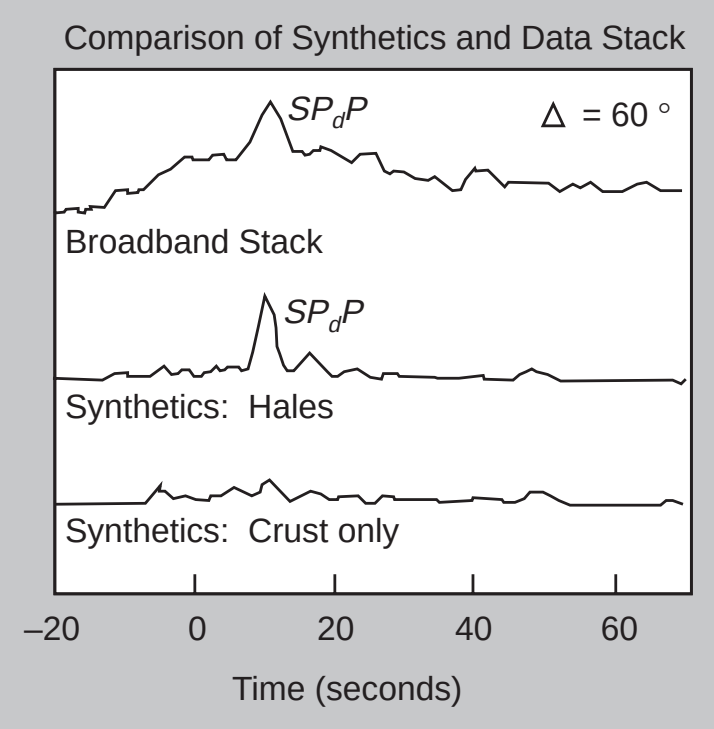


*Figure 3. Comparison of reflectivity synthetics and the broad-band data stack for a source-receiver range of 60°. The broad-band records and the synthetics are rotated to suppress the main S arrival and to enhance the $SP_dP$ phase. The envelope function is taken prior to stacking. One clearly sees S-to-P converted energy on the data trace and on the synthetics calculated using a velocity model with a Hales discontinuity.*

# Experimental Constraints on the Transport of Basaltic Melt in Earth's Mantle (GS96-31)

Principal Investigator: Quentin Williams (UC Santa Cruz)
LLNL Collaborators: F. J. Ryerson and Henry Shaw
Student: Craig Lundstrom (UC Santa Cruz)

## Abstract

*We have conducted a sequence of experiments designed to constrain how the trace element composition of basaltic liquid, the most abundant magma type on the planet, is produced. Such trace element compositions can yield unique insights into how basaltic magma is tranported and chemically evolves as it ascends from within the Earth.*

*We focus particularly on how trace elements are incorporated into coexisting solid phases, such as clinopyroxene (with an endmember formula of $CaMgSi_2O_6$), and how the detailed chemistry of the melt and solid modulate the behavior of a wide suite of elements.*

*Our results, derived from charges synthesized at temperatures in excess of 1200°C, demonstrate that increasing the amount of anorthite ($CaAl_2Si_2O_8$) within basaltic systems produces an increase of up to an order of magnitude in the degree to which highly charged elements are retained within clinopyroxene relative to liquid.*

*Such shifts in trace element behavior have both profound importance for the modeling of trace element signatures of natural magmas, as well as provide crystal-chemical insight into the manner in which such elements are retained as defects within solid crystalline phases.*

## Objectives

The geochemistry of natural magmas provides primary information on the source region of the liquid, the degree of partial melting that has occurred at depth, and the amount of interaction with solid phases occurring during ascent of the magma. As basaltic magma is responsible for the formation of oceanic crust, constraints on how this magma is formed provide fundamental insights into the geochemical and dynamic evolution of the planet.

Our goals are to produce a more detailed understanding of the underlying chemistry associated with basalt petrogenesis, through experimental measurements of element partitioning between minerals and melt in synthetic systems. Although basalt is the most abundant volcanic rock type on the surface of the solid Earth, many aspects of its formation remain uncertain:

- the depth at which ascending basaltic melt completely ceases to equilibrate with coexisting solids;

- the degree to which it equilibrates with solid phases during buoyant ascent; and
- the resultant efficiency with which it extracts trace elements from the solid mantle through which it rises.

For each of these topics, an improved knowledge of the solid/liquid partitioning behavior of different elements can, in conjunction with fluid dynamic modeling,[1] provide significant constraints.

## Progress

We utilized similar experimental and analytical techniques to our previous work on partitioning of actinide and alkaline earth elements[2] to examine the partitioning of a range of high field strength, rare earth, alkali and alkaline earth elements between coexisting clinopyroxene and model basaltic liquids.

Briefly, samples are completely melted at temperatures near 1275°C; their temperatures are then dropped over a 30-hour span to 6° below the initial crystallization temperature of clinopyroxene. The quenched samples, with coexisting solids and liquid, are subsequently analyzed using both an electron microprobe (for major elements) and the Lawrence Livermore National Laboratory ion microprobe (for trace elements).

The particular compositions we chose are 66 mol% $CaMgSi_2O_6$ – 34% $CaAl_2Si_2O_8$ and 57% $CaMgSi_2O_6$ – 43% $NaAlSi_3O_8$, each doped at the approximately 100 ppm level with trace elements and run at identical temperatures to minimize temperature effects on partitioning.

These two endmember compositions, which differ primarily in their relative amounts of sodium, calcium, and aluminum, are designed to examine the effects of shifting the major element content on the solid/liquid partitioning of trace elements, an effect that we have previously demonstrated to be important for thorium partitioning,[2] and which has not been widely considered in modeling of basalt petrogenesis.

Figure 1 shows the ratio of the partition coefficients of various elements between our calcic system and the sodic system. While many elements partition equally between these two systems of moderately different chemistry, it is clear that elements with intermediate ionic strengths (between about 4 and 8 $Å^{-1}$) are retained within crystalline clinopyroxene by up to an order of magnitude more in the calcium/aluminum-rich system than in the sodic system.

The importance of this shift in partitioning lies in the petrogenetic significance attached to elemental ratios such as Nb/Ta and Zr/Hf, elements which had previously been thought not to fractionate from one another, but which our results indicate probably behave differently from one another in aluminum-rich systems.

The underlying reason for this unexpected difference in behavior appears to lie in the degree to which cations with these ionic strengths can enter into clinopyroxenes in conjunction with aluminum: clinopyroxenes in the calcic system typically contain near 5 wt% $Al_2O_3$, while those in the sodic system contain near 1 wt% alumina. Thus, a coupled substitution of (for example) a $ThMgAl_2O_6$ component for $CaMgSi_2O_6$ appears likely to be responsible for the enhanced solubility of Th in the crystalline phase in the calcic system.

It is notable that the behavior of boron, with an ionic strength greater than 11, does not differ between the two compositions,[3] implying that these coupled substitutions are only able to accommodate cations within a relatively narrow range of ionic strengths.

Thus, compositionally-dependent, complex substitution mechanisms appear to modulate the behavior of a family of trace elements in basaltic liquid. A detailed understanding of such effects provides the prospect of generating a quantitative model of the processes that control the evolution of the elemental signature of the planet's most abundant magma type.

## References


1. Lundstrom, C. C., J. Gill, Q. Williams, and M. Perfit, "Mantle Melting and Basalt Extraction by Equilibrium Porous Flow," *Science* **270**, 1,958 (1995).

2. Lundstrom, C. C., H. F. Shaw, F. Ryerson, D. Phinney, J. Gill, and Q. Williams, "Compositional Controls on the Partitioning of U, Th, Ba, Pb, Sr and Zr between Clinopyroxene and Haplobasaltic Melts: Implications for Uranium Series Disequilibria in Basalts," *Earth Planet. Sci. Lett.* **28**, 407 (1994).

3. Neroda, E., J. M. Brenan, C. C. Lundstrom, H. F. Shaw, F. J. Ryerson, and D. L. Phinney, "Mineral-Melt Partitioning of B, Be, and Li: Implications for Mantle Melting," *EOS Trans. Am. Geophys. Union* **77** (1996).


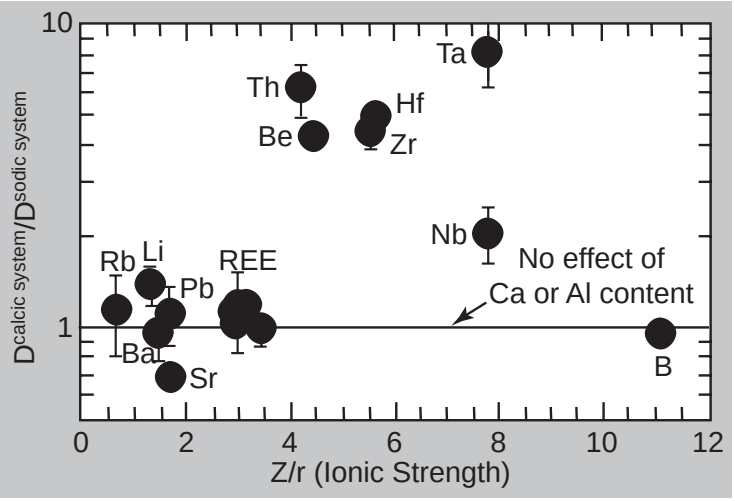


*Figure 1. The ratio of the partition coefficients (D, defined as wt% element in solid/wt% element in liquid) of a range of elements within a calcic model basalt composition relative to a sodic model basalt composition, as a function of ionic strength (the ratio of ionic charge to ionic radius). REE denotes the six rare-earth elements whose partitioning we have characterized.*

# Experimental Determinations of O and Si Self-Diffusion in Melts of Di-An-Ab Compositions at High Pressure (GS96-33)

Principal Investigator: Charles Lesher (UC Davis)
LLNL Collaborator: Ian Hutcheon
Student: David Tinker (UC Davis)

## Abstract

*Diffusion of network-forming components (O and Si) of silicate melts is a rate-limiting control on igneous processes involving crystallization, melting, mixing, and unmixing.*

*A study of self-diffusion of Si and O in melts with compositions in the system $CaMgSi_2O_6$(Di) – $CaAl_2Si_2O_8$(An) – $NaAlSi_3O_8$(Ab) was initiated to examine the effects of compression on the configurations of stable and transition-state network complexes up to 16 GPa.*

*The appropriate experimental procedures were developed for the MA6/8 multianvil apparatus, including the design of a stepped graphite heater with minimal thermal gradients, an improved gasketing configuration, and a pressure calibration for high temperature phase transformations.*

*Starting glasses enriched in $^{18}O$ and $^{28}Si$ and with normal isotopic abundances were synthesized for the Di endmember and the Di-An eutectic composition. Diffusion couples were formed by mating synthetic glass compositions with their isotopically normal counterparts.*

*Preliminary characterization of diffusion profiles was undertaken using the Cameca IMS 3f ion microprobe at Lawrence Livermore National Laboratory. The preliminary results were encouraging and indicate minimum self-diffusivities for O and Si of $4\times 10\ m^{-10}\ m^2/s$ in Di melt at 3 and 4 GPa and 1795°C.*

## Objectives

The goal of this project is to determine the pressure dependence of O and Si self-diffusion in melt compositions in the system Di-An-Ab. Previous work has demonstrated that the self-diffusion of network formers is sensitive to changes in pressure; diffusion rates for network formers increase with pressure in polymerized melt compositions and decrease with pressure in depolymerized melt compositions. This behavior suggests fundamental changes in the mechanism of diffusion for O and Si in polymerized and depolymerized melts on compression.

However, absolute values for the activation volume reported for the diffusion of O in both polymerized jadeite ($NaAlSi_2O_6$; O/T = 2, where T = Si+Al) melt and depolymerized Di (O/T = 3) melts are roughly equal to the molar volume of oxygen. This study attempts to reconcile these contradic-

tory pieces of evidence by comparing O and Si self-diffusion in melts along the compositional joins between depolymerized Di and polymerized An and Ab (O/T=2) endmembers. Observed changes in the activation volumes may be directly linked to changes in the mechanisms of diffusion for network formers in these melt compositions.

## Progress

A series of experiments on these compositions was begun in the multi-anvil apparatus at 3 and 4 GPa. Glasses, enriched in $^{18}O$ and $^{28}Si$ and isotopically normal, were synthesized for experiments on the Di endmember and on the Di-An eutectic composition. Preliminary experiments indicated a minimum self-diffusivity for O and Si of $4 \times 10^{-10}$ $m^2/s$ in Di at 3 and 4 GPa and 1795°C. The necessary developmental work was completed by the graduate student during the first year of this project, and results of an initial set of experiments are encouraging.

# Section IV. IGPP–LLNL Seminars

## *Astrophysics Research Center*

January 25, 1996
"Formation of the Planets"
Stan Peale, UC Santa Barbara

February 2, 1996
"LLNL Speckle Imaging of Planets"
Don Gavel, LLNL

February 9, 1996
"The Ghost of Lyman Alpha as Evidence for Radiative Acceleration in Quasars"
Nahum Arav, California Institute of Technology

February 16, 1996
"Discovery of Two Extrasolar Planets"
Paul Butler, UC Berkeley

February 23, 1996
"NIRSPEC: A High-Resolution Near-Infrared Spectrograph for the Keck II Telescope"
Ian Small McLean, UC Los Angeles

March 8, 1996
"Lighting in the Solar System"
Seran Gibbard, University of Arizona

March 15, 1996
"Measuring the Radius of a Neutron Star"
David J. Helfand, Columbia University, NY

March 22, 1996
"Cosmological Magnetic Fields"
Angela Olinto, Lawrence Berkeley National Laboratory

March 29, 1996
"Imaging with 30 Milliarcsecond Resolution at 10 Microns: Recent Results from UCB Infrared Spatial Interferometer"
William C. Danchi, UC Berkeley

April 5, 1996
"A Search for Low-Luminosity Active Nuclei in Nearby Galaxies"
Alex Filippenko, UC Berkeley

April 12, 1996
"Going Out with a Bang: Supernovae and Their Environments"
Schuyler Van Dyk, UC Berkeley

April 19, 1996
"Faint Starcounts, Red Dwarfs, and Dark Matter"
Neill Reid, California Institute of Technology

April 26, 1996
"Dwarf Galaxies also have Stellar Halos"
Dante Minniti, LLNL-IGPP

May 3, 1996
"Rings and Resonances"
Doug Hamilton, University of Maryland

May 17, 1996
"Speckle Interferometry with the Keck Telescope"
Andrea Ghez, UC Los Angeles

May 24, 1996
"Keck and HST Observations of High Redshift Radio Galaxies"
Wil van Breugel, LLNL-IGPP

May 31, 1996
"Tsunamis in Neutron Star Oceans"
Lars Bildsten, UC Berkeley

August 27, 1996
"From ULIRGs to Primeval Galaxies: Mergers across the Universe"
Dave Clements, European Southern Observatory, Chile

September 13, 1996
"Surface Composition of Solar System Objects Determined from Remote Sensing Observations"
Ted Rousch, NASA Ames Research Center

September 20, 1996
"Binary White Dwarfs and Type 1a Supernova"
James W. Liebert, Steward Observatory, University of Arizona

September 27, 1996
"Gravitational Magnification"
Tom Broadhurst, Astronomy Department, UC Berkeley

October 4, 1996
"The ROSAT HRI X-Ray Survey of the Cygnus Loop Supernova Remnant"
James Graham, UC Berkeley

October 11, 1996
"HST Imaging of Ellipticals with Kinematically Distinct Cores"
Duncan Forbes, Lick Observatory, UC Santa Cruz

October 25, 1996
"Complete Radio Surveys and the Unification and Evolution of Radio Sources"
Pat McCarthy, Carnegie Observatories

November 1, 1996
"First Detections of Solar-like Oscillations"
Tim Bedding, Department of Physics and Astronomy, University of Sydney, Australia

November 5, 1996
"Nucleosynthesis in Low and Intermediate Mass Stars"
John Lattanzio, Monash University, Australia

November 8, 1996
"CDM Cosmogony in an Open Universe"
Dr. Bharat Ratra, Department of Physics, Kansas State University

November 12, 1996
"Starbursts, Mergers, and the Formation of Elliptical Galaxies"
Dr. Steve Zepf, Astronomy Department, UC Berkeley

November 22, 1996
"Identifying the Origin of the Cosmic X-Ray Background"
Ed Moran, LLNL-IGPP

December 6, 1996
"The Role of Finite Photon Mass in Magnetohydrodynamics of Space Plasmas"
Dmitri Ryutov, LLNL

December 13, 1996
"Lensing and Lasers"
Brian McLeod, Harvard-Smithsonian Center for Astrophysics

# *Center for Geosciences*

December 7, 1995
"Permeability of Metamorphic Rocks"
Marian Holness, University of Edinburgh, United Kingdom

April 25, 1996
"BES Planned Projects"
Nick Woodward, Office of Basic Energy Sciences, Washington, DC

June 27, 1996
"Oxygen Isotope Analysis via Laser Probe: Applications to Rocks and Teeth"
Matt Kohn, University of Wisconsin

August 16, 1996
"Uplift of Tibetan Plateau"
Jet Propulsion Laboratory, Mazingarbe, France

November 6, 1996
"2D Models of Fluid Flow: Implications for Variable Permeability during Metamorphism"
Nathalie Marchildron, University of British Columbia, Rouyn, Quebec, Canada

# Section V. Bibliography

## *1996*


Alcock, C., "Gravitational Microlensing Searches and Results," 18th Texas Symposium on Relativistic Astrophysics, Chicago, Illinois, December 15–20, 1996.

Alcock, C., "The Search for MACHOs in the Galactic Dark Matter," International Symposium on Origin of Matter and Evolution of Galaxies, Atami, Japan, January 18–20, 1996.

Alcock, C., D. R. Alves, K. H. Cook, D. Minniti, S. L. Marshall, R. A. Allsman, T. S. Axelrod, D. P. Bennett, K. C. Freeman, B. A. Peterson, A. W. Rodgers, A. C. Becker, C. W. Stubbs, K. Griest, J. Guern, M. J. Lehner, M. R. Pratt, P. J. Quinn, W. Sutherland, and D. Welch, "Properties of LMC Planetary Nebulae and Parent Populations in the MACHO Database," IAU Symposium No. 180, Planetary Nebulae, Groningen, The Netherlands, August 26–30, 1996.

Alcock, C., R. A. Allsman, D. Alves, T. S. Axelrod, A. C. Becker, D. P. Bennett, K. H. Cook, K. C. Freeman, K. Griest, J. Guern, M. J. Lehner, S. L. Marshall, B. A. Peterson, M. R. Pratt, P. J. Quinn, D. Reiss, A. W. Rodgers, C. W. Stubbs, W. Sutherland, and D. L. Welch, "Real-Time Detection and Multisite Observations of Gravitational Microlensing," *Astrophys. J. Lett.* **463**, L67 (1996).

Alcock, C., R. A. Allsman, D. Alves, T. S. Axelrod, A. C. Becker, D. P. Bennett, K. H. Cook, K. C. Freeman, K. Griest, J. Guern, M. J. Lehner, S. L. Marshall, B. A. Peterson, M. R. Pratt, P. J. Quinn, A. W. Rodgers, C. W. Stubbs, and W. Sutherland (The MACHO Collaboration), "The MACHO Project: Limits on Planetary Mass Dark Matter in the Galactic Halo from Gravitational Microlensing," *Astrophys. J.* **471**, 774 (1996).

Alcock, C., R. A. Allsman, D. Alves, T. S. Axelrod, A. C. Becker, D. P. Bennett, K. H. Cook, K. C. Freeman, K. Griest, J. A. Guern, M. J. Lehner, S. L. Marshall, B. A. Peterson, M. R. Pratt, P. J. Quinn, A. W. Rodgers, C. W. Stubbs, and D. L. Welch (The MACHO Collaboration), "Gravitational Microlensing Results from MACHO," The Identification of Dark Matter Conference, Sheffield, United Kingdom, September 8–11, 1996.

Alcock, C., R. A. Allsman, D. Alves, T. S. Axelrod, A. C. Becker, D. P. Bennett, K. H. Cook, K. C. Freeman, K. Griest, J. Guern, M. J. Lehner, S. L. Marshall, D. Minniti, B. A. Peterson, M. R. Pratt, P. J. Quinn, A.

W. Rodgers, A. Rorabeck, C. Stubbs, W. Sutherland, and D. L. Welch, "Cepheids in the LMC: Results from the MACHO Project," Institute d'Astrophysique de Paris Astrophysics Colloquium, Paris, France, July 8–12, 1996.

Alcock, C., R. A. Allsman, D. Alves, T. S. Axelrod, D. P. Bennett, P. A. Charles, K. H. Cook, K. C. Freeman, K. Griest, J. Guern, M. J. Lehner, M. Livio, S. Marshall, B. A. Peterson, M. R. Pratt, P. J. Quinn, A. W. Rodgers, C. W. Stubbs, K. A. Southwell, W. Sutherland, and D. L. Welch, "Optical Variability of the LMC Supersoft Source RX J0513-69 from MACHO Project Photometry," *Mon. Not. R. Astron. Soc.* **280**(4), L49 (1996).

Alcock, C., R. A. Allsman, D. R. Alves, T. A. Axelrod, A. Becker, D. P. Bennett, G. C. Clayton, K. H. Cook, K. C. Freeman, K. Griest, J. A. Guern, D. Kilkenny, M. J. Lehner, S. L. Marshall, D. Minniti, B. A. Peterson, M. R. Pratt, P. J. Quinn, A. W. Rodgers, C. W. Stubbs, W. Sutherland, and D. L. Welch, "The MACHO Project LMC Variable Star Inventory: IV. New R Coronae Borealis Stars," *Astrophys. J.* **490**, 583 (1996).

Alcock, C., R. A. Allsman, T. S. Axelrod, D. P. Bennett, K. H. Cook, K. C. Freeman, K. Griest, S. L. Marshall, B. A. Peterson, M. R. Pratt, P. J. Quinn, A. W. Rodgers, C. W. Stubbs, S. Sutherland, and D. L. Welch, "The Macho Project LMC Variable Star Inventory. II. LMC RR Lyrae Stars—Pulsational Characteristics and Indications of a Global Youth of the LMC," *Astron. J.* **111**(3), 1146 (1996).

Alcock, C. R., Ed., "1995 Observatory Report," *Bull. Am. Astron. Soc.* **28**(1) (1996).

Alcock, C., R. A. Allsman, T. S. Axelrod, D. P. Bennett, K. H. Cook, K. C. Freeman, K. Griest, J. A. Guern, M. J. Lehner, S. L. Marshall, H.-S. Park, S. Perlmutter, B. A. Peterson, M. R. Pratt, P. J. Quinn, A. W. Rodgers, C. W. Stubbs, and W. Sutherland, "The MACHO Project First-Year Large Magellanic Cloud Results: The Microlensing Rate and the Nature of the Galactic Dark Halo," *Astrophys. J.* **461**, 84 (1996).

Alves, D. R., C. Alcock, K. H. Cook, R. A. Allsman, T. S. Axelrod, K. C. Freeman, B. A. Peterson, A. W. Rodgers, A. C. Becker, C. W. Stubbs, D. P. Bennett, K. Griest, M. J. Guern, J. J. Lehner, S. L. Marshall, M. R. Pratt, P. J. Quinn, W. Sutherland, and D. Welch, "The MACHO Project LMC Variable Star Inventory: The Cepheid Catalog," 187th AAS Meeting, San Antonio, TX, January 14–18, 1996.

Alves, D. R., C. Alcock, R. A. Allsman, T. S. Axelrod, A. C. Becker, D. P. Bennett, K. H. Cook, K. C. Freeman, K. Griest, J. Guern, M. J. Lehner, S. L. Marshall, D. Minniti, B. A. Peterson, P. J. Quinn, M. R. Pratt, A. W. Rodgers, C. W. Stubbs, W. Sutherland, and D. Welch, "Properties of

LMC Planetary Nebulae and Parent Populations in the MACHO Database," IAU Symposium No. 180, Groningen, The Netherlands, August 26–30, 1996.

Alves, D. R., and D. W. Hoard, "Near-Infrared Observations of the Proto-Planetary Nebula IRAS 07131-0147," *Astron. J.* **112**(1), 230 (1996).

Antolik, M., S. Larsen, D. Dreger, and B. Romanowicz, "Modeling Broad-Band Waveforms in Central California using Finite Differences," *Seism. Res. Lett.* **67**(2), 30 (1996).

Beck, S. L., G. Zandt, S. C. Myers, T. C. Wallace, P. G. Silver, and L. Drake, "Crustal Thickness Variations in the Central Andes," *Geology*, submitted (1996).

Becker, R. H., M. D. Gregg, D. J. Helfand, C. M. Cress, R. L. White, and R. G. McMahon, "First Results from the FIRST Survey," in *Extragalactic Radio Sources*, R. Ekers *et al*., Ed., p. 499 (1996).

Becker, R. H., M. D. Gregg, I. M. Hook, R. G. McMahon, R. L. White, and D. J. Helfand, "The FIRST Radio-Loud Broad Absorption Line QSO and Evidence for a Hidden Population of Quasars," *Astrophys. J. Lett.*, in press (1996).

Bennett, D. P., and S. H. Rhie, "Is There Evidence for Repeating Gamma Ray Bursters in the BATSE Data?", *Astrophys. J.* **458**, 293 (1996).

Bennett, D. P., and S. H. Rhie, "Detecting Earth-Mass Planets with Gravitational Microlensing," *Astrophys. J.* **472**, 660 (1996).

Brenan, C. J. H., I. W. Hunter, and J. Brenan, "Noninvasive Confocal Raman Imaging of Immiscible Liquids in a Porous Medium," *Anal. Chem.* **69**(1), 45 (1996).

Brenan, J. M., K. D. McKeegan, and F. J. Ryerson, "Oxygen Diffusion in Garnet at High Pressure: Experimental Technique and Initial Results," *EOS Trans. Am. Geophys. Union*, Spring Meeting (1996).

Caffee, M., M. L. Roberts, and I. D. Proctor, "$^{129}$I Interlaboratory Comparison," 7th International Accelerator Mass Spectrometry Conference, Tucson, AZ, May 20–24, 1996.

Caffee, M., M. L. Roberts, G. S. Bench, T. A. Brown, R. C. Finkel, S. Freeman, L. J. Hainsworth, M. Kashgarian, M. McAninch, I. D. Proctor, J. E. Southon, and J. S. Vogel, "The LLNL AMS Facility," 7th International Accelerator Mass Spectrometry Conference, Tucson, AZ, May 20–24, 1996.

Carilli, C. L., H. J. A. Röttgering, G. K. van Ojik, G. K. Miley, and W. J. M. van Breugel, "The Redshift Evolution of the Physical Sizes of Ultra-

Luminous Radio Galaxies," *Mon. Not. R. Astron. Soc.*, submitted (1996).

Chambers, K. C., G. K. Miley, W. J. M. van Breugel, and J.-S. Huang, "Ultra-Steep-Spectrum Radio Sources. I. 4C Objects," *Astrophys. J. Suppl. Ser.* **469**, 215 (1996).

Chambers, K. C. , G. K. Miley, W. J. M. van Breugel, M. A. R. Bremer, J.-S. Huang, and N. A. Trentham, "Ultra-Steep-Spectrum Radio Sources. II. Radio, Infrared, Optical, and HST Imaging of High-Redshift 4C Objects," *Astrophys. J. Suppl. Ser.* **106**, 247 (1996).

Cimatti, A., A. Dey, W. van Breugel, R. Antonucci, and H. Spinrad, "Keck Spatially Resolved Spectropolarimetry of Distant Radio Galaxy 3C 324," *Astrophys. J.* **465**, 145 (1996).

Cimatti, A., A. Dey, W. van Breugel, T. Hurt, and R. Antonucci, "Keck Spectropolarimetry of Two High-*z* Radio Galaxies: Discerning the Components of the Alignment Effect," *Astrophys. J.*, submitted (1996).

Colbert, E. J. M., S. A. Baum, J. F. Gallimore, C. P. O'Dea, M. D. Lehnert, Z. I. Tsvetanov, J. S. Mulchaey, S. Caganoff, and D. Gilmore, "Galactic Winds in Edge-on Seyfert Galaxies. I. Optical Emission-line Imaging and Optical Spectroscopy," *Astrophys. J.*, submitted (1996).

Cook, K. H., C. Alcock, D. Alves, S. Marshall, D. Minniti, R. A. Allsman, T. S. Axelrod, K. C. Freeman, B. A. Peterson, A. W. Rodgers, A. C. Becker, C. W. Stubbs, D. P. Bennett, K. Griest, J. Guern, M. J. Lehner, M. R. Pratt, P. J. Quinn, W. Sutherland, and D. L. Welch, "The Macho Project: Microlensing and Variable Stars," 12th Institute d'Astrophysique de Paris Astrophysics Colloquium, Paris, France, July 8–13, 1996.

Cook, K. H., D. R. Alves, C. Alcock, R. A. Allsman, T. S. Axelrod, A. Becker, D. P. Bennett, K. C. Freeman, K. Griest, J. A. Guern, M. J. Lehner, S. L. Marshall, D. Minniti, B. A. Peterson, M. R. Pratt, P. J. Quinn, A. W. Rodgers, C. W. Stubbs, W. Sutherland, and D. L. Welch (The MACHO Collaboration), "The MACHO Project: Microlensing and Variable Stars," 12th Institute d'Astrophysique de Paris Astrophysics Colloquium, Paris, France, July 7–12, 1996.

Cook, K., C. Alcock, P. Purdue, R. Allsman, D. Alves, T. Axelrod, K. Freeman, B. Peterson, A. Rodgers, A. Becker, C. Stubbs, D. Bennett, K. Griest, M. Guern, M. Lehner, S. Marshall, M. Pratt, P. Quinn, W. Sutherland, and D. Welch, "The MACHO Project Variables in the Bulge: 1st Year Results," 187th AAS Meeting, San Antonio, TX, January 14–18, 1996.

Cress, C. M., D. J. Helfand, R. H. Becker, M. D. Gregg, and R. L. White, "The Angular Two-Point Correlation Function for the FIRST Radio Survey," *Astrophys. J.* **473**, 7 (1996).

Dahlem, M., T. M. Heckman, G. Fabbiano, M. D. Lehnert, and D. Gilmore, "The Hot Gaseous Halo of the Spiral Galaxy NGC 3628 in the Lero Triplet," *Astrophys. J.,* submitted (1996).

Dey, A., A. Cimatti, W. van Breugel, R. Antonucci, and H. Spinrad, "On the Origin of the Ultraviolet Continuum Emission from the High-Redshift Radio Galaxy 3C 256," *Astrophys. J.* **465**,157 (1996).

Farber, D. L., Q. Williams, and F. J. Ryerson, "Chemical Diffusion in High-Pressure Olivine Polymorphs: Implications for Deep Upper Mantle Transport Properties," *J. Geophys. Res.,* submitted (1996).

Farber, D. L., Q. Williams, and F. J. Ryerson, "Divalent Cation Diffusion in $Mg_2SiO_4$-Spinel, B-Hase and Olivine: Implications for the Electrical Conductivity of the Mantle," *J. Geophys. Res.,* submitted (1996).

Gregg, M. D., "The Coma-Leo I Distance Ratio and the Hubble Constant," *New Astron.,* submitted (1996).

Gregg, M. D., R. H. Becker, R. L. White, D. J. Helfand, R. G. McMahon, and I. M. Hook, "The FIRST Bright QSO Survey," *Astron. J.* **112**(2), 407 (1996).

Gu, Z. Y., D. Lal, T. S. Liu, J. Southon, M. W. Caffee, Z. T. Guo, and M. Y. Chen, "Five Million Year $^{10}$Be Record in Chinese Loess and Red Clay: Climate and Weathering Relationships," *Earth Planet. Sci. Lett.* **144**, 273 (1996).

Harrison, T. M., A. Yin, and F. J. Ryerson, "Orographic Evolution of the Himalayan and Tibetan Plateau," in *Tectonics and Climate Changes* (1996).

Harrison, T. M., F. J. Ryerson, K. D. McKeegan, P. Lefort, and A. Yin, "The Pb Monazite Ages of Himalayan Metamorphic Rocks: Constraints on the Timing of Inverted Metamorphism and Slip on the MCT and STD," Tibet-Himalaya-Karakorum Workshop (1996).

Harrison, T. M., O. Lovera, F. J. Ryerson, and P. Lefort, "A Late Miocene-Pliocene Origin for the Central Himalayan Inverted Metamorphism due to Reactivation of the Main Central Thrust," *Earth Planet. Sci. Lett.,* submitted (1996).

Hart, J., J. van Harmelen, Hovey, K. C. Freeman, B. A. Peterson, T. S. Axelrod, P. J. Quinn, A. W. Rodgers, R. A. Allsman, C. Alcock, D. P. Bennett, K. H. Cook, K. Griest, S. L. Marshall, M. R. Pratt, C. W. Stubbs, and W. Sutherland, "The Telescope System of the MACHO Program," *Pubs. Am. Astron. Soc. 108*, 220 (1996).

Jedamzik, K., "Primordial Black Hole Formation during the QCD Epoch," *Nature,* submitted (1996).

Jedamzik, K., J. X. Prochaska, A. M. Wolfe, and G. M. Fuller, "Constraints on Structure Formation Scenarios by Observations of Damped Lyman-Alpha Systems at High Redshift," 1996 Joint American Physical Society/American Association of Physic Teachers Meeting (1996).

Jedamzik, K., V. Katalinic, and A. V. Olinto, "Damping of Cosmic Magnetic Fields," *Astrophys. J.,* submitted (1996).

Justtanont, K., C. J. Skinner, A. G. G. M. Tielens, M. Meixner, and F. Baas, "Modeling of the Dust and Gas Outflows from OH 26.5+0.6: The Superwind," *Astrophys. J.* **456**, 337 (1996).

Kersting, A. B., R. J. Arculus, and D. A. Gust, "Lithospheric Contributions to Arc Magmatism: Isotope Variations Along-Strike in Volcanoes of Honshu, Japan," *Science* **272**, 1464 (1996).

Kurki-Suonio, H., K. Jedamzik, and G. J. Mathews, "Stochastic Isocurvature Baryon Fluctuations, Baryon Diffusion, and Primordial Nucleosynthesis," *Astrophys. J.,* submitted (1996).

Lehnert, M. D., and T. M. Heckman, "Ionized Gas in the Halos of Edge-On Starburst Galaxies: Evidence for Supernova-Driven Superwinds," *Astrophys. J.* **462**, 651 (1996).

Lehnert, M. D., and T. Heckman, "The Nature of Starburst Galaxies," *Astrophys. J.* **472**, 546 (1996).

Liu, M., and G. Zandt, "Convective Thermal Instabilities in the Wake of the Migrating Mendocino Triple Junction, California," *Geophys. Res. Lett.* **23**(13), 1573 (1996).

Macintosh, B. A., E. E. Becklin, B. Zuckerman, and I. S. McLean, "A Near-Infrared Search for Low Mass Companions to Hyades Dwarfs," *Astrophys. J. Lett.,* submitted (1996).

McCarthy, P. J., V. K. Kapahi, W. van Breugel, S. E. Persson, R. M. Athreya, and C. R. Subrahmanya, "The Molonglo Reference Catalog/1 Jansky Radio Source Survey. I. Radio Galaxy Identifications," *Astrophys. J. Suppl. Ser.* **107**, 19 (1996).

McCarthy, P. J., V. K. Kapahi, W. van Breugel, S. E. Persson, R. Athreya, and C. R. Subramhanya, "The MRC/1 Jy Survey and Radio Source Unification," *Bul. Am. Astron. Soc.* **189**, 118.26 (1996).

McEvilly, T. V., and R. M. Nadeau, "Characteristic Microearthquakes at Parkfield as Deep Drilling Targets," *EOS Trans. Am. Geophys. Union,* submitted (1996).

McNamara, D., "Lateral Variations within the Upper Mantle across the Tibetan Plateau," *Am. Geophys. Union,* Fall Meeting (1996).

McNamara, D., "Velocity Structure across Northern Africa from Surface Wave Dispersion," *Am. Geophys. Union,* Fall Meeting (1996).

Meixner, M., C. J. Skinner, E. Keto, A. Zijlstra, M. G. Hoare, J. F. Arens, and J. G. Jernigan, "Mid-IR and Radio Images of IC 418: Dust in a Young Planetary Nebula," *Astron. Astrophys.* **313**, 234 (1996).

Minarik, W. G., and F. J. Ryerson, "Metal-Sulfide Melt Non-Interconnectivity in Silicates, Even at High Pressure, High Temperature, and High Melt Fractions," 27th Annual Lunar and Planetary Science Conference, Houston, TX, March 18–22, 1996.

Minarik, W. G., F. J. Ryerson, and E. B. Watson, "Textural Entrapment of Core-Forming Melts: Implication for Siderophile Element Abundances," *Science* **272**, 530 (1996).

Minarik, W. G., F. J. Ryerson, and I. D. Hutcheon, "More Immiscible Silicate Melt Partitioning: Light Lithophile and Platinum Group Elements," *Am. Geophys. Union*, Fall Meeting, San Francisco, CA (1996).

Minniti D., C. Alcock, D. Alves, K. H. Cook, S. L. Marshall, R. A. Allsman, T. S. Axelrod, K. C. Freeman, B. A. Peterson, A. W. Rodgers, A. C. Becker, C. W. Stubbs, D. P. Bennett, K. Griest, J. Guern, M. J. Lehner, M. R. Pratt, P. J. Quinn, W. Sutherland, and D. L. Welch, "RR Lyrae Stars in the MACHO Database," 12th Institute d'Astrophysique de Paris Astrophysics Colloquium, Paris, France, July 8–12, 1996.

Minniti, D., and A. A. Zijlstra, "Stellar Populations of the Dwarf Irregular Galaxy WLM," *Astron. J.,* submitted (1996).

Minniti, D., and A. Zijlstra, "Dwarf Galaxies also have Stellar Halos," *Astrophys. J. Lett.* **467**, L13 (1996).

Minniti, D., C. Alcock, D. R. Alves, R. A. Allsman, T. S. Axelrod, A. Becker, D. P. Bennett, K. H. Cook, K. C. Freeman, K. Griest, J. A. Guern, M. J. Lehner, S. L. Marshall, B. A. Peterson, M. R. Pratt, P. J. Quinn, A. W. Rodgers, C. W. Stubbs, W. Sutherland, and D. L. Welch (Le Groupe MACHO), "RR Lyrae Stars in the MACHO Database," 12th Institute d'Astrophysique de Paris Astrophysics Colloquium, Paris, France, July 7–12, 1996.

Minniti, D., G. Meylan, and M. Kissler-Patig, "Globular Cluster Halos around Dwarf Elliptical Galaxies," *Astron. Astrophys.*, submitted (1996).

Minniti, D., M. V. Alonso, P. Goudfrooij, P. Jablonka, and G. Meylan, "Globular Clusters in the Inner Regions of NGC 5128 (Centarus A)," *Astrophys. J.* **467**, 221 (1996).

Minniti, D., R. C. Peterson, D. Geisler, and J. J. Claria, "High-Dispersion Spectroscopy of Giants in Metal-Poor Globular Clusters. II. Oxygen and Sodium Abundances," *Astrophys. J.* **470**, 953 (1996).

Moran, E. C., D. J. Helfand, R. Becker, and R. L. White, "The Einstein Two-Sigma Catalog: Silver Needles in the X-Ray Haystack," *Astrophys. J.* **461**, 127 (1996).

Moran, E. C., J. P. Halpern, and D. J. Helfand, "Classification of IRAS-Selected X-Ray Galaxies in the ROSAT All-Sky Survey," *Astrophys. J. Suppl. Ser.* **106**, 341 (1996).

Murphy, M. A., A. Yin, T. Harrison, S. B. Durr, Z. Chen, X. Wang, X. Zhou, F. J. Ryerson, and W. S. F. Kidd, "Significant Crustal Shortening in the Lhasa Block Predates the Indo-Asian Collision," Tibet-Himalaya-Karakorum Workshop (1996).

Myers, S. C., T. C. Wallace, S. L. Beck, P. G. Silver, and G. Zandt, "Implications of Spatial and Temporal Development of the Aftershock Sequence for the Mw8.3 June 9, 1994, Deep Bolivian Earthquake," *Geophys. Res. Lett.* **22**(16), 2269 (1996).

Myers, S. C., T. C. Wallace, S. L. Beck, P. G. Silver, and G. Zandt, "Aftershock Source Mechanisms from the June 9, 1994, Deep Bolivian Earthquake," *Geophys. Res. Lett.*, submitted (1996).

Nadeau, R. M., "Recurrence Scaling of Characteristic Microearthquakes at Parkfield with Large Repeating Events on the San Andreas Fault in California," *Seism. Res. Lett.* **67**(2), 48 (1996).

Nadeau, R. M., and T. V. McEvilly, "An Analysis of the Feasibility of Microearthquake Hypocenters as Drilling Targets," *EOS Trans. Am. Geophys. Union*, submitted (1996).

Nadeau, R. M., and W. Foxall, "Implications of Characteristic Microearthquakes at Parkfield, CA, for Fractal Crustal Deformation Models," *EOS Trans. Am. Geophys. Union*, submitted (1996).

Neroda, E., J. M. Brenan, C. C. Lundstrom, H. F. Shaw, F. J. Ryerson, and D. L. Phinney, "Mineral-Melt Partitioning of B, Be, Li with Implications for Mantle Melting," *EOS Trans. Am. Geophys. Union*, Spring Meeting (1996).

Nishiizumi, K., M. W. Caffee, R. C. Finkel, and R. C. Reedy, "Exposure history of lunar meteorite QUE93069 and 94269," *Meteroritics Planet. Sci.*, submitted (1996).

Owens, T